NEW METHODS IN BIOGEOCHEMISTRY:

THE DEVELOPMENT OF ELECTROCHEMICAL TOOLS FOR THE MEASUREMENT OF DISSOLVED AND SOLID STATE COMPOUNDS IN NATURAL SYSTEMS

Dissertation

zur Erlangung des

Doktorgrades der Naturwissenschaften

am Fachbereich 5

der Universität Bremen

Vorgelegt von

Jochen Nuester

Bremen 2005

Die vorliegende Arbeit wurde in der Zeit von Mai 2000 bis August 2005 am Max Planck Institut für Marine Mikrobiologie erstellt.

1. Gutachter: Prof. Dr. Bo Barker Jørgensen

2. Gutachter: Prof. Dr. Jörn Peckmann

Prüfer:

Prof. Dr. Achim Kopf

Dr. Sabine Kasten

Tag des Promotionskolloquium: 26. August 2006

Acknowledgements

This PhD thesis deals with the development of new tools and methods to describe biogeochemical processes. Several aspects concerning the speciation have been studied; especially new methods were described for the determination of solid iron compounds, the detection of dissolved transition metals, and the complexation of such transition metals. The financial support for this thesis came from the Max Planck Society and the European Union is grateful acknowledged.

First of all, I would like to thank Prof. Bo Barker Jørgensen for accepting me as his PhD student, and the opportunity to carry out this work at the Max Planck Institute. I am very grateful to my mentor and friend Dr. Ole Larsen for the initiation of the work, for the way he taught me to think interdisciplinary, for his supervision, and his support. He always had an open ear, and he usually had very inspiring answers to my questions. I like to thank Prof. Stan van den Berg at the University of Liverpool for the opportunity to stay at his laboratory and the fruitful cooperation. The work at the Oceanographic Laboratories in Liverpool was very inspiring, and supports my understanding of electrochemistry.

Timothy Ferdelman, Michael Böttcher, and Dirk de Beer always had time for very fruitful discussions on various topics concerning electrochemical measurements and iron biogeochemistry. Their clear and critical analysis helps to structure my ideas and to develope new methods and tools. Dirk de Beer is also thanked for the opportunity to use the microsensor laboratories.

My special thanks go to Gaby Eickert, Ines Schroeder, Cäcilia Wigand, Karin Hohmann, Vera Hübner, and Ingrid Dohrmann for accepting me somehow as a part of *their* microsensor laboratory, for their helping hand, for the introduction to construct microsensors, and also for the way they handle my impossibility to be tidy.

Without the help of the Volker Meyer, Paul Färber, and Harald Osmers from the electronic workshop the microsensor development work would not have been possible. Thanks a lot!

Kirsten Imhoff, Swantje Lilienthal, Imke Busse, Gabi Schüssler, Gabi Klockgetter, and all the other technicians are thanked for their invaluable, never ending help in the laboratory. I like to thank Bernd Stickford for his help in the library, and for ordering so many articles and books not available, and to Ulrike Tietjen for all her organizing work.

Many thanks to Jutta, Niko, Verona, Lev, Stanislav, Kyriakos, Solveig, Sandra, Eli, Fanny, Tina, Hans, Marcel, Stefan, Uschi, Felix, Alex, Susanne, Anna, Heiko, Nina, Helge, Peter and all the other nice people at the institute, who support me in those days when I could not laugh anymore about the problems I had with my work. They made this time at the Max Planck Institute very special in providing a nice working atmosphere and a very pleasant time. Especially I would like to thank the members of the cheerleading group and the boy group, who made my Julefrokost parties to very exciting events.

I'm deeply grateful to Emily Fleming, who helped me in the last years with her support, her love, her patient, and also her knowledge about English language and grammar.

Last but not least I like to thank my parents, my brother, and my grandma, who saw me struggle, but always support my work and my goals. Uncountable thanks!

Table of Contents

Table of Figures

List of Tables

List of Important Abbreviations

Chapter 3:

Mn^{n+}	positive charged metal ion with n charges
M	metal
ML_n	metal ion complexed by a natural ligand
AL	added complexing ligand
MAL	metal ion complexed by an added ligand
WE	working electrode
RE	reference electrode
CE	counter electrode
AdSV	adsorptive stripping voltammetry
ASV	anodic stripping voltammetry
LSV	linear sweep voltammetry
DPV	differential pulse voltammetry
SWV	square wave voltammetry
CSV	cathodic stripping voltammetry
HDME	hanging drop mercury electrode
SDME	static drop mercury electrode
HOPG	highly orientate pyrolytic graphite
PIGE	paraffin impregnated graphite electrode

Chapter 4:

J	is the overall rate of dissolution (mol/s)
m	is the amount of undissolved crystals (mol)
m_0	m_0 is the initial amount of crystals (mol)
k	is the rate constant (s^{-1})
k'	is the product of the initial rate constant and *g(C)*
γ	describes the homogeneity of the dissolution process
g(C)	describes the effect of the solution composition
$f(m/m_0)$	describes the change in reactivity of the remaining mineral fraction
Q_t	is the charge required to dissolve the unreacted amount of particles
Q_0	is the charge required to dissolve all particles
Q_{chrono}	consumed charge of chronoamperometric measurements
Q_{LSV}	used charge to reduce the remain particle fraction after chronoamperometry
Fe_{total}	all extracted iron
Fe_{dith}	iron extracted with a sodium dithionite extraction protoll
Fe_{asc}	iron extracted with an ascorbate extraction protoll
$Fe_{reactive}$	$Fe_{reactive} = Fe_{asc}$
$Fe_{refractory}$	$Fe_{refractory} = Fe_{dith} - Fe_{asc}$
HCl-Fe_{total}	Ferrous and ferric iron extracted with 0.5 M HCl
HCl-Fe^{2+}	Ferrous iron extracted with 0.5 M HCl
HCl-Fe^{3+}	HCl-Fe^{3+} = HCl-Fe_{total} - HCl-Fe^{2+}
LSV	linear sweep voltammetry
CV	cyclic voltammetry
DPV	differential pulse voltammetry

Chapter 5:

LSV	linear sweep voltammetry
SWV	square wave voltammetry
SWASV	square wave anodic stripping voltammetry

Chapter 6:

K'CuL	complexing stability constant of CuL
C_L	concentration of a nature l ligand L
B'_{CuSA}	
K'_{CuSA}	complexing stability constant of CuSA
Cu'	inorganic copper
α_{Cu}	α coefficient of Cu
α_{CuSA}	α coefficient of CuSA
α_{CuSA2}	α coefficient of $CuSA_2$
X	X= Ip/ I_{max}
Ip	voltammetric signal for each addition of a ligand (i.e., SA)
I_{max}	maximum voltammetric signal
S	sensitivity
CSV	cathodic stripping voltammetry
CLE	competitive ligand equilibration

Chapter 7:

J_B	overall bulk dissolution rate ($mol \cdot s^{-1}$)
J_L	rate for ligand promoted dissolution
J_{RD}	reductive dissolution rate
J_P	rate for proton assisted dissolution
m	is the amount of undissolved crystals (mol)
m_0	m_0 is the initial amount of crystals (mol)
k	is the rate constant (s^{-1})
k'	is the product of the initial rate constant and *g(C)*
γ	describes the homogeneity of the dissolution process
g(C)	describes the effect of the solution composition
$f(m/m_0)$	describes the change in reactivity of the remaining mineral
C_L^S	
C_P^S	

Abstract

This PhD thesis deals with biogeochemical processes of transition metals (i.e., iron, manganese, and copper). Depending on chemical, physical, and biological processes these elements change their speciation. Thus, the knowledge about the distribution of solid, dissolved, or complexed compounds of these metals is an important factor in evaluating biogeochemical cycles.

Despite the importance of manganese and iron for biogeochemical processes, the possibilities for determination are limited due to their reactivity and their appearance in several solid state forms. In natural ecosystems iron and manganese minerals occur as amorphous to crystalline nanosize solid compounds. Previous established solid state extraction methods allow only the description of different solid state iron and manganese pools, but a detailed analysis of the single mineral composition was only possible with high technological expenditure. On the other hand, in-situ detection of aqueous iron, manganese, and trace metals at the scale of the processes is so far limited due to the size of the available instruments.

The primary aim of this thesis was to develop new tools and methods allowing a detailed characterization of solid and dissolved compound distribution in natural ecosystems. The detection techniques described in this thesis allow the identification of single iron and manganese minerals (i.e., iron (oxyhydr)oxides and sulfides), allow the detection of dissolved iron, manganese, and trace metals, and offer a new option to evaluate the strength of the complexing capacity of organic ligands to bind trace metals.

The application of Voltammetry of Immobilized Microparticles (VIM) allows a detailed and high resolution detection of the distribution of iron (oxyhydr)oxides (i.e., ferrihydrite, lepidocrocite, goethite, and hematite) in sediments and soils. The detection of ferrous iron minerals (i.e., mackinawite, greigite, and pyrite) gives evidence of the transformation of mackinawite to pyrite via greigite, which is otherwise only possible with magnetic susceptibility measurements. In addition to the detection of different mineral phases, it is also possible to describe the reaction kinetics of the iron (oxyhydr)oxide pool in soils and sediments. The application of a reaction continuum model to the results of chronoamperometric measurements reduces the time for such iron (oxyhydr)oxide reductive dissolution measurements from weeks to minutes. A combination of one-step batch extraction

methods with solid state electrochemistry enables a detailed evaluation of the biogeochemical processes in which the different iron fractions are involved.

The second report describes the construction and miniaturization of different microelectrodes, and their application possibilities to detect different transition metals. The miniaturization of these devices enables a detection level, which is similar to the level at which the detected compounds are involved in several reactions. This allows measurements with resolution of 100 to 200 µm without effects on the profiled sediment column. Iridium-based mercury microelectrodes are perfect for water column applications. The stability of the liquid mercury droplet at the iridium substrate restricts the use in sediments and soils. Compared with iridium-based microelectrodes, the application of amalgam microelectrodes based on silver enables sediment profiling. These microelectrodes can be used for the detection of oxygen, sulfide, iron, and manganese. An application to trace metals is not recommendable, because these metals could interact with silver substrate itself. A further development for application in Lander systems is possible.

The third report describes a new method for metal speciation by varying the concentration of a competing ligand using cathodic stripping voltammetry. The method is a *reverse titration*, because the increase of the added competing ligand decreases the free metal ion concentration and probes progressively into the already complexed metal fraction. These analysis based on the model ion copper can in principal be applied to any trace metal with corresponding competing ligands. This new method allows the reduction of the required amount of sample water by applying the whole titration in one electrochemical cell. However, this requires long equilibration times for each step of addition. The mathematical model of such reverse titrations allows the separation of two ligands with different complexing capacity. The application to natural waters with more than two ligands is limited.

The fourth report describes the comparison of abiotic and bacterial iron (oxyhydr)oxide bulk dissolution kinetics. Initial microbial dissolution rates do not correlate with the initial inorganic dissolution rate calculated from bulk dissolution studies in ascorbic acid (pH=3). These findings indicate that the dissolution mechanisms are fundamentally different. Abiotic experiments emphasize the importance of crystal structure for the dissolution rate, while microbiological experiments indicate a correlation to the gross surface area.

Zusammenfassung

Diese Doktorarbeit präsentiert die Ergebnisse von Untersuchungen zur Biogeochemie von Übergangsmetallen und der Entwicklung neuer Ansätze diese zu bestimmen. Chemische, physikalische und biologische Prozesse beeinflussen den Zustand dieser Übergangsmetalle, wobei besonders Eisen und Mangan sehr redox sensitiv sind. Eine genaue Bestimmung von Festphasen, gelösten Phasen und komplexierten Spezies dieser Übergangsmetalle ist daher nötig, um Aussagen über die beteiligten biogeochemischen Kreisläufe treffen zu können.

Im Gegensatz zu ihrer Gewichtung in biogeochemischen Prozessen sind die Nachweismöglichkeiten von Eisen und Mangan aufgrund ihrer Reaktivität and der Vielfalt der beteiligten Festkörperphasen sehr begrenzt. In natürlichen Ökosystemen haben Eisen- und Manganminerale eine unterschiedliche Kristallstruktur, wobei der Grad der Kristallinität variiert. Um die Zusammensetzung der unterschiedlichen Eisen- und Manganminerale in Sedimenten zu beschreiben sind Festphasen-Extraktionsmethoden entwickelt worden, welche jedoch nur die Einteilung in bestimmte Eisen- und Manganklassen erlauben. Eine genauere Bestimmung der einzelnen Mineralphasen war bisher nur durch hohen technischen Aufwand möglich. Eine In-Situ-Bestimmung der gelösten Eisen- und Manganfraktion, in einer Auflösungsdichte entsprechend der stattfindenden Prozesse, war ebenso nur eingeschränkt möglich.

Das Hauptziel dieser Dissertation war die Bereitstellung neuer Methoden und Werkzeuge, welche eine genauere Unterscheidung der festen und gelösten Phasen in natürlichen Ökosystemen ermöglichen. Die in dieser Dissertation beschriebenen Untersuchungstechniken vereinfachen die Bestimmung von einzelnen Eisen- und Manganmineralen (z.B.: Eisenoxide und -sulfide), erlauben die Messung von gelösten Übergangsmetalionen, und bieten die Möglichkeit die Stärke von komplexierenden organischen Molekülen abzuschätzen.

Die Anwendung von Festkörperelektrochemie auf natürliche Sedimente bietet eine neue Möglichkeit Eisenfestphasen detailliert zu bestimmen. Diese Methode erlaubt sowohl Eisen(oxihydr)oxide (Ferrihydrit, Lepidokrokit, Goethit und Hematit), als auch Eisensulfide (Mackinawit, Greigit und Pyrit) zu bestimmen. Die Option gleichzeitig verschiedene Eisensulfidphasen zu bestimmen, unterstützt die in der Literatur beschriebene Theorie, dass sich Mackinawit zu Pyrit wandelt, wobei Greigit als Übergangsphase existiert. Dies war bisher nur durch gleichzeitige Messungen der magnetischen Suszeptibilität und des Pyritgehaltes möglich. Zusätzlich zu den Mineralbestimmungen kann durch chronoamperometrische Messungen die Reaktivität der verschiedenen Eisenmineralzusammensetzungen über die Tiefe kalkuliert werden. Die mathematische Beschreibung dieser chronoamperometrischen Messungen durch ein Kontinuummodel reduziert den Messaufwand im Vergleich zu nass-chemischen Reduktionsexperimenten von Wochen zu Minuten. Die kombinierte Anwendung von Extraktionsmethoden und elektrochemischen Festkörperanalysen ermöglicht eine detaillierte Beschreibung und genaue Einschätzung der ablaufenden biogeochemischen Prozesse.

Die zweite Studie dieser Dissertation beschäftigt sich mit der Miniaturisierung von Elektroden, so dass Messungen in einer Auflösungsdichte möglich sind, welche der stattfindenden Prozesse ähnelt. Die Konstruktion und die Anwendungsmöglichkeiten verschiedenster Elektroden werden beschrieben. Eine auf Iridium basierende Quecksilber-Mikroelektrode eignet sich besonders für Spurenmetalmessungen in der Wassersäule. Der Einsatz in Sedimenten ist jedoch durch die Stabilität des flüssigen Quecksilbertropfens auf der Iridiumoberfläche limitiert. Amalgamierte Mikroelektroden mit Gold oder Silbersubstraten eignen sich besser für die Anwendung in Sedimenten. Diese amalgamierten Mikroelektroden erlauben die Bestimmung von gelösten Eisen-, und Manganphasen, von H_2S und Sauerstoff. Die Bestimmung von Spurenmetallen ist limitiert, da diese eine Reaktion mit den Elektrodensubstraten eingehen können. Ein Einbau in autonomme Lander-Systeme ist mit diesen Mikroelektroden möglich.

Die dritte Studie dieser Dissertation beschreibt die neue Methode der *reversen Titration*, wobei die Metalkomplexierung in Abhängigkeit von der Zunahme eines konkurrierenden Liganden elektrochemisch gemessen wird. Dabei wird die freie Metalionenkonzentration erniedrigt und der schon bestehende Anteil des komplexierten Metalls untersucht. Kupfer wurde als Modelion ausgewählt, jedoch kann diese Methode auf alle Metalle angewendet werden, für die es einen synthetischen, komplexierenden, organischen Liganden gibt. Diese

Methode ermöglicht es Komplexierungsstudien auch dann durchzuführen, wenn nur geringe Probenmengen zur Verfügungen stehen. Eine direkte Anwendung in einer voltammetrischen Zelle ist möglich, jedoch benötigt dies eine lange Equilibrationszeit. Die mathematische Beschreibung solcher reverser Titrationen erlaubt die Einbeziehung von zwei Liganden mit unterschiedlicher Komplexierungsstärke, eine Ausweitung darüber hinaus ist aber beschränkt.

Die vierte Studie dieser Dissertation präsentiert die Ergebnisse des Vergleichs von bakterieller and abiotischer Auflösungskinetik von Eisen(oxihydr)oxiden. Der Vergleich der initialen Geschwindigkeiten der bakteriellen, und der anorganischen Auflösung zeigte keine Übereinstimmung. Während bei den abiotischen Experimenten der Einfluss der Kristallstruktur ein prägender Faktor darstellte, konnte dieser für mikrobielle Experimente nicht festgestellt werden. Bei letzteren Experimenten zeigte sich, dass die initiale Auflösungsgeschwindigkeit mit der Brutto-Oberfläche korreliert.

Chapter 1

In-Situ Applications to Modern Biogeochemistry

1.1 Introduction

Natural aqueous and sedimentary environmental samples can potentially be altered, chemically, physically, and biologically, while they are sampled on the seafloor, brought to the surface, processed, and analyzed. Therefore, a detailed characterization of natural systems needs new and miniaturized tools for undisturbed measurements and monitoring. A further aspect for developing miniaturized tools is the opportunity to measure the products of chemical, physical, or biological processes at the same scale at which these processes take place. The size of the instruments used determines the resolution of the measurement and also if the measurement is affected by a response from several microniches (Joergensen 1977; Fenchel 1996; Fenchel 1996; Schramm, Stantegoeds et al. 1999; Shuttleworth, Davison et al. 1999; Krom, Mortimer et al. 2002; Nielsen, Gribsholt et al. 2004). It was suggested that such microniches with a diameter of 50 to100 µm play a major role in metal remobilization, and depending on the applied measurement tool caution has to be taken on the estimation of fluxes from one-dimensional concentration gradients (Shuttleworth, Davison et al. 1999).

The understanding of biogeochemical processes was dramatically increased by the introduction of the first in-situ tools in environmental related research disciplines (Jørgensen 1977; Revsbech, Jørgensen et al. 1980). The application of instruments allowing two-dimensional profiling further increased the knowledge about the spatial heterogeneity and the time dependence of biogeochemical processes (Davison, Zhang et al. 1994; Davison, Fones et al. 1997). Since then, rapid progress in technology development (i.e., Glud et al. (1996)) has enabled a more detailed and precise description of chemically heterogeneous natural systems. The developments and experiments described in this thesis provide new tools to evaluate biogeochemical processes that involve the reactivity of solid state electron acceptors, the ligand complexing capacity of trace metals, and the distribution of dissolved trace metals including manganese and iron. All applications enable the decrease of needed sampling material, and a higher measuring resolution in comparison to commonly applied methods.

1.2 In-Situ Technologies

The highest amount of biogeochemical activity in sediments occurs close to the sediment-water interface. Activities in this spatially heterogeneous zone are very sensitive to disturbances. Therefore, micro-electrochemical sensors are invaluable tools to study the small scale chemical heterogeneity of such systems. Such tools also allow rapid data acquisition and

consequently provide real time data. As a variety of anaerobic processes is shown to be relevant for many biogeochemical cycles, the need for the development of new analytical tools for in-situ and on-site measurements has increased. With the discovery of dissimilatory iron and manganese reduction (Lovley and Phillips 1986; Lovley and Phillips 1988)), and the observation of small scale chemical heterogeneities in spatial distributions of sediments (e.g., Ziebis et al. (1996)), a better understanding for biogeochemical zonation has been evolved. These findings increase the need for miniaturized analytical tools to detect chemical changes with time and depth. With such tools dramatic submillimeter changes of chemical species were discovered in microbial mats and sedimentary environments (Gundersen and Joergensen 1990; Davison, Grime et al. 1991; Gundersen, Jørgensen et al. 1992). Unlike microsensors that provide a one dimensional view, gel measurements by diffusive equilibrium in thin films (DET) provided a picture of the spatial distribution of different chemical species and the related environmental processes (Davison, Grime et al. 1991; Fones, Davison et al. 1998; Fones, Davison et al. 2001).

The initial use of microsensors focused on the detection of single compounds with amperometric sensors (Reimers, Fischer et al. 1986; Revsbech and Jørgensen 1986) and only with the combination of more than one sensor per casing enabled the simultaneously measurements of two or more compounds (Revsbech and Jørgensen 1986; Visscher, Beukema et al. 1991). In addition to the use of amperometric microsensors, optical fiber sensors ("opt(r)odes") and planar opt(r)odes were developed for the detection of oxygen and pH in sedimentary environments or microbial mats (Glud, Ramsing et al. 1996; Polerecky, Franke et al. 2005). Planar optrodes allow the visualization of two dimensional heterogeneities of pH and oxygen at high spatial and time resolution in the natural environment. Diffusive gradients in thin films (DGT) and DET provide similar spatial information about trace metal distribution (Davison, Grime et al. 1991; Davison and Zhang 1994). DET allows the detection of spatial trace metal distribution and DGT enables the measurement of a combination of trace metal concentration and fluxes, but unfortunately both techniques do not provide real time information (Davison, Fones et al. 2000).

In order to provide real-time information about metal distribution (including manganese and iron), and to detect several compounds simultaneously (including O_2, S^{2-}, Fe^{2+}, Mn^{2+}) voltammetric microsensors and microarrays were developed (Brendel and Luther 1995; Tercier and Buffle 1996; Belmont-Hebert, Tercier et al. 1998; Luther, Brendel et al. 1998; Luther, Glazer et al. 2001). The sensors developed by Buffle and colleagues are made of an

iridium wire plated with liquid mercury and an agarose protection membrane. These sensors are primarily used for the detection of trace metals like Cd, Cu, or Pb in water column studies of aquatic systems. Luther and co-workers constructed an amalgam gold electrode that can be used in sedimentary systems to detect dissolved manganese and iron. Both of the approaches allow the detection of metals, sulfide species, and oxygen, but the dimensions of these devices are 10 to 100 times bigger than other microsensors used in sediment and biofilm studies (i.e., a Clark microsensor for O_2 detection), and can cause perturbations of the chemical gradients and zonations in the local structure of sediments and biofilms.

In contrast to oxygen, nitrate, or sulfate, the oxidized species of iron and manganese form a variety of particulate compounds (e.g., iron and manganese (oxyhydr)oxides)) under natural pH conditions. The reactivity of this heterogeneous group of iron and manganese (oxyhydr)oxides constrains their use by microbial or chemical processes, and consequently controls small scale changes between dissolved and particulate fractions of iron and manganese.

1.2 Thesis Outline

To analyze sedimentary biogeochemical processes, techniques for measuring the dissolved and particulate compounds are required. The aim of this work was to develop sensitive techniques and miniaturized devices for in-situ and on-site trace metal detection and speciation (including iron and manganese). Furthermore, this work focuses on the complexation of trace metals in aquatic environments, and on the reactivity of the particulate fraction of iron minerals.

Is it possible to describe the reactivity of solid phase iron using Voltammetry of Microparticles and a continuum model?

To date there only a few reports (Postma 1993; Larsen and Postma 2001) using a continuum approach to describe the reactivity of synthetic and natural iron mineral suites. It was hypothesized that chronoamperometric measurements would allow the application of a reaction continuum model to describe the reactivity of the iron (oxyhydr)oxide pool in recent sediments, and additionally, the use of voltammetric measurements would enable a detailed identification of the single participating iron minerals. The results of this study are presented in chapter 4.

The development and miniaturization of microelectrodes for the investigation of dissolved iron, manganese, and other trace metal species.

Several electrochemical tools have developed for the detection of iron, manganese, and trace metals (i.e., Tercier et al.(1995) and Brendel and Luther (1995)), but the actual size of the electrode does not allow high resolution profiling. It was hypothesized that a miniaturization of microsensors would offer the option to increase the resolution of the measurements and consequently result in a better estimation of vertical fluxes of transition metals. The results of this study are presented in chapter 5.

How does the increased addition of a competitive ligand affect the complexing capacity titrations by cathodic stripping voltammetry (CSV)?

The method of choice for the determination of metal complexing ligands in natural ecosystems is a complexing capacity titration using CSV (i.e., Campos and van den Berg (1994), and van den Berg (1988)). To date nobody has analyzed the influence of steady additions of a competitive ligand, and if such a method would result in additional information to discriminate between different natural ligands of different strength in comparison to usual complexing capacity titrations. The results are presented in chapter 6.

How does iron oxide heterogeneity affect the bacterial ferric iron reduction?

Several kinetic experiments have been carried out to study the abiotic bulk reductive dissolution of iron (oxyhydr)oxides. Additionally, the importance of Fe-oxide mineralogy and surface area were studied in experiments with *Shewanella putrefaciens* strain CN32 by quantifying the initial dissolution rate. The abiotic and the microbiological studies were compared, and the results are presented in chapter 7.

The following chapters give an overview and introduction about the importance of iron, manganese, and other trace metal speciation for carbon oxidation and the importance of detecting dissolved and solid state compounds of the same element (chapter 2). Secondly, an introduction to the used voltammetric techniques will be given (chapter 3). This introductory part is followed by the presentations of the main studies of this thesis.

Chapter 2

Iron and Manganese Biogeochemistry

2.1 Introduction

Iron is the most abundant element in the Earth as a whole and iron and manganese represent the first and third most abundant transition metal in the earth's crust (8.8×10^4 ppm and 1.5×10^3 ppm, respectively) (Wedepohl 1995). Iron occurs primarily in three oxidation states, metallic iron (Fe(0)), ferrous iron (Fe(II)), and ferric iron (Fe(III)), and manganese occurs in four redox states (Mn(0), Mn(II), Mn(III), and Mn(IV)). Due to the strong adsorption capacity of solid state iron and manganese (oxyhydr)oxides, transportation, precipitation, and dissolution processes of these minerals have major environmental impacts with respect to anthropogenic pollution and biogeochemical processes (Stone and Morgan 1987; Erel, Morgan et al. 1991; Huang 1991; Waychunas, Rea et al. 1993; Cornell and Schwertmann 1996; Farrell, Huang et al. 1998; Elbaz-Poulichet, Dupuy et al. 2000; Morgan 2000).

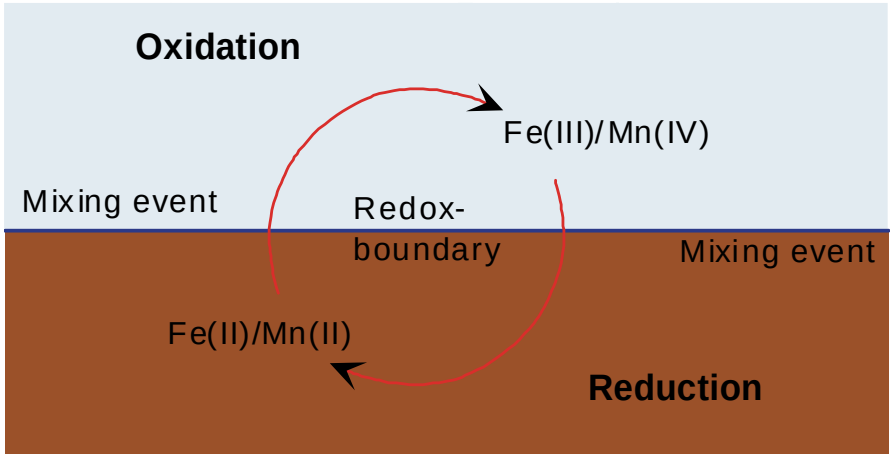

Figure 2.1 Metal cycling across a redox boundary either within the sediment or across the sediment-water interface. The term 'mixing' involves the cycling of dissolved and particulate compounds via bioturbation and bioirrigation.

Redox chemistry in natural environments strongly influences the precipitation (oxidation) and dissolution (reduction) of Fe and Mn solid phases (Figure 2.1). In natural waters at neutral pH, aqueous iron and manganese are only abundant in significant concentrations under anoxic conditions (i.e., porewater of marine sediments). Under oxic conditions iron and manganese form insoluble (oxyhydr)oxides limiting the dissolved

concentration of iron and manganese species (Dixon and Skinner 1992; Schwertmann and Fitzpatrick 1992; Stumm and Morgan 1996; Drever 1997). The interconversions among redox states and physical states, while often thermodynamically favorable, are frequently slow in the absence of a catalyst. For example, aqueous solutions of Mn(II) in the presence of O_2 at pH 8.4 are exothermic toward oxidation, yet the uncatalyzed reaction proceeds slowly (Diem and Stumm 1984). Compared to the oxidation of dissolved manganese, the oxidation rate of ferric iron with oxygen is ~10^6 faster at circumneutral pH (Martin in press). Surfaces (i.e., particles surfaces or cell surfaces), ligands (i.e., organic ligands like oxalate or cysteine), and other metal ions have different impacts of catalytic activity for iron and manganese oxidation, reduction, and mineral transformation (Cornell and Schwertmann 2003). In addition to these chemical and physical influences, microbial activity can also catalyze these oxidation and reduction processes (Banfield and Nealson 1997; Ehrlich 1998).

Iron and manganese species participate in several environmental processes, which can be classified in at least four categories:

- **Dissimilatory reactions:** In the absence of a more favorable terminal electron acceptors like oxygen or nitrate, the oxidized forms of iron and manganese in either oxyhydroxides, clay minerals, colloids or complexes are used as the terminal electron acceptor (Lovley and Phillips 1988; Lovley 1991; Nealson and Myers 1992; Kostka, Stucki et al. 1996; Canfield and Raiswell 1999; Kusel, Dorsch et al. 1999; Thamdrup 2000; Straub, Benz et al. 2001).
- **Assimilatory reactions:** In oxic natural waters and soil zones, trace amounts of iron and manganese are required for many respiratory pigments, proteins, and enzymes of prokaryotes and eukaryotes (Hudson and Morel 1989). In order to utilize these micronutrients many micro-organisms release organic ligands or siderophores (Barbeau, Rue et al. 2001; Macrellis, Trick et al. 2001), and consequently increase the bioavailability of iron and manganese (oxyhydr)oxides.
- **Chemical transformations:** In abiotic reactions iron and manganese can be dissolved by protons, ligands (i.e., oxalate and citric acid), and reductants (i.e., HS^- and ascorbate)) (i.e., Haese (2000)). Ferric iron has also the thermodynamic potential to reduce nitrate, however this reaction is not spontaneous, but can proceed with trace metals as serving catalysts (Ottley, Davison et al. 1997). In the sulfur chemistry of

marine sediments several abiotic reactions are affected by the availability of iron or manganese (oxyhydr)oxides.

- **Heavy metal cycling:** The transport and fate of heavy metals in natural waters is strongly affected by iron and manganese (oxyhydr)oxide precipitation and dissolution. Heavy metals can be adsorbed to mineral surfaces of iron and manganese minerals, or also be incorporated as impurities in iron and manganese precipitates (Dzombak and Morel 1986; Brown, Henrich et al. 1999; Ferris, Konhauser et al. 1999; Banfield, Welch et al. 2000; Ferris, Hallberg et al. 2000).

2.2 Iron and Sulfur Cycle

2.2.1 Organic Matter Degradation

Oxidation and mineralization of organic carbon involves a number of chemical, physical, and biological processes. In addition to other factors, the quality of the organic matter pool controls its degradability. The composition of the organic pool is thereby strongly dependent on the microbial degradation pathway. Organic matter in marine sediments is predominantly produced in the photic zone and the flux to the sediment is primarily controlled by the primary productivity and the water column depth. The organic carbon produced in the photic zone can either be oxidized to CO_2 in the water column or sinks to the sediment surface. After sedimentation, diagenetic reactions (physical, biological, and/or chemical reactions) further change the composition of the organic matter pool (Berner 1980).

The degradation of organic matter occurs in the oxic and in the anoxic zone of natural systems. In the oxic zone, organic carbon is oxidized completely to CO_2 using oxygen as electron acceptor. In coastal areas oxygen is typically consumed prior to complete mineralization of organic material (Canfield 1993). In the anoxic zone, which can start either in the water column (i.e., Black Sea) or below the sediment surface (i.e., coastal areas), the anaerobic degradation of organic matter involves several reaction steps. These degradation processes are usually accompanied by an increase of refractory organic compounds with depth (Middelburg 1989) due to the preferential breakdown of high energy yielding reactive organic material. Parallel to the degradation of organic matter changes in porewater chemistry can be measured, which arise from microbial respiration. This results in a vertical sequence of biogeochemical zones (Froelich, Klinkhammer et al. 1979; Santschi, Hohener et al. 1990).

After depletion of oxygen, micro-organisms utilize other electron acceptors in a consecutive sequence of respiratory processes including nitrate, manganese and iron (oxyhydr)oxides, and sulfate. In the absence of these entire electron acceptors methanogenesis will dominate (Table 1). The energy yield for the organic matter oxidation is dependant on the electron acceptor used. Due to the spatial heterogeneity of dynamic sedimentary systems (i.e., bioturbation, bioirrigation, microniches (see below)) the vertical separation is not rigid and several respiratory processes may occur concomitantly in patches at the same depth (Davison, Fones et al. 1997; Harper, Davison et al. 1997).

Table 2.1 Pathways of organic matter oxidation and their standard free energy yield $\Delta G°$ per mol C_{org} (Berner 1989).

Process	Reaction	$\Delta G°$ (kJ mol^{-1} C_{org})
Aerobic respiration	$CH_2O + O_2 \rightarrow CO_2 + H_2O$	-475
Denitrification	$5CH_2O + 4NO_3^- \rightarrow CO_2 + 2N_2 + 4HCO_3^- + 3H_2O$	-448
Mn(IV) reduction	$CH_2O + 3CO_2 + H_2O + 2MnO_2 \rightarrow 2Mn^{2+} + 4HCO_3^-$	-349
Fe(III) reduction	$CH_2O + 7CO_2 + 4Fe(OH)_3 \rightarrow 4Fe^{2+} + 8HCO_3^- + 3H_2O$	-114
Sulfate reduction	$2CH_2O + SO_4^{2-} \rightarrow H_2S + 2HCO_3^-$	-77
Methanogenesis	$CH_3COO^- + H^+ \rightarrow CH_4 + CO_2$	-58

Postma and Jakobsen (1996) used a partial equilibrium approach to explain the simultaneously occurrence of iron and sulfate reduction. In this approach, the initial fermative step is rate controlling, whereas partial equilibrium controls the sequence of the terminal electron acceptors. The stability of the iron oxides and the pH are the dominant factors regulating whether ferric iron or sulfate reduction is energetically most favorable.

2.2.2 The Role of Iron and Manganese in Organic Carbon Mineralization

In the past decades denitrification, sulfate reduction and methanogenesis have been studied extensively (i.e., Abram and Nedwel (1978), Cappenberg and Prins (1974), Martens and Berner (1974), Jørgensen (1978; 1978; 1978)). More recently it has been shown that iron and manganese (oxyhydr)oxide reduction can be important processes for biogeochemical cycles in sedimentary environments (Lovley and Phillips 1986; Lovley and Phillips 1988; Canfield, Joergensen et al. 1993; Canfield, Thamdrup et al. 1993). Bacterial dissimilatory iron reduction is used to oxidize organic matter (Hyacinthe, Anschutz et al. 2001), i.e.:

$$424\ Fe(OH)_3 + \text{Organic Matter} + 704\ CO_2 \rightarrow$$
$$424\ Fe^{2+} + 846\ HCO_3^- + 16\ NH_3 + 320\ H_2O + HPO_4^{2-} \quad 2.1$$

Iron (oxyhydr)oxides can also react with hydrogen sulfide produced during bacterial sulfate reduction to form ferrous iron and oxidized sulfur products (Pyzik and Sommer 1981; Yao and Millero 1996), i.e.:

$$8\ Fe(OH)_3 + 16\ H^+ + 8\ HS^- \rightarrow 8\ Fe^{2+} + S_8 + 24\ H_2O \quad 2.2$$

Nitrate, a dissolved potential electron acceptor for the oxidation of organic carbon, can also be biotically reduced by iron and manganese oxidation (Straub, Benz et al. 1996). In addition to the biotic oxidation of dissolved manganese by nitrate, oxygen can be involved as electron acceptor (Luther 1989). Recently, it was demonstrated that adsorbed Mn(II) on hematite (Fe_2O_3) surfaces can chemically be oxidized to Mn(III) (Junta and Hochella 1994; Madden and Hochella 2005). Such abiotic processes of manganese oxidation are typically not taken into account. The importance of manganese as electron acceptor is strongly dependent on the availability of manganese (oxyhydr)oxides in natural ecosystems. Usually dissimilatory manganese reduction is of minor importance, but there exists some natural settings, where manganese (oxyhydr)oxides are important electron acceptors, i.e. Skagerrak station S9 (Canfield, Thamdrup et al. 1993) and the Panama Basin (Aller (1990)). At these locations, manganese as electron acceptor accounts for up to 100% of organic carbon degradation. Recently, Vandienken (2005) showed similar results for a site NE of Svalbard. These high manganese reduction rates are accompanied by high bioturbation rates and low organic carbon input. Manganese (oxyhydr)oxide reduction can also be coupled to the chemical oxidation of dissolved ferrous iron (Postma 1985), mackinawite, and pyrite (Schippers and Joergensen 2001).

Like manganese, iron is involved in a variety of biogeochemical important processes, but in most marine settings, the concentration of iron is much higher than that of manganese. The importance of iron as electron acceptor for the oxidation of organic matter varies. In freshwater environments iron (oxyhydr)oxides are the most important electron acceptors (i.e., Roden and Wetzel (1996)), whereas their importance in marine systems is far more variable. Canfield et al. (1993) showed that iron reduction accounts for 78% of mineralization at Skagerrak site S4, while usually the mineralization in other typical marine sediments is dominated by sulfate reduction (i.e., Jørgensen (1982), and Thamdrup (2000)).

Iron (oxyhydr)oxides can be reduced coupled to the reoxidation of sulfide (Sorensen and Jørgensen 1987). The rate of hydrogen sulfide formation and the availability of reactive iron (see below) exert an important control on the initial "acid volatile sulfide (mostly FeS)/pyrite" ratio. The precipitation of amorphous iron sulfides (mackinawite) occurs in the presence of excess sulfide versus ferrous iron. These iron monosulfides can either be completely oxidized by manganese (oxyhydr)oxides to sulfate (Aller and Rude 1988):

$$FeS + 4\ MnO_2 + 8H^+ \rightarrow Fe^{2+} + SO_4^{2-} + 4Mn^{2+} + 4\ H_2O \qquad 2.3$$

or be oxidized by several pathways to pyrite resulting in an oxidation state of –I for the S in the S_2^{2-} moiety. This oxidation is accompanied by addition of sulfur to or loss of iron from the FeS structure. Three pathways have been reported to convert FeS to pyrite:

- Addition of sulfur with sulfur as the electron acceptor ("Polysulfide-pathway") (Berner 1970; Berner 1984):

  $$FeS + S^0 \rightarrow FeS_2 \qquad 2.4$$

- Addition of sulfur with a non sulfur electron acceptor ("H_2S-pathway") (Rickard 1997; Rickard and Luther 1997):

  $$FeS + H_2S \rightarrow FeS_2 + H_{2(g)} \qquad 2.5$$

- Loss of iron combined with an additional electron acceptor ("iron-loss-pathway") (Wilkin and Barnes 1996):

  $$2FeS + 2H^+ \rightarrow FeS_2 + Fe^{2+} + H_{2(g)} \qquad 2.6$$

The H_2S-pathway and the iron-loss-pathway are controversial. Benning et al. (2000) showed that the degree of crystal order of FeS increases in the presence of H_2S, but oxidation of FeS was not observed. It is generally accepted that the low temperature conversation of mackinawite to pyrite proceeds via greigite (Fe_3S_4). The mechanism of iron loss involving a greigite intermediate was shown by Lennie et al. (1997), but whether further iron loss is involved in the transformation to pyrite has not yet been demonstrated.

In addition to the importance for organic matter degradation pathways, the occurrence, precipitation, and dissolution of iron minerals including iron sulfides and iron (oxyhydr)oxides are important for trace metal cycling. Many trace metals, for example cadmium and lead, are adsorbed on or incorporated in sedimentary manganese or iron (oxyhydr)oxides. The dissolution of iron and manganese(oxyhydr)oxides, either by dissimilatory or chemical processes, may affect the distribution of trace metals in the anoxic environments of sedimentary settings (Zachara, Smith et al. 1992; Tessier, Fortin et al. 1996; Voigt, Brantley et al. 1996; Wang and Tessier 1999). The released trace metals can further be included in the precipitation of new minerals (i.e., sulfide minerals) (Skei, Loring et al. 1988). As a consequence, the bioavailability and the mobility of these trace metals are affected by redox transformations (Morse 1994; Morse 1994). This cycling of trace metals is an important factor controlling pollution and toxification in soils and sediments (Voigt, Brantley et al. 1996; Foster, Brown et al. 1997; Wolthers, van der Weijden et al. 2002). Iron and manganese (oxyhydr)oxides are also involved in controlling the distribution of chlorinated and aromatic organic compounds. Some dissimilatory iron and manganese reducing bacteria can gain energy by the oxidation of these hydrocarbons to CO_2 (Lovley, Baedecker et al. 1989; Lovley, Holmes et al. 2004).

Besides the influence of redox processes on manganese and iron (oxyhydr)oxides dissolution and precipitation, a major factor in controlling the biogeochemical cycling of these elements is the bioturbating activity of higher organism changing the gradients of electron acceptors.

2.2.3 Bioturbation

The dominant transport mode for dissolved species in porewater of fine grain sediments is via molecular diffusion. Because iron and manganese (oxyhydr)oxides are particulate compounds, active transport due to bioturbation greatly effects biogeochemical processes in which these compounds are involved (Figure 2.2). Aller (1980; 1984; 1990; 1994) described the effect of bioturbation on manganese reduction and consequently organic matter degradation.

Particle mixing moves solid state electron acceptors like manganese or iron (oxyhydr)oxides from the oxic to the anoxic zone of a natural system and vice versa. Bioirrigation is another process, in which the porewater gradients are changed by intrusion of overlaying oxygenated water through burrows.

Ferro (2003) showed that particle mixing strongly affects iron reduction, whereas manganese reduction is affected by both, particle mixing and irrigation. It was postulated that this is due to the differences in reduction chemistry of both metals. A ventilation of a sediment column with dissolved oxidants would result in a longer oxygen-Mn(II) contact, which would support a retainment of manganese in a sediment body, and hinder diffusion into the overlaying water column. In contrast, the oxidation kinetics of iron with dissolved oxygen is much faster and a diffusion of iron into the oxygenated water column mostly suppressed.

2.3 Iron Oxide Reactivity

The importance of iron oxide reduction for anaerobic degradation of organic matter is not only regulated by the quantity and quality of the organic matter, but the availability of other competitive electron acceptors, and also dependent on the characteristics of the iron and manganese oxide pool itself.

Sedimentary iron oxides form a heterogeneous group of minerals with different structures and reactivities. The structure and the reactivity of these iron oxides range from minerals with a low degree of crystal order (i.e., freshly precipitated iron (oxyhydr)oxides and lepidocrocite) to more ordered and nearly inert iron oxides (i.e., hematite, goethite) (Schwertmann and Murad 1983; Schwertmann 1991; Postma 1993; Sulzberger and Laubscher 1995; Larsen and Postma 2001).

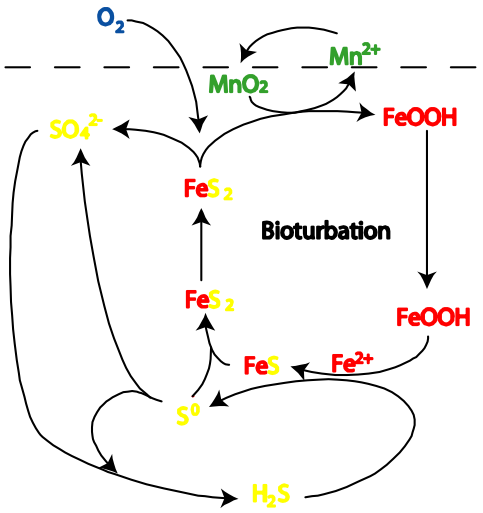

Figure 2.2 Schematic illustration of the coupled sedimentary sulfur-iron cycle (Jørgensen and Nelson, 2004).

Sedimentary iron oxides originate from two major sources. They are either allochtonous which includes input by fluvial and aeolian processes, and formation in the water column (Zachara, Kukkadapu et al. 2004), or they are autochthonously, and are formed in the sediments (Ferris, Konhauser et al. 1999; Haese 2000). The external iron oxide input, i.e., detrital iron oxides, results from settling particles. They may originate either from the adjacent land (recycled from rocks or formed during weathering), formed during riverine and marine transport (Hunter 1983; Hunter 1983), or originate from re-suspension of nearby or distal sediments (Croot and Hunter 2000). The variety of transport mechanism and sources may affect the composition of the iron oxides. These differences in mineralogy, chemical composition, grain size, and crystallinity are crucial for the reactivity of the different iron oxide fractions.

The different formation processes of iron (oxihydr)oxides in sediments result in a heterogeneous pool with minerals of different reactivity. The reaction of ferrous iron with oxygen is fast at neutral and slows down with decreasing pH (Millero, Sotolongo et al. 1987). Ottley et al. (1997) reported that the presence of catalysts, such as trace metals, stimulates the oxidation of ferrous iron with the concurrent reduction of nitrate. The interaction of manganese and iron is an important mechanism for the formation of ferric oxides (Schippers and Jørgensen 2001). Postma (1985) described that the precipitation of iron (oxyhydr)oxides has the potential to block further iron oxide precipitation. In addition to chemical pathways of ferrous iron oxidation, microbially mediated processes are also possible (Nealson 1983; Mandernack and Tebo 1993; Mandernack, Post et al. 1995; Fredrickson, Zachara et al. 1998). The ratio of pyrite iron/(pyrite iron + reactive iron) of total iron using 6N HCl as extratant has been defined by Berner (1970) as the degree of pyritization. Canfield (1989) used dithionite extractions and defined “reactive” iron as the fraction, which would react with sulfide. Canfield et al. (1992), and Raiswell and co-authors (1994; 1996) constructed a reactivity scheme for the sulfidization of iron minerals based on sulfide oxidation, Fe(III) dissolution rates, and some experimental applications. The reactivity of iron (oxyhydr)oxides towards dissolved sulfide was recently revised by Poulton et al. (2004) (Table 2.2). They demonstrated that minerals with a lower degree of crystal order react within minutes to hours, and more ordered minerals react on time scales of days to years (Table 2.2). The largest discrepancy in reactivity between the studies of Canfield et al. (1992) and Raiswell et al. (1994) on one hand and Poulton et al. (2004) on the other hand exists for the mineral magnetite (105 years to 72

days). This difference is explained by the surfaces area, which is taken into consideration by the study of Poulton et al. (2004). A further notable difference is the faster reactivity of lepidocrocite determined by Poulton et al. (2004), where they show that the reactivity time with sulfide is similar to the reduction rate of a 2-line ferrihydrite.

Table 2.2 Half-lives ($t_{1/2}$) for reductive dissolution of Fe (oxyhydr)oxides in seawater at pH 7.5 at a sulfide concentration of 1000µM.

Mineral	$t_{1/2}$ [a]	$t_{1/2}$ [b]
Freshly precipitated hydrous ferric oxide	5 min	
2-line ferrihydrite	12.3 hours	2.8 hours
Lepidocrocite	10.9 hours	< 3 days
Goethite	63 days	11.5 days
Magnetite	72 days	105 years
Hematite	182 days	< 31 days

References: a :(Poulton, Krom et al. 2004), b: (Canfield, Raiswell et al. 1992; Raiswell, Canfield et al. 1994)

In natural settings the iron and manganese (oxyhydr)oxide pool contains a mixture of fast or slower reacting minerals. This mixture with variable crystallinity, mineralogy, surface property, and size can be described as a reactive continuum (Postma 1993; Larsen and Postma 2001). Boudreau and Ruddick (1991) developed a mathematical model in order to describe such a reactive continuum for the degradation of organic matter. In their model, the pool of organic matter consists of an infinite number of varying reactive compounds, which is equivalent to the iron (oxyhydr)oxide spectrum in natural sediments. In comparison to the approach of determining a reaction constant for every possible degradation pathway, Boudreau and Ruddick (1991) describe a complex continuum with two parameters, where k is an expression for the initial reaction rate and γ is a parameter for the heterogeneity of the degradation progress with time.

Postma (1993) used the mathematical approach of Boudreau and Ruddick (1991) to describe of the dissolution of an unknown mixture of iron oxides. For kinetic modeling it is advantageously that the mathematical solution to describe the dissolution process of an unknown continuum is identical to the mathematical approach to describe the dissolution of a single compound (Christoffersen and Christoffersen 1976). Postma (1993) and Larsen and Postma (2001) have been able to determine the reductive bulk dissolution kinetics of single iron (oxyhydr)oxides and of unknown iron (oxyhydr)oxide mixtures of natural environments (Rømø, Bight of Aarhus) using an ascorbic acid extraction protocol. They showed that the reactivity decreases in the order ferrihydrite>lepidocrocite>goehtite>hematite, which is in agreement with the relative decrease in solubility. Recently, Bonneville et al. (2004) showed

that microbial reduction of iron (oxyhydr)oxides is also positively correlated to the solubility of these minerals, and they suggest that the parameter controlling the rate for abiotic and enzymatic reduction of iron (oxyhydr)oxides is the solubility. In contrast, Roden (2004, 2003) found that abiotic and microbial reduction of iron (oxyhydr)oxides differs significantly in long term experiments. The author suggests that produced Fe(II) adsorption on the mineral surface inhibits enzymatic reduction, and therefore abiotic and biotic experimental results cannot be compared. After removal of the adsorbed ferrous iron from iron oxide surface, the microbial reduction process could be reactivated. Furthermore, Roden and Zachara (1996) suggest that the oxide surface area is the controlling parameter for cell growth and Fe(II) production in soils and sediments. They showed a linear relationship between surface area and microbially reduced ferric iron. This is supported by studies of Liu et al. (2001) who reported that the microbial reduction of goethite was constrained by the surface site availability and the overall free reaction energy.

In an effort to evaluate the role of iron in biogeochemical processes, several studies attempted to quantify the different reactive mineral groups, and to differentiate between ferrous and ferric iron in natural settings. Several assays have been described in the literature since the early 1960´s (Mehra and Jackson 1960; Schwertmann 1964). Haese (2000) has provided an overview of iron mineral fractions, which can be extracted or leached by these assays reported. Recently, Poulton and Canfield (2005) reported a new extraction scheme for the separation of seven iron pools including:

- Fe_{carb}: carbonate assisted iron including siderite and ankerite
- Fe_{ox1}: easily reducible iron oxides including ferrihydrite and lepidocrocite,
- Fe_{ox2}: reducible oxides including goethite, hematite, and akaganéite
- Fe_{mag}: Magnetite
- Fe_{prs}: poorly reactive sheet silicate bound iron
- Fe_{pyr}: pyrite bound iron
- Fe_{u}: unreactive silicate bond iron

These extraction protocols include for the first time a separation method for the magnetite fraction, and for ferrous iron bound in carbonate minerals. This differentiation of seven classes of iron containing minerals shows the complexity in evaluating the significance of iron in biogeochemical processes. The reaction continuum model used to evaluate the

reactivity of the iron pool in sediments is a possibility to simplify the description of such a heterogeneous pool of iron minerals. Because these processes can be of chemical or biological nature, it is important to understand how mineral-microbe interaction takes place.

2.4 Mechanism of Microbial Fe(III) Reduction

The group of *Bacteria* and *Archaea* capable of using solid state ferric oxides as electron acceptor for dissimilative iron reduction is phylogenetically diverse. The most studied organisms belong to the *Geobacteraceae* family in the *δ-Proteobacteria* (e.g. Caccavo et al. (1994), Coates et al. (1996), Lovley and Phillips (1988)(1988), and Lovley (1987)) and *Shewannella* species in the γ subclass of the *Proteobacteria* (Caccavo (1999), DiChristina (1992), Dollhopf et al. (2000)(2000), Kostka et al. (1992), Meyers and Meyers (1994) and Nealson et al.(1995)). Because iron and manganese (oxyhydr)oxides are solid state particles, several mechanism have been proposed to transfer electrons from microorganisms to the mineral surfaces.

In the early work of Munch and Ottow (1980), it was suggested that direct contact between iron oxides and the bacteria cell is necessary to reduce particulate iron oxides. They shield iron oxides from microorganisms by a dialysis membrane, but they could not observe a production of ferrous iron. Assuming that electron transfer molecules would have the ability to pass the dialysis membrane, they concluded that direct contact is necessary for the reduction of ferric iron. By now several molecules, such as cytochromes, quinones, and dehydrogenases have been identified as part of this transfer process (Myers and Myers 1997; Myers and Myers 1998; Myers and Myers 1998; Seeliger, Cord-Ruwisch et al. 1998; Blakeney, Moulaei et al. 2000). Although a direct contact for the reduction of particulate ferric iron maybe true in special circumstances, it was shown that electron shuttles cannot inevitably pass such a dialysis membrane. Soluble shuttles, such as organic compounds with quinone moieties, can be used to transfer electrons from the bacterial cell to the mineral surface (Lovley, Coates et al. 1996), and may be extracellularly or intracellularly synthesized (Newman and Kolter 2000). Kappler et al. (2001) found that enzymatic reduction of humics and the subsequent chemical reduction of iron (oxyhydr)oxides by these reduced humic substances represent an important pathway for electron transfer in anoxic natural environments. Bacteria may dissolve minerals by producing chelating molecules, but so far, it was only conclude in a few studies that this mechanism is used in respiration. However,

Turick et al. (2002) showed that *Shewanella algae* could produce melanin, and further that melanin associated with cell surfaces can promote iron reduction (Turick, Caccavo et al. 2003). These studies clearly demonstrate that *Shewanella Algae* has the potential to use ifself-produced chelating agents.

The bacterial mechanisms used to access solid state electron acceptors are phylogenetically heterogeneous. Lower et al. (2000; 2001; 2001) used a new approach (Biological Force Microscopy, BFM) to measure the attraction forces between different bacteria and various iron and aluminum minerals. Lower et al. (in review) expand this approach by combining it with 2D-gel-electrophoresis to specify the involved proteins. With this method, it is simple to investigate different organisms and their way to access solid state electron acceptors.

Recently, Glasauer and coworkers (2002, 2004) showed that the formation of intracellular iron and manganese minerals was coupled to dissimilatory reduction. The reason for this intracellular precipitation of iron and manganese (oxyhydr)oxides is unknown, and the mechanism remains unclear. A direct role of dissimilatory metal reducing organism in transferring manganese via cellular uptake has not been considered for a long time, because the possibility of intracellular manganese precipitation was unknown.

In conclusion, the mechanisms proposed for the use of solid state electron acceptors are diverse. The mechanisms determined by laboratory studies with pure cultures cannot easily be generalized to environmental systems, where the diversity of the microorganisms controls the predominant mechanism in accessing solid state electron acceptors. The identification of the microorganisms and the detection of possible electron carrier are therefore necessary to evaluate the electron cycling of individual ecosystems

Chapter 3

Principles of Voltammetry

3.1 Introduction

Recently voltammetric studies in which the redox active components are soluble in the solution phase have reported the use of a wide range of potential waveforms (staircase, differential pulse, square wave, …) and also combinations of macroelectrodes, microelectrodes, and different forms of mass transport. At the same time studies with solids attached to electrodes surfaces have emerged a very important area of both pure and applied research. With this chapter, I will give a short overview about the applicability of electrochemistry (voltammetry) to environmental problems.

Since Faraday's pioneering studies (Table 3.1), it has been known that the transfer of electrons between a dissolved redox active species and an electrode results in interesting electrode reactions. Since the 1940s, the instrumentation was available to conduct voltammetric studies. These studies involve the measurement of a current (I) arising from a time-dependent potential change (E(t)). The recording and the interpretation of such I-E-t diagrams was mainly affected by the development of new electrodes and the introduction of personal computers. The events in the development of voltammetry are described in Table 3.1. Especially the development of computer controlled potentiostats, the introduction of square wave voltammetry, and the development of microelectrodes were most important to increase the sensitivity of voltammetric techniques.

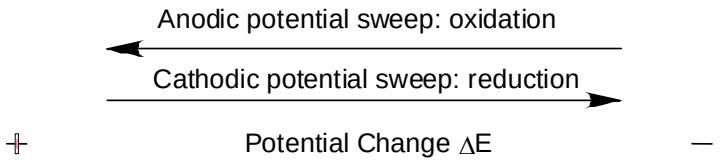

Figure 3.1 Schematic illustration about the potential variation during a voltammetric measurement.

In voltammetric studies, an applied potential is swept over a potential range and the resulting current is measured. In anodic processes the potential is swept towards more positive potentials resulting in an oxidation of the redox active compound, whereas in cathodic electrochemical processes the potential is changed towards more negative values resulting in a reduction of the redox active compound (Figure 3.1).

Table 3.1 A chronology of some important events in history of electrochemistry. Adapted from A.M. Bond (2004).

1791	L. Galvani published his results on electrical experiments with frogs. De Bononiensi Scietiarum et Artium Instituto atque Academia Commentarii VII (1791) 363.
1800	A. Volta communicated the construction of his electrochemical pile (voltaic battery) in a letter to Sir Joseph Banks. Philos. Trans. 90 (1800) 403. W. Nicholson and A. Carlisle used Volta's pile to demonstrate electrolytic conduction (electrolysis). Nicholson's Journal 4 (1800) 179. W. Cruikshanks published the first qualitative analysis (copper) performed with the aid of electrolysis. Nicholson's Journal 4 (1800) 187.
1807	H. Davy published his theory of electrolysis. Philos. Trans. 97 (1807) 1.
1812-19	J.J. Berzelius published his electrochemical theory and developed the concept of the electrochemical series. Journal für Chemie und Physik 6 (1812) 119, Essai sur la Théorie des Proportions Chimiques et sur l´Influence Chimique de Électricité, Paris 1819.
1826	G.S. Ohm published his law. Schweiger´s Journal 46 (1826) 137.
1832-34	M. Faraday published numerous observations based on data obtained from electrochemical experiments, and introduced modern electrochemical nomenclature (i.e., ion, anion, cation, electrolyte, electrode) Philos. Trans. (1832-34).
1839	W.R. described the first practical fuel cell. Philos. Mag. 14 (1839) 127. E. Becquerel reported the photovoltaic effect. Compt. Rend. Acad. Sci. 9 (1839) 561.
1860	R. L. G. Planté demonstrated the operation of the lead-acid battery. Compt. Rend. Acad. Sci. 50 (1860) 640.
1864	W. Gibbs published the first electrogravimetric analysis. Fresenius´ Z. Anal. Chem. 3 (1864) 334.
1889	W. Nernst published his fundamental equation, which relates the potential to ion activities in his dissertation. Die elektromotorische Wirksamkeit der Jonen, Leipzig 1989.
1903	F.G. Cottrell published the "Cottrell"-equation. Z. phys. Chem. 42 (1903) 385. B. Kučera introduced the dropping mercury electrode for electrocapillary studies. Ann. Phy. 11 (1903) 529.
1922	J. Heyrovský used a dropping mercury electrode to introduce the technique of polarography. Chem. Listy 16 (1922) 256, Philos. Mag. J. Sci. 45 (1923) 303.
1934	D. Ilkovic published the "Ilkovic"-equation. Coll. Czech. Chem. Comm. 6 (1934) 498
1940	I. M. Kolthoff and Laitinen H. A. introduce the technique of voltammetry. Science 92 (1940) 152.
1948	J. E. B. Randles and A. Sevčik independently described the technique of cyclic voltammetry. Trans. Faraday Soc. 44 (1948) 327, Coll. Czech. Chem. Comm. 13 (1948) 349.
1952	G. C. Barker and I. L. Jenkins introduced square wave techniques. Analyst 77 (1952) 685.
1953	T. Berzins and P. Delahay developed a hanging mercury drop electrode (HMDE). J. Am. Chem. Soc. 75 (1953) 5716.
1960	G.C. Barker and A. W. Gardner developed pulse techniques Anal. Chem. 173 (1960) 79.
1962	A. Y. Gohkstein and Y. P. Gohkstein described a static mercury drop electrode (SMDE). Zh. Fizicheskoi Khimii 36 (1962) 651.
1980´s	The research group developed square wave voltammetry allowing lower detection limits. Odea J. J., Osteryoung J., and Osteryoung R. A., Anal. Chem. 53 (1981) 695. The development of microelectrodes was introduced by several groups. Wightman R. M. Anal. Chem. 53 (1981) 1125A, and Fleischmann et al. J. Electroanal. Chem. 177 (1984) 179.

The important components of a voltammetric cell are a working electrode (WE), a reference electrode (RE), and an auxiliary (counter) electrode (CE) (Figure 3.2). These three electrodes are inserted in an electrolyte and placed in close proximity. Especially the small distance of the reference to the working electrode is important to minimize contributions of an ohmic drop during the measurement. The voltammetric study is concentrated on the electron transfer reactions (redox reactions) at the working electrode, while the reactions at the counter and reference electrode are not studied. The three electrodes are connected to a potentiostat, which regulates the current flow between the working electrode and the counter electrode and drives the potential between the working electrode and the reference electrode. Hence, the potentiostatted circuitry reduces the effect of ohmic drop by decoupling the current circuit form the potential circuit.

The following chapters describe the necessity for a three-electrode assembly, and the demands for the electrochemical tools used in this project.

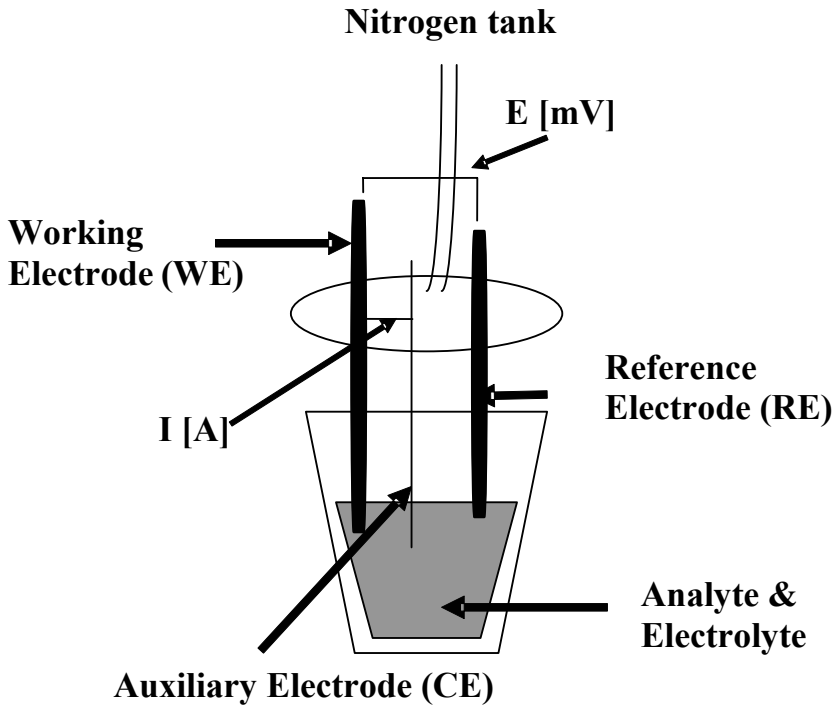

Figure 3.2 Illustration of a voltammetric cell with major components: working electrode, reference electrode, auxiliary electrode (counter electrode).

3.2 Theory

Voltammetry describes the current-potential relationship in an electrochemical environment. In particular, voltammetry describes this relationship as a function of time and controlled electrode potential. If a potential is stepped to or held at a value at which a faradaic process takes place at an electrode in an electrolyte, the resulting current at this special potential can be used to identify and to quantify the concentration of the species undergoing the electrode process. Figure 3.3 shows the results of an anodic oxidation (stripping) of lead and cadmium after preconcentration of these ions at a mercury microelectrode. The peak potential is characteristic for a special oxidized or reduced species. The current is the rate, at which a charge passes through the electrode-solution interface. A current arising from a faradaic process is a direct measure of the rate of the process, and if the rate is proportional to the concentration, it is also a measure of the concentration of the species undergoing the electrode process (Buffle and Tercier-Waeber 2000; Bard and Faulkner 2001).

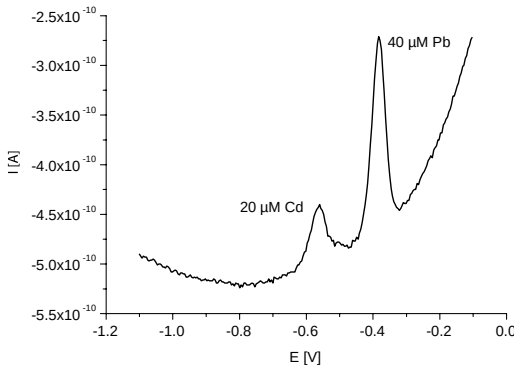

Figure 3.3 Results of Square Wave Stripping Voltammetry (SWV) of cadmium and lead in 0.1 M $NaNO_3$ and 0.01 M HEPES. Conditioning potential: 0.1 V; conditioning time: 60 s, deposition potential: -1.1 V; deposition time: 60 s; equilibration time: 5 s; initial potential: -1.1 V, final potential: -0.1 V; frequency: 50 Hz; step potential: 4 mV; amplitude: 25 mV.

At the interface of any electrode immersed in an electrolyte solution, a specific interfacial electrical double layer is formed. This electrical double layer arises from a potential difference between an immersed electrode and the surrounding solution. In a simplified way this layer can be described as a capacitor, which includes a charged plane on the electrode surface and a layer of oppositely charge ions on the solution side (Stojek 2002). A change of the potential difference in this electrical double layer will create a so-called

capacitive current (charging current), which does not involve any charge transfer. If no electrochemical treatment were made, the measured current of a reduction or oxidation process at an electrode would be a composite of a capacitive and a faradaic fraction. As only the faradaic current is specific for the reaction, electronic modulations have been developed to decrease or eliminate the capacitive fraction of the composite current signal, and to improve consequently the analytical signal.

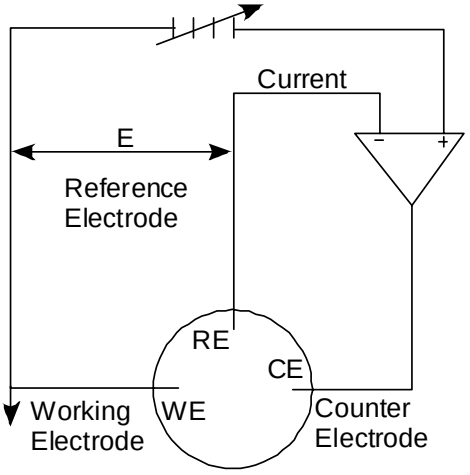

Figure 3.4 Schematic drawing of the electronic circuit of a potentiostat and about a voltammetric electrode arrangement. E: imposed potential, RE: reference electrode, CE: counter electrode, WE: working electrode. Modified after Buffle and Tercier-Waeber (Buffle and Tercier-Waeber 2000).

As the resulting current of a reduction or oxidation process is a function of the exact applied potential, a voltammetric circuit has to be constructed using a three-electrode array, which avoids effects of a charge transfer process to the applied potential. Therefore, a voltammetric cell contains three electrodes: a working electrode (WE), a reference electrode (RE) and a counter electrode (CE) (Figure 3.4). In such a voltammetric cell, a potential difference E is imposed between WE and RE, and the resulting current I is simultaneously measured between the working and the counter electrode. The electronic circuit in the potentiostat is constructed in such a way that the absolute potential of RE remains constant, independent of a flowing current I (Buffle and Tercier-Waeber 2000). Any applied potential change is directly passed to the working electrode.

This electronic circuit and the electrode array allow precise detection and identification of an electrochemical redox process. The polarization range of the working electrode limits the detection window, in which redox active species can be measured. The polarization range of a working electrode is defined by the oxidation of the electrode material (positive limit), and the production of hydrogen gas at the negative potential limit of the electrode. For the detection of ferrous iron ($E°= -1.47$ V) and dissolved manganese ($E°=-1.51$ V) a high overpotential of the working electrode is necessary, because otherwise the reduction to metal iron and manganese would be mask by a hydrogen wave. Therefore, the most used electrode material for such applications is mercury. To improve the sensitivity and to lower the detection limit, other modifications have been established and are described in the following chapters.

3.3 Stripping Voltammetry

3.3.1 Preconcentration Step

Stripping analysis requires the preconcentration (Figure 3.5) of the analyte from the sample solution onto (adsorptive) or into (amalgamation with Hg) the working electrode. The most common preconcentration step involves the deposition of the analyte into the mercury electrode. The deposition step is carried out by employing a controlled potential electrolysis for a defined time under reproducible hydrodynamic (mass-transport) conditions. Mass transport of the analyte to the electrode occurs by stirring the solution or rotating the electrode (Bard and Faulkner 2001). The reactions of the metals deposited into the working electrode (mercury is a common electrode material for stripping analysis) is given as followed:

$$M^{n+}_{(aq)} + ne^- \rightarrow M(Hg) \qquad 3.1$$

In contrast, the reaction for the deposition of metals on solid electrodes is given by:

$$M^{n+}_{(aq)} + ne^- \rightarrow M_{(s)} \qquad 3.2$$

The deposition time has to be controlled very carefully, as this will influence the amount of analyte preconcentrated into the electrode. Thus, a longer deposition time would result in a larger amount of analyte being available for the stripping step, and hence the voltammetric signal will increase. The deposition time varies between some seconds and minutes depending on the concentration of the analyte and the reversibility of the redox process. Thus, the extent of amalgamation of the preconcentrated metal on the mercury electrode depends on the metal's solubility in mercury (Galus 1984).

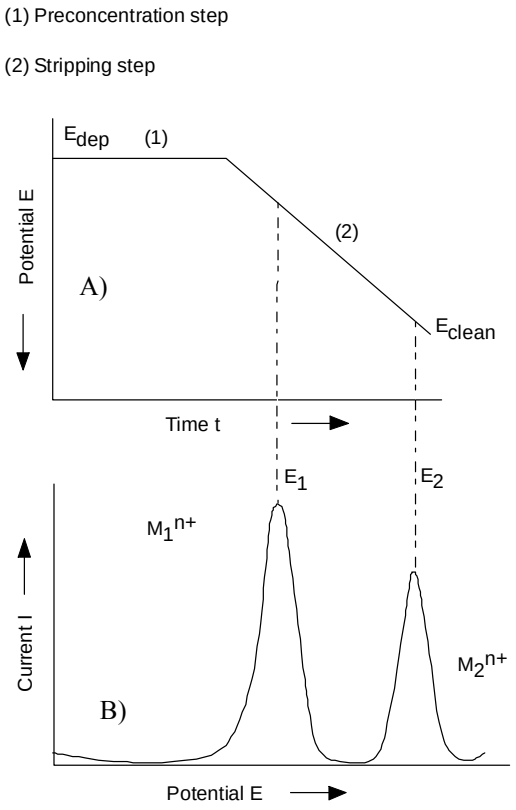

Figure 3.5 Principle of anodic stripping voltammetry. A): (1) indicates the deposition step, and (2) indicates the stripping step. B) resulting voltammogram of two analyzed metal ions M_1^{n+} and M_2^{n+}. Inversion of the potential to lower values results in a cathodic stripping process.

The main advantage of stripping voltammetry is that low analyte concentration can be compensated by increased deposition time. This advantage is dependent on the solubility of the redox active compound in mercury. The solubilities for some metals are given in Table 3.2.

Table 3.2 Solubility of some metals in mercury.

Element	Solubility in Hg (atomic %)
Cd	10
Zn	5.83
Ti	4.3
Pd	1.3
Au	0.133
Pt	0.1
Cu	0.007
Mn	0.007
Fe	No
Ir	No

Reproduced from: Stojek, Z., Stepnik, B., Kulik Z., J. Electroanal. Chem., **74 (**1976) 277.

Exceeding the solubility of the elements in mercury can have a detrimental effect on the subsequent stripping step (Galus 1975). When the solubility is exceeded, a crystalline phase of pure metal can be adsorbed on the mercury drop surface or enriched in the mercury droplet. In these cases the surface of the electrode is changed, and is no longer uniform. Such processes affect the stripping step of a voltammetric measurement, and for nonrenewable electrodes is this of particular importantance. In a subsequent measurement, the preconcentration step would be affected, and a quantification of a compound is negatively influenced (Galus 1975).

In general, good results are obtained with stripping voltammetry, when metal-mercury solubilities are not exceeded (Ostapczuk and Kublik 1978). In case of irreversible and quasi-irreversible redox reactions like Fe^{2+}/Fe^{0} and Mn^{2+}/Mn^{0}, a deposition step during the voltammetric measurement has to be avoided, or at best, for quasi-irreversible reactions such deposition step has to be in the range of seconds (Galus 1975; Tercier-Waeber, Belmont-Hebert et al. 1998; Buffle and Tercier-Waeber 2000).

3.3.2 Equilibration Period

The concentration of the metal deposited into the mercury electrode increases parabolically towards the surface of the mercury droplet for short deposition times (Shain and Lewinson 1961; Devries and Vandalen 1964). The concentration within the mercury becomes uniform if longer deposition periods are applied or thinner mercury films are used. To obtain a uniform distribution of the metals in the mercury film, a rest period has to be employed at the end of the preconcentration step and before the stripping step (Figure 3.5) (Bard and Faulkner 2001).

3.3.3 Stripping Step

In the stripping step, the material is redissolved ("stripped") from the electrode using some voltammetric technique. This involves the application of a positive (anodic) potential scan for anodic stripping voltammetry (ASV) – *reoxidation* - and a cathodic potential scan for cathodic stripping voltammetry (CSV) - *reduction*. In the case of ASV, the scan proceeds linearly towards more positive potentials, or may involve the superimposition of more complex potential-time waveforms (Bard and Faulkner 2001). Once a potential, close to the standard potential of a metal/metal-ion redox couple is reached, the reoxidation of the metal-amalgam proceeds and the reoxidized metal-ion is released into the solution:

$$M(Hg) \rightarrow M^{n+} + Hg + ne^{-}. \qquad 3.3$$

The resulting potential-current stripping voltammogram is illustrated in Figure 3.5. Under reproducible deposition conditions, the peak current (i_p) is proportional to the metal ion concentration in solution and the metal species is identified by the peak potential E_{peak}.

3.3.4 Potential-Time Waveforms

The deposition step is usually the same for all stripping techniques. The main difference consists in the potential modulation of the stripping step. The optimization of the electrochemical response (analytical and background currents) is depending on different parameters, which describe the potential modulation during the anodic or cathodic scan. The following sections describe and discuss the different possibilities of a potential modulation,

beginning with the classical case of linear modulation, and is followed by a short description of more advanced voltammetric modulation techniques (Bard and Faulkner 2001).

3.3.4.1 Linear Scan (Sweep) Modulation

In 1948, Randles published the first theoretical considerations of reversible processes for linear potential (sweep) voltammetry (Randles 1948). In linear scan voltammetry (LSV) the electrode, potential is varied linearly with time (Figure 3.6A). A limiting factor for the use of linear scan voltammetry is a particular high current at high polarization rates. This current is the result of the electrode double layer charging, which produces high capacitive currents (Loveland and Elving 1952). A more advanced modulation of the potential sweep reduces the capacitive currents and increases the resolution of the measurements.

3.3.4.2 Pulse Modulations

Differential Pulse Voltammetry

Differential pulse voltammetry (DPV) is the most widely used potential modulation (Galus 1975), which was designed to overcome capacitive background current problems (Figure 3.6C) (Rifkin and Evans 1976). In the differential pulse mode, positive (anodic) or negative (cathodic) scans are superimposed by pulses of equal potential amplitude. Each pulse is determined by its pulse width t_p and height ΔE_p as shown in Figure 3.6C. Applying a differential pulse mode, the total current in the system was found to increase (Galus 1975). This is due to the resulting increase in Faradaic and capacitive currents. The capacitive (charging) current decays more rapidly than does the Faradaic current, the Faradaic current is therefore more predominant at the end of each pulse cycle. The current is consequently sampled at the end of each pulse cycle. This technique provide a high discrimination towards charging currents and consequently, the signal-to-background response is improved (see section 1.2.2) (Galus 1975; Osteryoung, Christie et al. 1975; Osteryoung, Christie et al. 1979; Bard and Faulkner 2001).

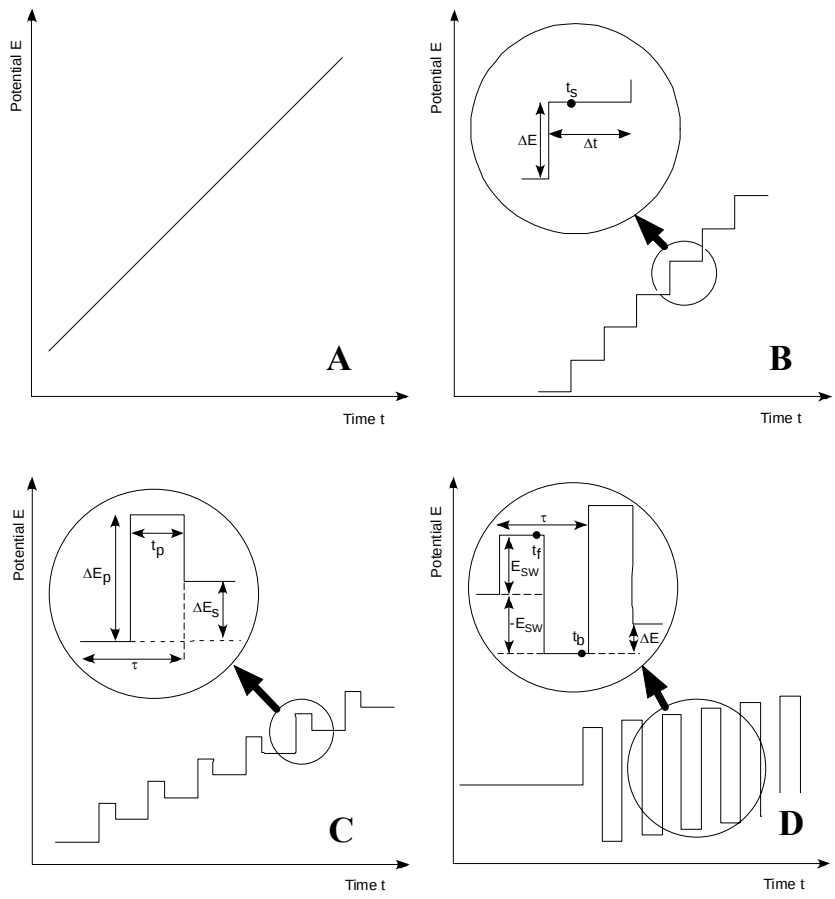

Figure 3.6 Schematic potential time diagrams of different voltammetric potential modulations: A): Linear modulation - B): Staircase modulation: t_s: sampling time, Δt: pulse (step) width, ΔE: pulse (step) height – C) Differential pulse modulation: ΔE_s: step potential, ΔE_p: pulse height, τ: pulse period, t_p: pulse width – D) Square Wave modulation: ΔE: step potential, t_f, t_b: forward and backward sampling time, E_{SW}, $-E_{SW}$: forward and backward square wave amplitude, τ: wave period

Staircase Voltammetry

Staircase voltammetry is another approach used to reduce charging currents (Barker and Gardner 1960). In this modulation, the potential variation is done by applying potential steps of distinct amplitude using a measurement dependent frequency. A schematic diagram of the staircase potential-time modulation is shown in Figure 3.6B. The capacitive (charging)

current is largely eliminated from the measured signal because the current is measured near the end of each incremental potential step, where the charging current was found to be very small (Barker and Gardner 1960). This mode is very useful for the detection of low concentrated compounds, where charging current interference may be quite significant.

Square Wave Voltammetry

Square wave voltammetry (SWV) is similar to staircase and differential pulse voltammetry, which discriminate against charging currents. Using this modulation the current is measured at the end of the forward step, and at the end of the backward step. The subtraction of these signals improves sensitivity by extensive removal of the capacitive current, due to current sampling just before a new square wave polarization. The potential-time waveform and the current sampling positions (indicated by t_f (forward) and t_b (backward)) are shown in Figure 3.6D.

The square waveform is a combination of a large amplitude square-wave modulation and a staircase ramp. The square wave is a variation of the differential pulse wave, and is sometimes called Osteryoung´s square wave (Osteryoung and Odea 1986; Barker and Jenkins 1992; Bond 1994). To allow rapid decay of the charging current the square wave techniques requires solutions of high supporting electrolyte content. Square wave voltammetry is the most sensitive modulation technique and allows the measurement at low analyte concentrations.

3.4 Voltammetric Applications

3.4.1 Cathodic Stripping Voltammetry (CSV)

It is well known that organic complexation dominates the chemical speciation of trace metals in natural waters. It has been assumed that these ligands are soluble molecules that serve to maintain free metal ion activities within the physiological tolerance range for microorganisms, as well the scavenging loss of bioactive metals to sinking particles in natural waters. Therefore, the complexation controls the residence time of trace metals in their natural environment. Hence, it is important to determine the complexed fraction of metals in addition to their dissolved concentration in natural waters.

Recently, the new technique of cathodic stripping voltammetry (CSV) has been developed for analytes like copper, zinc, nickel, and cobalt (Campos and Van den Berg 1994; Van den Berg 1995; Colombo and Van den Berg 1998; Lam, Murimboh et al. 1999) that cannot be preconcentrated onto or into electrodes by electrolysis, or where the sensitivity of anodic stripping voltammetry is limited (Van den Berg 1984).

Cathodic stripping voltammetry with competitive ligand equilibration (CSV-CLE) has two major advantages. First, any oxidation state of an electroactive compound can be controlled in the stability range of the electrode between mercury oxidation and hydrogen evolution. The second advantage is that the adsorbed material is collected as monomolecular layer on the electrode surface, so that all material is instantaneously accessible to the stripping process. Accordingly, the reduction current of the stripping step is independent of diffusion of the reactive species and very fast potential scanning techniques can be employed producing larger currents. This kind of voltammetric technique is usually carried out with hanging drop mercury electrodes to provide clean and renewable electrode surfaces for each measuring step. This chapter will explain the background for cathodic stripping voltammetry with competitive ligand equilibration.

3.4.1.1 Hanging Mercury Drop Electrode

Traditionally a mercury electrode consists of a mercury drop that is periodically created and dispatched at the tip of a glass capillary. This electrode is immersed in a solution during the measurement. A reservoir feeds the capillary with the required amount of mercury, and controls thereby the mercury flow. The controlling mechanism can performed either mechanically or electronically. Controlling the flow of the mercury through the capillary can regulate the drop time within a wide range. A manual decoupling of the mercury drop from the mercury reservoir leads to a stable mercury drop within the used measuring time. Such a device is called hanging drop mercury electrode (HMDE). If the decoupling is controlled electronically, the device is called a static mercury drop electrode (SDME). Both controlling systems guarantee a constant drop size during each measurement step. After each step, the mercury drop is mechanically knocked off, and a new one is created. The main advantage of such an electrode device is the easily renewable electrode surface. This leads to a clean mercury surface for each measuring step, which is isotropic with respect to its physicochemical properties. A disadvantage of such a device is the size of the electrode. The

in-situ use of such an electrode is however not possible because renewal of the mercury drop would lead to contamination of the environment (Bard and Faulkner 2001).

3.4.1.2 Cathodic Adsorptive Preconcentration and Stripping

In cathodic adsorptive stripping voltammetry (AdSV) the analyte is reduced during the stripping step, instead of oxidized as in anodic stripping voltammetry (ASV). The preconcentration step typically involves adsorption of the analyte after complexation with a specific complexing ligand, causing the formation of a complex with adsorptive properties:

$$ML_n + AL \rightarrow L_n + MAL \quad 3.4$$

$$MAL_{(aq)} \rightarrow MAL_{(ads)}. \quad 3.5$$

Equation 3.4 describes the addition of the chelating ligand (AL) to a Metal (M) complexed by a natural ligand (L_n) to form an absorbable metal chelate (MAL) complex. Equations 3.4 and 3.5 describe the preconcentration of a metal chelate onto an electrode surface. Several ligands are available for the preconcentration step including salicylaldoxime, 8-hydroquilonine, catechol, pyrrolidine, dithiocarbamate, and others. About twenty elements can be detected by this technique (Bruland, Donat et al. 1991; Van den Berg 1991; Boussemart, Vandenberg et al. 1992; Campos and Vandenberg 1994; Donat, Lao et al. 1994; Gledhill and Vandenberg 1994; Gerringa, Herman et al. 1995; Rue and Bruland 1995; Van den Berg 1995; Le Gall and Van Den Berg 1998; Lam, Murimboh et al. 1999; Witter, Lewis et al. 2000; Laglera and van den Berg 2003).

The addition of chelating ligands results in a competition between the complexing ability of the added chelating ligand AL and the natural ligands L_n. This addition results in a shift of the equilibrium of the original speciation, and the increased formation of a complex of the metal with the added ligand AL. The magnitude of this alteration can be varied by changing the concentration of AL, or by selecting ligands forming more or less stable complexes. The labile metal concentration in CSV therefore equals all metal bound by the added ligand, and the fraction of the total metal that is labile depends on the relative stabilities of the complexes. In the stripping step, which can be done by pulse or linear voltammetric techniques, the metal chelate (MAL) is removed from the electrode by reductive stripping:

$$MAL_{n(ads)} + ne^- \rightarrow M^0 + nAL^-. \quad 3.6$$

The reduction of the metal is preferable to ligand reduction because the reduction peak potential is more specific to the redox process of metal, and interferences by other metals are minimized. Furthermore, a reduction of the added ligand also tends to reduce the sensitivity. However, in the case of metal species with a very negative redox potential close to that of hydrogen evolution, a reduction of the ligand is preferred. The total metal concentration is measured by pretreating the sample with UV irradiation, and then analyzing it as described above. The mathematical description of the resulting voltammetric signals in relation of metal additions and added ligand equilibration have been developed by Ruzic and van den Berg (Ruzic 1982; Ruzic and Nikolic 1982; Vandenberg 1982; Gerringa, Herman et al. 1995).

3.4.2 In-Situ Application of Voltammetric Microelectrodes

The development of microelectrodes in voltammetry has extended the scope of electroanalytical measurements. Until the end of the 1970s, the majority of the working electrodes employed in electroanalytical chemistry were based on a mercury drop or solid electrodes of silver, gold, platinum, or carbon with millimeter sized dimensions. During the last decades, the application of miniaturized working electrodes has substantially increased. In the early 1980's Wightman and Fleischmann and their coworkers developed the theoretical background for microsensor applications (Ewing, Withnell et al. 1981; Wightman and 1981; Bond, Fleischmann et al. 1984; Bond, Fleischmann et al. 1984; Fleischmann, Lasserre et al. 1984; Howell and Wightman 1984; Deakin, Wipf et al. 1986; Wightman and Wipf 1989).

The geometries of such electrodes are quite diverse: There are spheres, hemispheres, disks, cylinders, bands, rings, and electrodes containing many microelectrodes very close together in arrays (Bixler, Fifield et al. 1989; Heinze 1993; Tallman 1994; Buffle and Tercier-Waeber 2000). The materials mainly used for manufacturing microelectrodes are gold (Bond, Henderson et al. 1986; Brendel and Luther III 1995), platinum (Daniele, Baldo et al. 2002; Daniele, Bragato et al. 2002), carbon fibers (Zhang and Ogorevc 1998), silver (Ciszkowska, Donten et al. 1994; Pizeta, Billon et al. 2003), copper (Bond, Brainina et al. 1994), mercury (Tercier, Parthasarathy et al. 1995; Belmont, Tercier et al. 1996), and iridium (Kounaves and Deng 1991; Kounaves and Deng 1993; Tercier, Parthasarathy et al. 1995; Belmont, Tercier et al. 1996; Belmont-Hebert, Tercier et al. 1998). The most favorable electrode material is plated

on substrates of micrometer size either as liquid film (iridium, carbon) (Tercier, Parthasarathy et al. 1995; Tercier and Buffle 1996; Tercier-Waeber, Belmont-Hebert et al. 1998; Tercier-Waeber, Pei et al. 2000), or as amalgam wit the electrode substrate (gold, silver, platinum) (Brendel and Luther 1995; Luther, Brendel et al. 1998).

Microelectrodes are defined by the ratio between the electrode diameter (r) and the diffusion layer thickness (δ) around the electrode: $1/r \rangle\rangle 1/\delta$. Under such geometric conditions the current (I) is independent of both time and stirring conditions. Typically, $r \leq 10$ µm corresponds to micro-behavior, while macroelectrodes have usually an electrode radius (r) larger than 100 µm. The redox signal of such macroelectrodes is dependent on time and the hydrodynamic conditions

$$\delta = \sqrt{\pi \overline{D} t} \qquad 3.7$$

where $\overline{D}$ is the average diffusion coefficient and t the time.

The major difference between micro- and macroelectrodes is that the dimension of a macroelectrode is larger than the diffusion layer thickness, so that linear diffusion can be considered as transport mechanism independent on the geometry of the electrode. On the contrary at microelectrodes occurs spherical or semi-spherical diffusion.

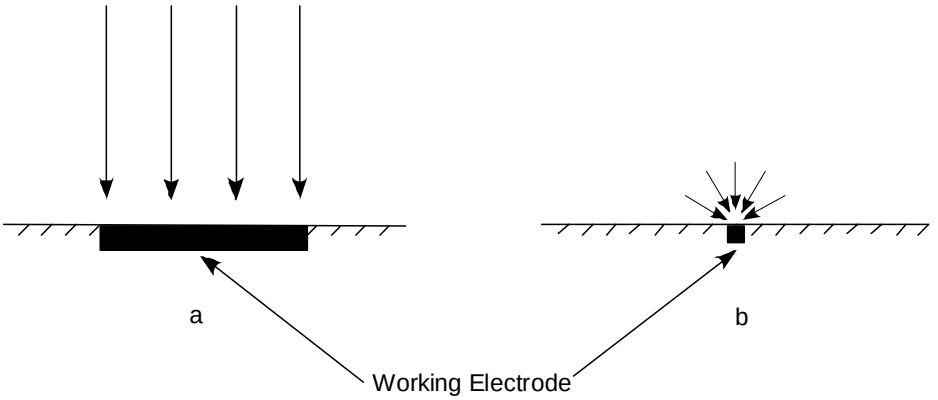

Figure 3.7 Schematic drawing of the diffusion conditions: a) macroelectrode: linear diffusion, b) microelectrode: spherical diffusion

The presence of spherical diffusion around a microelectrode improves the signal to noise ratio. For a microdisk electrode, the thickness of the diffusion layer (δ) can be estimated from equation 3.8 and 3.9:

$$\delta = \left(\frac{\pi}{4}\right) r \qquad 3.8$$

$$i = 4nFDCr \qquad 3.9$$

where r is the radius of the disk, F the faraday constant, D the diffusion coefficient, and C the concentration of the analyte. As in Figure 3.7b indicated, the shape of the diffusion layer will be spherical, because a microelectrode acts as a point like electrode. This is especially true for electrodes smaller than 1 µm. In comparison, the diffusion layer at a macroelectrode is planar due to linear diffusion (Figure 3.7a).

Due to spherical diffusion the transport of analyte to a microelectrode surface is increased, which yields a higher current per unit area (i.e. current density), and therefore a higher signal to noise ratio. The steady state diffusion limited current for a disk microelectrode is given by equation 3.9. The development time to establish a complete diffusion layer decreases with electrode size. Reducing the electrode size enables therefore fast electroanalytical measurements (Bond 1994; Buffle and Horvai 2000; Buffle and Tercier-Waeber 2000).

For in-situ application where the convection around the electrode cannot be controlled, the diffusion layer thickness may vary with time, and this variation would influence the results of the measurements by macroelectrodes. The flux of the analyte to the electrode should be time independent during the preconcentration step of voltammetric stripping analysis. This cannot be ensured using macroelectrodes. Therefore, microelectrodes are better suited for in-situ application. The advantages of microelectrodes can be summarized as follows:

- *Higher sensitivity*: higher signal to noise ratio (lower background currents)
- *Higher spatial resolution*: the small dimension of the electrode and its glass body decreases the perturbation of sediments or microbial mats
- *Easier discrimination between analyte bound to mobile ligands and colloids:* analyte transport is only dependent on molecular diffusion and independent on the convection in the surrounding environment

- *Reduced ohmic drop:* microsensors allow measurements in low ionic strength waters (Bond, Fleischmann et al. 1984; Bond, Fleischmann et al. 1984; Bond, Fleischmann et al. 1984; Bond, Henderson et al. 1986). A data distortion caused by a drop in *IR,* where *R* is the resistance of the solution, is avoided, because the resulting current of a measurement is in the range of pA or nA. For macroelectrodes, an electronic compensation is necessary to remove the influence of an *IR* drop. However, a complete compensation is not possible
- *Independence of time and stirring conditions:* the curvature radius of spherical or semi-spherical microelectrodes is smaller than the diffusion layer thickness; therefore, microelectrodes are independent on time and stirring conditions

The electrode material has to be chosen with regard to the redox potentials of the test compounds. The polarization range of the electrode material is limited by the reduction potential of water at the electrode surface, and by the oxidation potential of the electrode material itself. Platinum, gold, iridium, and carbon are most suitable materials for electrode reactions with a positive reaction potential, whereas mercury is the best material for reactions occurring at negative redox potentials. For in-situ measurements of iron, manganese, and trace metals in natural waters, mercury is the electrode material of choice. Special demands have to be fulfilled for the mercury carrier substrate:

- No or very low solubility of the substrate with mercury to avoid formation of an amalgam
- Formation of intermetallic compounds of the carrier substrate and the analyzed test compound should be excluded
- High stability of the mercury adhesion on the electrode substrate

Iridium is the substrate of choice for mercury microelectrodes, because the surface tension and the Hg-Ir cohesion forces are such that the stability of a hemispherical mercury cap formed on microsized iridium discs is optimal. Such electrodes are stable in open circuit and can be transferred and rinsed with water easily without affection of the electrode surface. The solubility of iridium in mercury is much smaller than 10^{-4} w% (Buffle and Horvai 2000; Buffle and Tercier-Waeber 2000; Bard and Faulkner 2001). Beside iridium substrates, gold and silver are also useful electrode materials. The formation of an amalgam with the plated

mercury may lead to a reduced stability in comparison with iridium based electrodes. The advantage of such amalgam electrodes is the solid nature of such devices. Therefore, the handling in sedimentary setting is easier.

3.4.3 Electrochemical Studies of Solid Compounds

3.4.2.1 Voltammetry of Microparticles

Traditionally, analytical electrochemistry is associated with studies of dissolved species in solutions. Recently, a new technique has been developed to analyze solid state particles as well: Voltammetry of Immobilized Microparticles (VIM) or Abrasive Stripping Voltammetry (Scholz, Nitschke et al. 1989; Scholz, Nitschke et al. 1989; Scholz, Nitschke et al. 1989; Scholz, Nitschke et al. 1989; Komorsky-Lovric and Scholz 1998; Scholz and Meyer 1998; Grygar, Bezdicka et al. 1999; Komorsky-Lovric, Mirceski et al. 1999; Schroder, Oldham et al. 2000).

Especially in the field of environmental science, information about solid state particles is necessary to understand the biogeochemical cycles. Figure 2.1 shows that solid particles are major sinks, and sources of the iron-sulfur cycle, i.e., pyrite and goethite. The change of the valence state during the oxidation and reduction processes is accompanied with precipitation and dissolution reactions, thus different iron (oxyhydr)oxides, like ferrihydrite, lepidocrocite, goethite, and hematite, play a major role in the carbon cycle. VIM offers the opportunity to detect, and to distinguish between the different iron (oxyhydr)oxides and other solid state particles in environmental samples. This technique allows also the kinetic description of the bulk dissolution of a sample.

There are only two requirements for the compounds and the materials to be used by VIM: they should be insoluble in the electrolyte solution, and it must be possible to reduce or oxidize the compounds at an available potential window. The whole electrochemical solid state characterization is done by a paraffin-impregnated graphite electrode (PIGE), but other electrodes could also have a potential for VIM:

- Electrodes made of highly orientated pyrolytic graphite (HOPG)
- Pencil mine electrodes
- Metal electrodes

In order to re-use the electrodes, the electrode surface has to be mechanically cleaned after each measurement.

3.4.4.2 Paraffin-Impregnated Graphite Electrode (PIGE)

Paraffin-impregnated graphite electrodes (PIGE) (Figure 3.7) are made from porous spectral quality graphite rods. The material is usually used in spark analysis. The typical size of such rods for VIM experiments is 50 mm long and 5 mm in diameter. In untreated condition, these graphite rods are microporous. The porosity would lead to high background currents in electrochemical analysis. This would result in the constant penetration of electrolyte into the graphite electrode and lead to contamination of the electrode body. It can be avoided by impregnation of the graphite body with solid paraffin, which chemical is rather stable. Impregnation is done by immersing the graphite body in molten paraffin in a closed vessel in a water bath. The whole vessel is then evacuated until no more gas bubbles evolve from the graphite rod. After impregnation, the warm electrodes are placed on filter paper and allowed to cool down. The lower end of the graphite rod is polished carefully on smooth paper, filter paper or a lapping film to enable a smooth and plain surface. The sampling powder is inserted in the polished surface by carefully rubbing of the electrode over a powdered material (Fiedler and Scholz 2002).

A voltammetric cell for the detection of solid state particles with a paraffin impregnated graphite working electrode (PIGE) is illustrated in Figure 3.8. In contrast to other voltammetric applications, the working electrode (PIGE) touches only the meniscus of the electrolyte solution. This ensures that redox reactions are only taking place at a three phase boundary of the electrolyte, the incorporated sample, and the graphite electrode. Additionally, the low surface contact of the electrode body and the electrolyte minimizes the penetration of the electrolyte into the electrode body.

Before starting the experiment, the electrode has to be cleaned with a soft tissue to remove any particles on the outside of the electrode surface. Depending on the electrode surface state, the electrode can be regenerated for new sample loading by sliding the electrode over a piece of paper or filter paper, but sometimes it is necessary to add some silica gel, or to use abrasive papers with a low grain size (1µm or less).

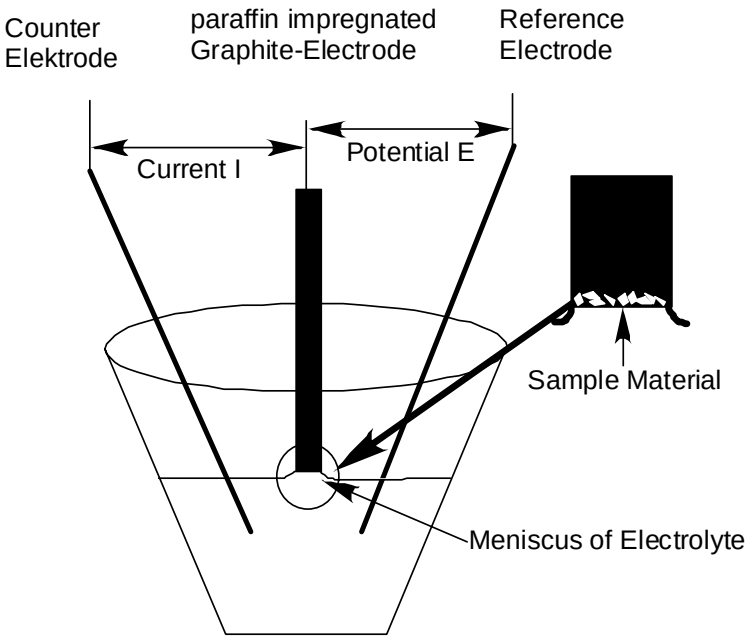

Figure 3.8 Schematic drawing of VIM

The mechanical incorporation of solid analyte into the electrode during VIM resembles the preconcentration step of voltammetric stripping analysis. But in contrast to controlled adsorption or electrode plating during voltammetric stripping analysis, the amount of mechanically incorporated material is unknown. This restricts direct quantification with VIM. The benefits of VIM are the identification of amorphous materials, the kinetic description of the material, the low sample amount, and the fast measuring time.

Chapter 4

Electrochemical Determination of the Reactivity of Sedimentary Iron Minerals

Jochen Nuester and Ole Larsen*§*

*Max Planck Institute for Marine Microbiology, Celsiusstr. 1, D-28359 Bremen, Germany

DHI Water and Environment, Krusenberg 31, D-28857 Syke, Germany

Submitted to Environmental Science and Technology

Abstract

The availability of particulate Fe(III) to microbial or chemical processes is generally inferred by performing one-step, chemical extractions. In this study, a continuum reaction model was used to assess and to test the reactivity changes of the total iron pool in different environmental and intertidal settings. A detailed electrochemical analysis and the comparison to previous ascorbate extractions (pH=3) verified the applicability to use Voltammetry of Immobilized Microparticles to detect different iron (oxyhydr)oxides and iron sulfides, and to describe their influence on the total reactivity of the bulk iron pool in recent marine and freshwater environments. Chronoamperometric measurements at -200 mV allowed good discrimination between the reactive and the refractory fraction of the iron mineral continuum. Electrochemical and wet chemical dissolution rates correlate for a defined potential window. The electrochemical kinetic calculations of the natural iron (oxyhydr)oxide pool are limited by the defining of the total reduction charge (Q_0), and kinetic dissolution experiments in 10 mM ascorbic acid at pH 3 are limited by defining the amount of undissolved crystals (m), due to the influence of ferrous iron minerals. In defined borders, solid state electrochemical can be compared to wet chemical dissolution experiments. The combination of solid state electrochemical measurements with classical extractions methods improved the informational value of the single mineral compounds in a sedimentary iron pool. It was found that an electrochemical discrimination between FeS, pyrite, and greigite was possible. This enables the direct observation of the transformation process from mackinawite to pyrite via greigite.

4.1 Introduction

In environmental systems like soils, aquifers and sediments iron occurs as Fe(II) and Fe(III) in different minerals. In sediments iron(III)-compounds serve particularly as important electron acceptors for carbon and sulfide oxidation, while Fe(II) serve as important sink for sulfides ultimately buried as pyrite. The dissolution and formation of these iron bearing minerals are controlled by a variety of biogeochemical processes (Luther 1989; Jørgensen 1990; Stumm and Sulzberger 1992; Canfield, Joergensen et al. 1993; Canfield, Thamdrup et al. 1993; Kostka and Luther 1994; Thamdrup, Fossing et al. 1994; Brendel and Luther 1995; Luther, Brendel et al. 1998; Taillefert, Bono et al. 2000; von Gunten and Furrer 2000; Krom, Mortimer et al. 2002; Schippers and Jørgensen 2002). Organic matter degradation studies in freshwater (Lovley and Phillips 1986; Lovley and Phillips 1986; Roden and Wetzel 2002; Roden 2003) and marine habitats (Canfield, Thamdrup et al. 1993; Thamdrup, Fossing et al. 1994; Thamdrup 2000) indicate that dissimilatory Fe(III) reduction can contribute substantially to this process.

The different forms of Fe(III) compounds in sediments cover a wide range in reactivity from nearly inactive silicate bound Fe(III) to a highly reactive oxyhydroxide species. Important properties of Fe(III) and Fe(II) minerals as adsorption capacity and bioavailability for iron reducing organisms depend on the mineral phase (Deng and Stumm 1994; Morse 1994; HamiltonTaylor, Davison et al. 1996; Canfield 1998; Neubauer, Furrer et al. 2002).

Usually chemical extraction methods are used as operational tools to distinguish different fractions of iron in soils and sediments. These classical extraction protocols are often used to discriminate between iron oxide, carbonate and phosphate phases (Lovley and Phillips 1986; Lovley and Phillips 1987; Phillips and Lovley 1987; Jensen and Thamdrup 1993; Phillips, Lovley et al. 1993; Church, Sarin et al. 1996). These methods yield operatively defined measures, but lack the ability to describe the continuum of phases present in sediments. This limitation can be overcome by performing kinetic experiments, in which the reduction of Fe(III) to Fe(II) is followed as a function of time.

Solid phase extraction methods for the different iron minerals result in a heterogeneous classification of reactivity groups for the different mineral phases (Schwertmann 1984; Canfield, Joergensen et al. 1993; Canfield, Thamdrup et al. 1993; Kostka and Luther 1994; Thamdrup, Fossing et al. 1994; Anshutz, Hyacinthe et al. 1999). The reduction capacity of ferric minerals in sedimentary environments depends on their reactivity, which in turn is

related to their mineralogy and their crystal properties. Hence, the rate and extent of iron (oxyhydr)oxide reduction in sediments are influenced by parameters including: particle size, mineralogy, surface adsorption, presence of ligands enhancing the dissolution process, and the reactivity of the electron donors including microorganisms (Postma 1993; Larsen and Postma 2001). The deconvolution of each individual factor and their formulation in reactivity models has only been successfully applied in initial rate experiments (Banwart, Davies et al. 1989; Sulzberger, Suter et al. 1989; Yao and Millero 1996).

Postma (1993) and Larsen and Postma (2001) have successfully applied a bulk reactivity model for reduction of iron (oxyhydr)oxides in ascorbate (pH=3) based on a general rate law for mineral dissolution developed Christoffersen and Christoffersen (Christoffersen and Christoffersen 1976):

$$J = \frac{-dm}{dt} = km_0 f\left(\frac{m}{m_0}\right) g(C), \qquad (1)$$

where J is the overall rate of dissolution (mol/s); m is the amount of undissolved crystals (mol); t is the time (s); k is the rate constant (s^{-1}); and m_0 is the initial amount of crystals (mol). The functions $f(m/m_0)$ describe the change in reactivity (e.g. change in available surface over time) of the remaining mineral fraction while the function $g(C)$ describes the effect of the solution composition (i.e., undersaturation).

Grygar an co-workers (1995; 1995) applied the same approach to determine the dissolution kinetics of different iron oxides using the "Voltammetry of Immobilized Microparticles (VIM)" method (Scholz, Nitschke et al. 1989; Scholz and Lange 1992). This method was formerly known as Abrasive Stripping Voltammetry (Grygar, Subrt et al. 1995). This method can be used to characterize and to identify the composition of solid state materials. Grygar and co-authors have applied this technique to characterize synthetic iron oxides, and iron oxides in paleo-soils and laterites (Grygar 1995; Grygar 1996; Grygar 1998; van Oorschot, Grygar et al. 2001; Grygar and van Oorschot 2002; Grygar, Dedecek et al. 2003).

In the present study, we used ascorbate extractions, chronoamperometric dissolution, and voltammetric dissolution experiments to describe the dissolution kinetics of synthetic iron minerals and of iron mineral phases in natural sediments. With a detailed analysis of the electrochemical method, we want to verify the applicability of this method for fast solid state

characterization of sedimentary material. Kinetic experiments using ascorbate extractions (pH=3) and chronoamperometric dissolution were tested for comparability. A voltammetric method was additionally used to identify the different iron minerals at the different sampling sites. Traditional one-step, chemical extraction experiments were further used to quantify the different reactive iron pools. For the first time we will present a detailed depth related electrochemical characterization of solid state iron containing minerals and their contribution to the reactivity change of the iron pool in recent sediments. This comparison was focused on the main iron (oxyhydr)oxides and sulfides in marine and freshwater sediments. The comparison of VIM with the results from one-step batch extraction experiments allowed a detailed evaluation of particulate iron in different environmental settings.

4.2 Experimental Section

4.2.1 Study Sites

Sediments from various N´German sites were obtained for testing solid state electrochemical procedures to describe sedimentary iron mineral reactivity. The types of sediments comprise a variety of environments with respect to geochemical conditions. The station Eckernfoerde Bay E8-3 is located in an elongated inlet extending southwestward from the Kiel Bight of the western Baltic Sea (54°28'N, 9°55'E), and the sediments consists of fine grained anoxic mud. The highly bioturbated sediments of the sampling site Weddewarden are located in the intertidal zone of the estuary of the River Weser in northern Germany (53°45'N, 8°05'E). Wuemmewiesen is a freshwater site in a wetland area north of Bremen (53° 4'N, 8° 48'E). The sediment at this station consists of sandy sediments with a 2 to 3 cm peat top layer. Sediments incubated in a flume have been collected from a north German harbor.

4.2.2 Equipment

We used two voltammetric systems, a computer controlled AMEL 433B and a Metrohm µ-Autolab3 polarograph. The working electrode was a paraffin impregnated graphite electrode (PIGE) (diameter: 0.4 mm) connected to the surface meniscus of the used electrolyte. The preparation of the PIGE electrode is described elsewhere (Scholz, Nitschke et al. 1989; Scholz and Lange 1990; Scholz and Lange 1992; Scholz and Meyer 1998). The reference electrode was a double-junction Ag/AgCl (3M KCl) electrode (Metrohm,

Germany), and the counter electrode was a platinum rod (Metrohm, Germany). All electrochemical experiments were carried out in a Metrohm three electrode cell connected to purified nitrogen system to avoid oxygen penetration during the measurements. The electrochemical experiments were carried out using an acetate buffer (pH 5.6) or a 0.01 M chloro-acetate buffer solution.

4.2.2 Voltammetry

(CV) and (LSV) have been used to oxidize or to reduce iron (II) and (III) containing minerals. (DPV) has been applied to improve sensitivity of the analytical detection limit. All experiments were started at open circuit potential (OCP). The potential was swept from OCP to –1000 mV for linear sweep voltammetry (LSV) and differential pulse voltammetry (DPV), and for cyclic voltammetry (CV), the potential was swept from OCP to 1200 mV as first turning point and than to –1000 mV as second turning point. The scan rate was 10 mV/s for LSV and CV, and for DPV the following parameters have been used: step potential, 5 mV; modulation amplitude, 25 mV; interval time, 0.5 s. Chronoamperometric experiments were performed at a constant potential for up to 1000s with a time interval of 0.2 s until no change in the current I was measurable. The recorded change of I(t) was recalculated to the accumulated charge Q for each time interval. The total charge (Q_0) was calculated from the sum of the charge recorded during chronoamperometric measurements (Q_{chrono}) and the charge calculated from following linear sweep voltammetric experiments (Q_{LSV}) to detect a unreacted fraction of the sample ($Q_0 = Q_{LSV} + Q_{chrono}$). All kinetic experiments have been fitted using a nonlinear least square procedure using SOLVER in Microsoft EXCEL.

4.2.3 Sample Preparation

FeS. Poorly crystalline mackinawite was prepared by a method adapted from Lennie and Vaughan (1996). Under argon atmosphere, 50mL polyethylene centrifuge tubes were filled with stoichiometric quantities of aqueous Fe(II) solution and aqueous Na_2S at pH (4.5) resulting in a spontaneous precipitation of microcrystalline FeS. The synthesis of a second crystalline mackinawite sample was carried out N_2 atmosphere. 0.5 M acetic acid/acetate buffer (pH=4.6) was prepared using 500 ml of freshly boiled MilliQ water. 5 g of pure iron wire (Goodfellow, UK) was then added to the acetic acid solution. After a couple of hours, the hydrogen development was large enough to ensure a reducing environment to which 30mL of a 0.45 M Na_2S solution was added. An immediate precipitation of black FeS particles was

observed. This suspension, containing the iron wire, was allowed to stand open for 24 h. Both mackinawite samples have been used directly from the synthesize solution for electrochemical investigations to avoid any further transformations. For storage the minerals were washed and freeze dried.

Pyrite. Pyrite (FeS_2) was prepared as previously described (Berner 1969; Sweeney and Kaplan 1973; Fossing and Jørgensen 1989; Schippers and Jørgensen 2001). A solution of 14.4 g Na_2S x 9 H_2O in 50 mL deionized water was mixed with a solution of 16.7 g $FeSO_4$ x $7H_2O$ in 50 mL deionized anoxic water in a 250 mL flask. FeS precipitated immediately and 2.1 g elemental sulfur was added under stirring. All chemicals were used of analytical grade. The flask was flushed with dinitrogen gas, sealed, and incubated at 65 °C for 4 d and at 85 °C for another 4 d. The precipitated FeS_2 was cleaned by washing with 1 N HCl to remove free sulfide and FeS.

Greigite. Greigite (Fe_3S_4) was provided by H. F. Passier (Netherlands Institute of Applied Geosciences, Netherlands) and a detailed description of the synthesis procedure is given by Dekkers et al. (2000). This Greigite sample was synthesized by injection of a Mohr salt solution into a sodium sulfide solution containing elemental sulfur at 140°C.

Iron (oxyhydr)oxides. The lepidocrocite samples (l5, l6, l7) have been differently synthesized to provide synthetic samples with different physical and chemical properties. The lepidocrocites were synthesized by oxidizing a 0.06 M aqueous Fe^{2+} solution with pure oxygen. The physical and chemical properties of the lepidocrocites were altered by manipulating the temperature and the Cl/Fe ratio. L5 was synthesized at 15 °C and at a Cl/Fe ratio of 6, while l6 and l7 were synthesized at 20 °C and at a Cl/Fe ratio of 8. The pH (5.5) of the synthesis was for all three lepidocrocites identical. Lepidocrocite l5 was synthesized in two steps by adding slowly twice an amount of Fe^{2+}. A 2-line ferrihydrite was synthesized by rapid hydrolysis of $Fe(NO_3)_2$ according to the method of Schwertmann and Cornell (1991). Other iron minerals (i.e., hematite, goethite, maghemite) have been purchased commercially.

4.2.4 Solid Phase Extractions

The synthetic and sedimentary iron (oxyhydr)oxides were characterized by four extraction methods targeting phases with different reactivity. Hydrochloric acid, ascorbate (pH 8), and dithionite were used in one-step extractions and ascorbate (pH=3) was used in a kinetic extraction. Reactive iron ($Fe_{reactive}$) was defined as the fraction extractable with

ascorbic acid (pH=8) (Fe_{asc}). Total extractable iron was defined using dithionite extraction (Fe_{dith}). Accordingly, refractory iron ($Fe_{refractory}$) were calculated as $Fe_{refractory} = Fe_{dith} - Fe_{asc}$. HCl extractions were used as a parallel method for the quantification of reactive iron oxides. The following description gives an overview of the applied extraction procedures:

1) The cold HCl extraction (HCl-Fe) dissolves the amorphous or poorly crystalline Fe oxides, FeS and $FeCO_3$, and might dissolve some Fe from silicates (Canfield, Raiswell et al. 1992; Canfield, Thamdrup et al. 1993; Thamdrup, Fossing et al. 1994): 0.4 g of sediment have been added to 10 mL of 0.5 M cold HCl solution and extracted for one hour at 200 rpm on a shaker at room temperature. Spinning down and measuring iron has been performed as described below (Stookey 1970; Kostka and Luther 1994; Thamdrup, Fossing et al. 1994). The extracted total (HCl-Fe_{total}) and ferrous iron (HCl-Fe^{2+}) concentration was then measured with the ferrozine method as indicated below.

2) The dithionite extraction has been applied to determine total extractable iron ($Fe_{dith} = Fe_{total}$) (Kostka and Luther 1994; Luther, Glazer et al. 2003). But it has to be taken into account that magnetite cannot be extracted with this method, but otherwise $FeCO_3$ and FeS will at least partly be extracted from the sediment (Kostka and Luther 1994): Approximately 0.25 g of sediment was mixed with 10ml of dithionite solution. The dithionite solution was prepared by dissolving 20 g of dithionite into 200 mL of an anoxic 0.35 M Na-accetate/0.2 M Na-citrate solution. The samples have than been shaken for 2 days at 200 rpm at room temperature. The extract was spun down and left in a closed plastic container on the lab desk for at least 2 weeks to oxidize excess dithionite. The Fe_{total} concentration of iron was then measured with the ferrozine method as indicated below.

3) Fe extracted by ascorbic acid (Fe_{asc}) is defined as reactive iron, including FeS (Ferdelman, Church et al. 1991; Kostka and Luther 1994): 10ml of ascorbic acid solution were add to approximately 0.4 g of sediment according to the method of Ferdelman et al. (1991) and Kostka and Luther (1994). The anaerobic ascorbic acid solution consists of 10 g Na-citrate and 10 g bicarbonate in 200 mL Milli-Q water. Slowly 4g of ascorbic acid were added to obtain a slightly basic pH (pH~8). The

samples have than been shaken at 50 °C for 48 hours at 150 rpm and spinned down to measure the Fe concentration after the Ferrozine method of described below.

4) All kinetic experiments were carried out in a 600 mL glass reaction vessel. For each experiment, 0.1 g to 0.2 g of sediment was given to 0.5 mL of anoxic 10 mM ascorbic acid solution under nitrogen atmosphere and pH control (pH 3). Filtered (0.2 µm pore size) samples were periodically collected with a syringe and immediately measured in a Na-acetate buffered Ferrozine solution (Stookey 1970)). For a complete description, the reader is referred to the protocol of Larsen and Postma (2001).

Dissolved Fe(II) was measured calorimetrically at 562 nm. 10 to 50 µl of extract were added to 2 to 3 ml of Ferrozine solution. The ferrozine solution consisted of 50 % of a 2.5 M ammonium acetate buffer and 50 % of 0.01 M ferrozine. To reduce any extracted iron HCl-hydroxylamine (final conc. 0.1 M) was added to the Ferrozine solution. Hence, HCl extracted ferric iron was calculated from the concentration difference between measurements with (HCl-Fe_{total}) and without HCl-hydroxylamine (HCl-Fe^{2+}).

4.3 Results and Discussions

4.3.1 Model for Bulk Electrochemical Dissolution Kinetics

4.3.1.1 Kinetic Theory.

Postma (1993) and Larsen and Postma (2001) has previously applied a general rate law originating from Christoffersen and Christoffersen (Christoffersen and Christoffersen 1976) to describe the kinetics of the reductive dissolution of iron (oxyhydr)oxides (Eq. 1) Often the function $f(m/m_0)$ is approximated by $(m/m_0)^{\eta}$. The function $g(C)$ depends on the solution composition such as concentration, type of reductant and pH. The experiments of Christoffersen and Christoffersen (1976) showed that $g(C)$ correspond to the degree of undersaturation. In our experiments, the solution composition was kept constant. Hence, we cannot separate $g(C)$ from the rate constant k and a more simple equation is derived with k' being the product of the initial rate constant and $g(C)$:

$$\frac{J}{m_0} = k'\left(\frac{m}{m_0}\right)^{\gamma}. \quad (2)$$

At the initial conditions *($m/m_0=1$)*, the rate normalized to the initial mass equals the rate constant *k'*. The exponent γ can be considered a number describing the homogeneity of the dissolution process (Larsen and Postma 2001). The dissolution process is among others influenced by the grain size distribution and the surface reactivity. A more detailed explanation of γ is given by Larsen and Postma (2001). This mathematical description equals the reactive continuum of Boudreau and Ruddick (Boudreau and Ruddick 1991; Postma 1993). Electrochemical bulk dissolution experiments can be treated in a similar manner as kinetic experiments with ascorbate (pH 3). Consequently, the charge is used as a function for the mass of sample material being reduced. The kinetics of electrochemical dissolution can be described analogously to Eq. 2:

$$\frac{J}{Q_0} = k'\left(\frac{Q_t}{Q_0}\right)^{\gamma} \quad (3)$$

where Q_t is the charge required to dissolve the unreacted amount of particles, and Q_0 is the total charge to dissolve the whole electroactive material. Integration of equation (2) and (3) results for $\gamma \neq 1$ in:

$$\frac{m}{m_0} = \left[-k'(1-\gamma)t+1\right]^{\frac{1}{1-\gamma}} \quad (4)$$

$$\frac{Q_t}{Q_0} = \left[-k'(1-\gamma)t+1\right]^{\frac{1}{1-y}} \quad (5)$$

The applicability of the reactive continuum model is depending on the definition of a value decribing the total reactive material, m_0 and Q_0 respectivley. Hence, the type of extractant, the dissolution mechanism, the experimental setup, the nature and the reactivity of the material, and the fitting process affect the results of the model. Van der Zee and Raaphorst (2004) defined m_0 as the maximum amount of iron a given extractant is able to dissolve from a particular sample. In this case, the value of m_0 is specific for a particular sample, a particular fraction of the iron pool, and the extractant solution considered. In other studies, the concentration of the reactive material (m_0) is determined by a more powerful extraction

method than used in the kinetic experiments (Postma 1993; Roden and Wetzel 2002; Ferro 2003). In those studies, the continuum model always predicts incomplete dissolution at the end of the extraction experiment. For the chronoamperometric approach used in this study, we used the approach of incomplete dissolution at the end of the kinetic experiments and verified the completeness of the reduction at a given chronoamperometric potential by a following voltammetric experiment. In the case of incomplete reduction, we added the reduction charge for the not reacted material (Q_{LSV}) to the charge of the chronoamperometric experiments (Q_{chrono}) to define the necessary charge to reduce all iron particles (Q_0).

Equations (4) and (5) were fitted to experimental data (Figure 4.1). A strong correlation was observed between the chronoamperometric measurements (solid lines) and the fitting model (dotted lines) at -200 mV, while the correlation was weak at -500 mV. The correlation decrease with decreasing potential is due to increased background currents at more negative potentials. The most striking differences between Figures 4.1A and 4.1B are the increased initial reactivity by decreasing the potential from -200 mV to -500 mV and the similarity in reactivity change of l6 and Ferri at -500 mV in comparison to experiments carried out at -200 mV. At both potentials, Ferri has the steepest decrease of Q_t/Q_0 within the first 50 seconds. A reductive dissolution of goethite was not possible at –200 mV and pH 5.6. Q_t/Q_0 is always positive because of background currents resulting from not dissolved remnants calculated by following voltammetric measurements (Q_{LSV}).

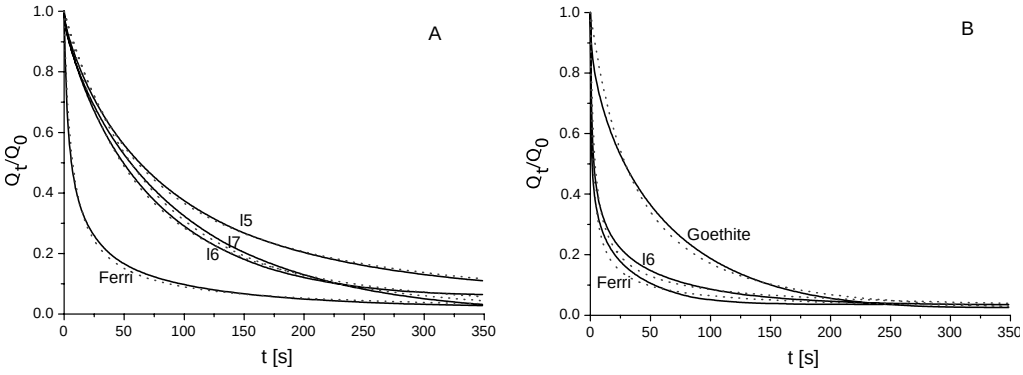

Figure 4.1 Chronoamperometric reductive bulk dissolution of different iron oxides at –200 mV (A) and –500 mV (B) in an acetate buffer (pH 5.6). The solid lines represent the actual data and the dotted lines are the fit to the data using a continuum model approach. Goethite could not be reduced at –200 mV and the initial reactivity increases with decreasing potential. Ferri: 2-line ferrihydrite; l5, l6, l7: three different lepidocrocites, goethite (Bayferrox).

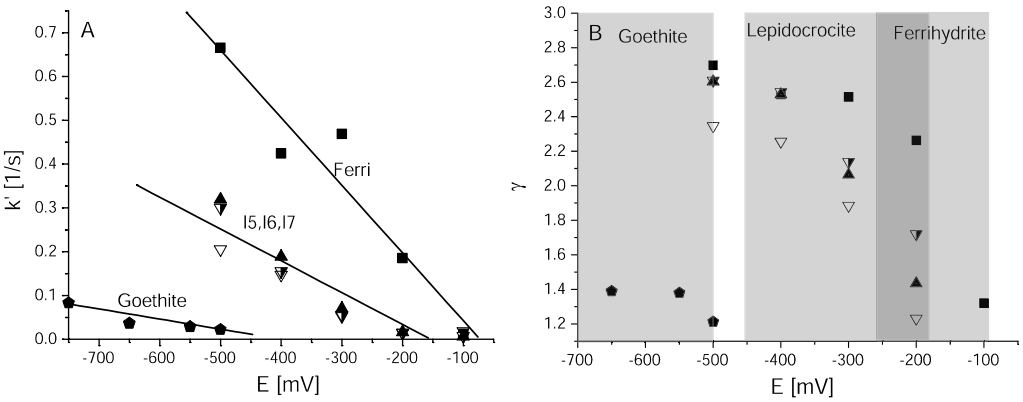

Figure 4.2 Chronoamperometric bulk dissolution studies in dependence of the applied potential E. A) K' shows an increase in initial reactivity with decreasing potential E. B) γ increases with decreasing potential E. The differentiation between g values for different ferrihydrites and lepidocrocites diminishes by lowering the reduction potential E. The shadowed areas show the preferential reduction potential for the different minerals. Ferrihydrite: Ferri - filled squares, Lepidocrocites: l5 – filled upright triangle, l6 – half-filled triangle, l7 – open triangle, Goethite: Goethite – filled polygons.

Figure 4.2 shows the change in electrochemical reactivity with decreasing applied potential. A strong correlation was observed between initial reaction rates (*k´*) and applied potential (Figure 2A). The potential effect of on the initial reaction rate was strikingly, and dissolution of goethite could only occur at potentials more negative than -500 mV. Assuming that *k´* is the product of *k* and *g(C)* a linear increase in *k'* with increasing potential is expected. Furthermore, for chronoamperometric experiments it was expected that *g(C)* would depend only on the potential and not on the mineralogy, but the different slopes for the different iron (oxyhydr)oxides seem to show that this assumption is not true (Figure 4.2A). Considering the ratio $k'_{Ferri}/k'_{l5,l6,l7}$ shown in Table 4.1 an effect of the applied potential on the mineralogy of the ferric (oxyhydr)oxides cannot be excluded, but is not obvious. For –100 mV, -400 mV and –500 mV the calculated $k'_{Ferri}/k'_{l5,l6,l7}$ values are 1.87, 2.55, and 2.42, respectively, and indicate a two times faster reaction of ferrihydrite over lepidocrocite. The experiments at –200 mV and –300 mV showed a 7.8 to 12 times faster reactivity for ferrihydrite to the lepidocrocites (l5, l6 ,l7) (Table 4.1). These differences in the initial reactivity ratio could be attributed to experimental errors, and the effect of the potential on the mineralogy could only be an artifact.

In contrast, lowering the reduction potential results in almost identical γ values for the different iron (oxyhydr)oxide pools (Table 4.1). This is presented in figure 4.2B, where the γ values for Ferri and l5, l6, and l7 became more similar at –500 mV than at –200 mV. The behavior of Goethite is less defined, because reduction of Goethite does not occur at low potentials.

Table 4.1 Comparison of electrochemical calculated initial reactivities of different iron oxyhydroxides.

	Ferri		l5		l6		l7		Goethite			
E [mV]	*k' [s^{-1}]*	γ	*k' [s^{-1}]*	γ	*k' [s^{-1}]*	γ	*k' [s^{-1}]*	γ	*k' [s^{-1}]*	γ	k'_{terr}/k'_{lepi}	$\gamma_{terr} - \gamma_{l5,l6,l7}$
-100	0.01	1.32	0.01	n.d	0.01	n.d.	0.02	n.d	n.d.	n.d.	1.87	n.d.
-200	0.19	2.26	0.01	1.72	0.02	1.43	0.02	1.23	n.d.	n.d.	12.08	0.80
-300	0.47	2.51	0.06	2.14	0.07	2.06	0.05	1.88	n.d.	n.d.	7.88	0.49
-400	0.42	2.53	0.16	2.54	0.19	2.53	0.15	2.26	n.d.	n.d.	2.59	0.09
-500	0.67	2.70	0.30	2.61	0.32	2.60	0.21	2.35	0.02	1.21	2.42	0.18
-550	n.d	n.d	n.d	n.d	n.d	n.d	n.d	n.d	0.03	1.38	n.d	n.d.
-650	n.d	n.d	n.d	n.d	n.d	n.d	n.d	n.d	0.04	1.39	n.d	n.d.

Overall the calculated γ values comprise a range from 1.2 to 2.7. As described in detail by Larsen and Postma (2001) γ values in the range 1/2 to 2/3 can be explained by a shrinking core model of crystals with different morphology. Higher γ values can be explained by more broad distribution of particle size and reactivity of surface sites. Figure 4.2 and Table 4.1 show unambiguously that an electrochemical, kinetic description of the more reactive iron compounds (ferrihydrite and lepidocrocite) is more favorable at high potentials (i.e., -200 mV, pH=5.6), because a concurrent distinction in k' and γ for the different reactive ferric (oxyhydr)oxides is constricted at –500 mV.

A comparison of kinetic experiments using ascorbate (pH 3) and chronoamperometric experiments showed a good correlation between these two different methods. As an example, Figure 4.3 displays linear correlations for k' and γ values for electrochemical (–200 mV) against ascorbate dissolution experiments for the three different lepidocrocites l5, l6, and l7. Positive correlations have also been found for similar experiments at more negative potentials. The correlation of the γ values especially indicates that both methods are comparable under defined conditions.

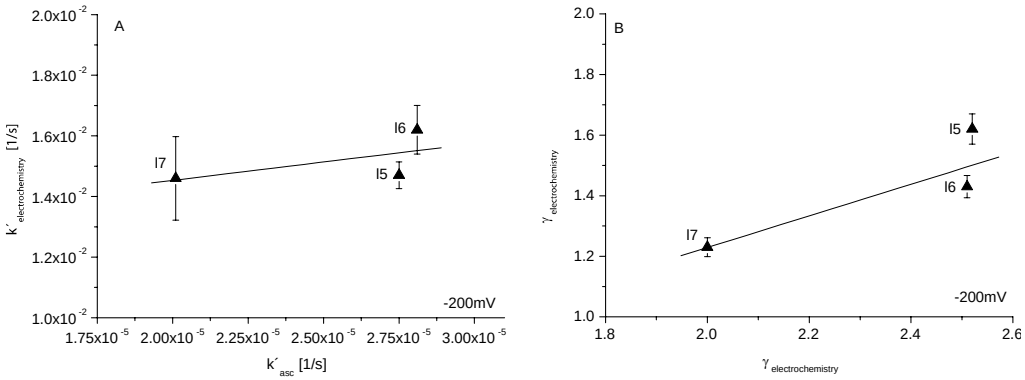

Figure 4.3 Comparison of bulk reductive dissolution experiments using chronoamperometry at –200 mV or 10 mM ascorbic acid. A) Correlation between k'_{asc} and $k'_{electrochemistry}$, B) Correlation between γ_{asc} and $\gamma_{electrochemistry}$. Lepidocrocites: l5, l6, l7: filled triangles.

The applied rate laws (Eq. 5, Eq. 6) assume that the γ values depend on mineralogical factors, i.e., particle size distribution. Different methods of synthesis result in different mineral properties (Larsen and Postma 2001), which again should be reflected in different γ values. The correlation of both methods illustrates that both methods have the potential to describe reactivity changes. On the other hand, it has to be stated that decreasing the chronoamperometric potential diminishes the differentiation in γ, and the description of mineral properties is therefore limited to high potentials (Figure 4.2B).

4.3.2 Electrochemical Detection of Different Synthetic Iron Oxides

As exemplified in Figure 4.4, the open circuit potential for all different ferric iron (oxyhydr)oxides immersed into the PIGE electrode was fairly identically at around 300 mV. The different onset of the electrochemical reaction is affected by their phase structure and morphology (Grygar 1995; Grygar 1996; Grygar 1997). Figure 4.4 shows sets of voltammograms of various ferric (oxyhydr)oxide minerals in acetate buffer at pH 5.6. Two distinct maxima for goethite and hematite reduction could be detected at -516 mV and –595 mV, respectively. To illustrate the electrochemical separation between different iron (oxyhydr)oxides a mixture of ferrihydrite and goethite was reduced, and two distinct peaks

occurred at 17 mV and –500 mV, respectively. The lepidocrocite samples l5, l6, and l7 have their maximum current signal between -75 mV and -85 mV. Broad peaks at approximately -630 mV following the reduction signal for lepidocrocite are an indication for small impuries of hematite in the lepidocrocite samples. Small impurities of hematite cannot be avoided during the synthesis of ferrihydrite and lepidocrocite and a partial phase transformation of lepidocrocite to hematite could have occurred over time. Reduction of maghemite powder reveals two distinct voltammetric peaks at –140mV and –740mV. The presence of these two peaks refers to reduction of ferric iron in tetrahedral and octahedral sites or to the inclusion of impurities.

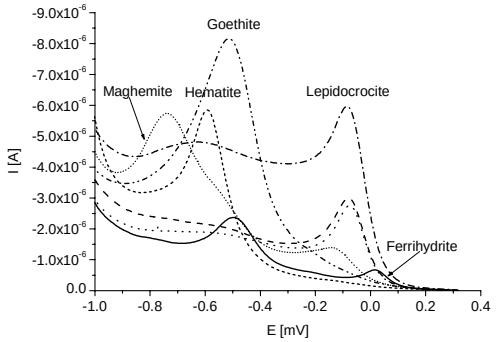

Figure 4.4 Comparison of different iron oxides by voltammetric reduction in acetate buffer (pH 5.6).

4.3.3 Electrochemical Dissolution of Synthetic Iron Sulfides

Different synthetic iron sulfide minerals were used as probe compounds to investigate the electrochemical oxidation of natural sulfide minerals. Two different mackinawite minerals ($FeS_{poorly\ cryst.}$ and $FeS_{crsyt.}$) have been synthesized to investigate the crystallinity effects on the electrochemical behavior, and synthetic pyrite and greigite samples have been chosen to probe the natural oxidation sequence from mackinawite to pyrite (Wang and Morse 1996; Benning, Wilkin et al. 2000).

Figure 4.5 shows sets of cyclic voltammograms of crystalline mackinawite, pyrite, and greigite. The oxidation of crystalline mackinawite showed three distinct voltammetric oxidation signals at 310 mV (A), 556 mV (B), and 760 mV (C) in the anodic branch of a cyclic voltammogram (Figure 4.5). Three electrochemical shoulders occurred at 420 mV (X_1), 0 mV (X_2) and –840 mV (X_3) indicating the reduction of produced compounds. X_1 and X_2

could be correlated to the reduction of adsorbed ferric iron at the electrode. The anodic oxidation of greigite resulted in a maximum between 940 mV to 950 mV (F, Figure 4.5). In contrast two oxidation steps were observed for the oxidation of pyrite, with one maximum at a lower peak potential (840 mV to 850 mV, (D)) and one maximum more positive than the greigite signal (1150 mV, (E)).

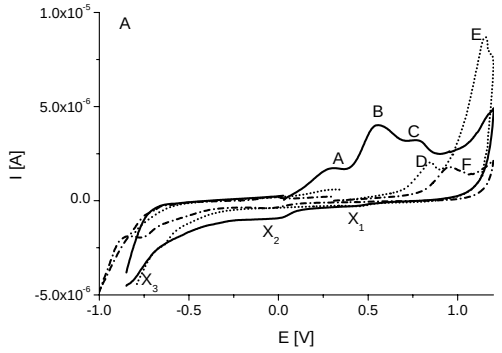

Figure 4.5 Cyclic voltammograms of different synthetic iron sulfide minerals (mackinawite: solid line, pyrite: short dots, greigite: dashed line). A to F indicate different anodic voltammetric maxima, and X_1 to X_3 indicate different cathodic maxima. CSV: start potential – OCP, first vertex - 1.2 V, second vertex - -1V, scan rate - 10mV/s, electrolyte: 0.01 M chloro-acetate buffer.

Figure 4.6 displays the cyclic voltammograms of poorly crystalline mackinawite ($FeS_{poorly\ cryst.}$) and crystalline mackinawite ($FeS_{crsyt.}$). The electrochemical oxidation signals of poorly crystalline mackinawite are more positive than those of the crystalline sample. Voltammetric signals for $FeS_{poorly\ cryst}$ were detected at ~20 mV (Y_1), ~190 mV to 220mV (Y_2), and at ~530 mV to 550 mV (Y_3). The peak Y_1 with a strong increase just after OCP (Figure 4.6) is due to the oxidation of adsorbed ferrous iron and was not recorded for the crystalline sample, because of the different synthesis pathways. Peak Y_3 is asymmetrical broad, and contains peak B and C of $FeS_{cryst.}$ (Figure 4.6).

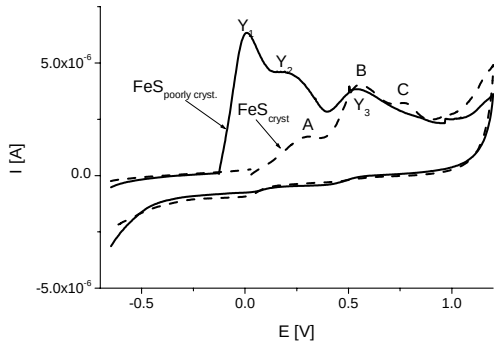

Figure 4.6 Comparison of poorly crystalline and crystalline mackinawite. Y_1 to Y_3 indicate voltammetric maxima of the poorly crystalline FeS (solid line) and A to C describe the voltammogram of crystalline FeS (dotted line). Conditions used are the same as in Figure 5.

The electrochemical oxidation of the three different iron sulfide minerals resulted in distinct pattern allowing the identification of the different minerals. The linkage of the different voltammetric maxima of the different minerals to specific redox processes is fairly unstudied because of the metastable character of FeS and greigite in natural ecosystems.

Electrochemical analysis of iron sulfide minerals are carried out in the context of mineral and metal processing as in flotation and acid mine drainage studies. In those electrochemical studies, bulk electrodes of the interested material have been usually applied, like pyrrhotite and pyrite rod electrodes (Doyle and Mirza 1886; Mikhlin 2000; Buswell and Nicol 2002). The electrochemical oxidation of FeS (mackinawite) is not well understood. For pyrrhotite (tetragonal FeS) Mikhlin (2000) describes three anodic maxima. The first anodic maximum was attributed to the formation of S_0^{2-} species and polysulfide clusters (Figure 4.5, peak A):

$$2S_0^{2-} \rightarrow 2S_1^{-} + 2e \qquad 4.1$$

$$S_0^{2-} + 2S_1^{-} + (S_2)_n^{2-} \rightarrow 2S_1^{-} + (S_2)_{n+1}^{2-} + 2e \qquad 4.2$$

the second maximum was due to the oxidation of the terminal S atoms (S_1^{-}) resulting in the formation larger S-S chains (Figure 4.5, peak B):

$$4S_1^{-} + (S_2)_n^{2-} + (S_2)_p^{2-} \rightarrow 2S_1^{-} + (S_2)_{n+p}^{2-} + 2e \qquad 4.3$$

and the third maximum resulted from the oxidation of the residual S_1^- (Figure 4.5, peak C):

$$S_1^- \rightarrow S_1^+ + 2e, \quad 4.4$$

where S_1^+ species are unstable and react further to S-S clusters. Mikhlin (2000) assumes that S_1^+ and S_3^+ species have the ability to oxidize ferrous to ferric iron. The analysis of pyrrhotite showed the same three anodic maxima as the crystalline mackinawite used in our study but with different peak potentials. An explanation of the more positive peak potentials is the difference in the pH of the electrolyte (1 M HCl in the study of Mikhlin versus 0.01 chloro-acetate buffer in our study). Taking into account the pH difference of the electrolytes used in the two studies, the electrochemical pyrrhotite oxidation model of Miklhlin could be used as an analog for the electrochemical oxidation of mackinawite.

Doyle and Mirza (1886) studied pyrites from several environments with solid pyrite electrodes. They concluded that no simple relationship exist between fundamental properties like S/Fe ratio and the electrochemical behavior. All their pyrite electrodes showed a sharp increase in the current density at potentials more positive than 900 mV. This is identically with our findings, but in comparison to their study, the strong current increase resulted in a voltammetric peak at approximately 1150 mV (Figure 4.5). According to Doyle and Mirza (1886) the strong current increase at potentials higher than 900 mV measured with solid state pyrite electrodes can be explained by the initial surface layer oxidation of iron deficient pyrite according to the following model:

$$Fe_{1-x}S_2 + 8H_2O \rightarrow 1\text{-}x\ Fe^{3+} + 2HSO_4^- + 14H^+ + 3(5\text{-}x)e. \quad 4.5$$

Accordingly, the peak at 840 to 850mV reflects the oxidation of Fe^{2+} and the formation of iron deficient pyrite (Doyle and Mirza 1886)

$$FeS_2 \rightarrow Fe_{1-x}S_2 + xFe^{3+} + 3xe \quad 4.6$$

Kelsall et al. (1999) showed using electrochemical and spectroscopic techniques that the oxidation of pyrite involves a complex series of parallel reaction steps, ultimately producing Fe^{2+}/Fe^{3+} and $S/S_2O_3^{2-}/HSO_4^-$, depending on pH and potential. The most important steps in pyrite oxidation are the breaking of the Fe-S bond and the formation of intermediate sulfoxy species (like $S_2O_3^{2-}$, $S_2O_4^{2-}$, $S_2O_5^{2-}$, HSO_3^-, and SO_4^{2-}). These sulfoxy species are then further oxidized to elemental sulfur and sulfate. The ratio of elemental sulfur to sulfate depends on

several parallel reactions (Kelsall, Yin et al. 1999). At potentials below 0.7 V the favored oxidation product is sulfate (Davis and Chatterjee 1975; Meyer, Ospina et al. 1980; Holman, Thompson et al. 1994; Kelsall, Yin et al. 1999).

To our knowledge, no electrochemical oxidation studies have been carried out with greigite due to its metastable nature. The peak at ~950 mV is probably due to the oxidation of ferrous iron in the greigite structure (Figure 4.5). We propose a partly to total oxidation of ferrous iron in the crystal lattice of greigite:

$$Fe^{II}Fe_2^{III}S_4 \rightarrow Fe_{1-x}{}^{II}Fe_2^{III}S_4 + xFe^{3+} + 3xe \qquad 4.7$$

Measurements with low amounts of incorporated material did not show any voltammetric peak signals in a second cyclic scan. It is therefore assumed the all greigite was oxidized. The probable oxidation of the sulfide to sulfate is not visible at high positive potentials, but the passivation of the electrode at high negative potentials could be an indication for sulfate adsorption at the electrode surface. The electrochemical oxidation of ferrous iron in the greigite structure resulted in a slight shoulder at 200 mV indicating a ferric iron product. To explain the voltammetric signals in detail, VIM studies need to be coupled to spectroscopic studies.

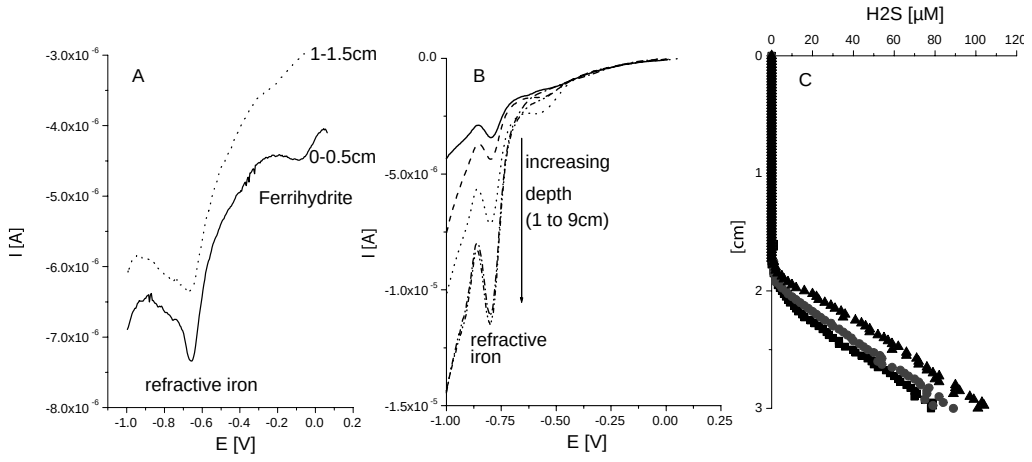

Figure 4.7 Eckernfoerde Bay. A) Differential pulse voltammogram of different depth intervals (0-0.5 cm and 1-1.5cm): start potential – OCP, final potential - -1V, step amplitude – 5mV, modulation amplitude – 25 mV, interval time – 0.5 s, electrolyte – 0.01 M chloro-acetate buffer. B) LSV voltammograms recorded for different depths after chronoamperometric measurements used to calculate Q_{LSV}: start potential – OCP, final potential - -1V, scan rate – 10 mV/s, electrolyte – 0.01 M chloro-acetate buffer. C) Hydrogen sulfide microsensor depth profile

4.3.4 Electrochemical Characterization of Iron Oxides in Natural Sediments

To monitor and to test the iron mineral dissolution kinetics, we focused our studies on four different environmental settings with different geochemical characteristics, and on the interpretation of electrochemical and classical extraction measurements.

Eckernfoerde Bay E8-3. Iron (oxyhydr)oxide reduction using DPV at different depth intervals showed distinct pattern. Figure 4.7A presents two typical voltammograms. The depth interval of 0 to 0.5 cm was the only level, ferrihydrite could be detected with a peak potential of approximately –50 mV. At the same depth a more refractory iron (oxyhydr)oxide compound was also found with a peak potential of ~ -680 mV close to the peak potentials of synthetic hematite and goethite. Further down only the iron (oxyhydr)oxide with a peak potential at –680 mV was detected (i.e., 2-3 cm, Figure 4.7A). Using in comparison the LSV signal of the remaining refractory iron (oxyhydr)oxides measured after chronoamperometric experiments (at –200 mV), an increase of the peak height was observed for the remaining, not dissolved refractory iron (oxyhydr)oxide fraction with increasing depth (i.e., 1-7 cm, Figure 4.7B). This signal increase is a qualitative information indicating that the amount of refractory iron (oxyhydr)oxides increases with depth. Quantitative information could not be obtained from the peak signal, because the amount of sample incorporated into the electrode is unknown.

An increase of free dissolved H_2S was detected below 17 mm (Figure 4.7C). The voltammetric and microsensor measurements showed the coexistence of refractory iron (oxyhydr)oxides with free dissolved H_2S. This points out the refractory manner of these iron minerals, because a strong reducing agent such as hydrogen sulfide would have reduced reactive iron oxyhydr(oxide) compounds immediately (Poulton, Krom et al. 2002; Poulton, Krom et al. 2004). These data are confirmed by classical extractions measurements (ascorbate, HCl, dithionite shown in Figure 4.8A).

The reactive iron pool calculated either from HCl or ascorbate extractions decreased within the first centimeter. The refractory part of the total iron pool was constant over the analysed depth interval. CSV experiments of different depth intervals provided evidence for precipitation of FeS below 5 mm depth (not shown). The occurrence of FeS accounts for the inability to detect free dissolved hydrogen sulfide in this depth zone.

The overall reaction kinetics have been measured and calculated by chronoamperometry (Figures 4.8 B, C). *k'* decreased steeply from values of ~0.03 s^{-1} to ~0.003 s^{-1} below 1.75 mm depth (Figure 8B). At the same depth, γ increases from values below 5 to above 20 (Figure 4.8C). Referring to Larsen and Postma (2001) only γ values up to 3.4 can be explained by grain size distribution (Taplin 1974; Dixon and Hendrix 1993). Therefore, other effects are contributing to the high γ values, like remaining undissolved particles.

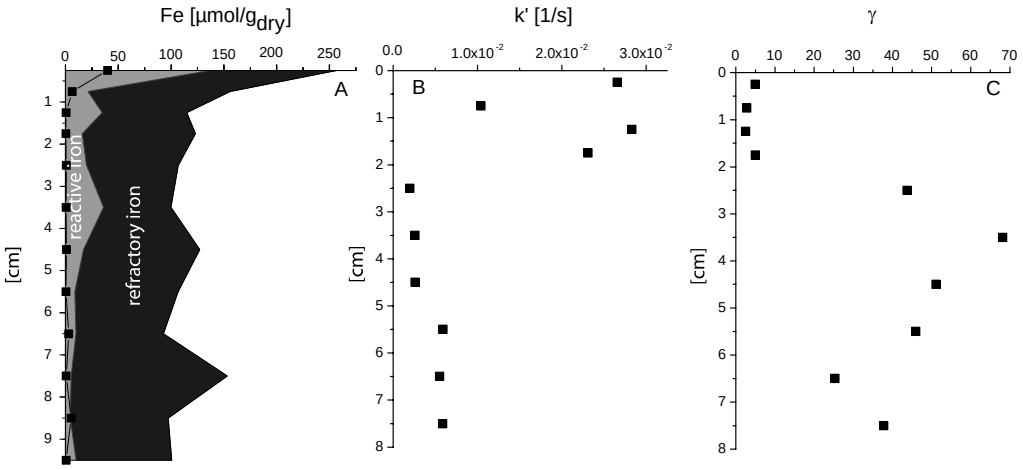

Figure 4.8 Eckernfoerde. A) Iron extraction depth profile: refractory iron is calculated from the subtraction of iron extracted by ascorbate from iron extracted by dithionite - $Fe_{refractory} = Fe_{dith} - Fe_{asc}$, reactive iron - $Fe_{recative} = Fe_{asc}$, filled squares: HCl-Fe^{3+}. B, C) Reactivity profiles applying a continuum reaction model to chronoamperometric experiments at –200 mV, k' (B) and γ (C). All parameters show a strong decrease of the iron (oxyhydr)oxide reactivity within the first cm.

The whole concept used for describing mineral reactivity in this study is based on bulk dissolution, but the application of chronoamperometric measurements at –100 mV to –200 mV assumes that very refractory mineral compounds (i.e., hematite or goethite) do not react at this high potentials. The addition of LSV measurements and the calculation of the charge necessary to dissolve the remaining fraction direct after the chronoamperometric experiments solve this contradiction. The results of the chronoamperometric and the LSV measurements are listed in Table 4.2.

Table 4.2 Charge comparison of reduced and remaining ferric iron chronoamperometric dissolution process.

Eckernfoerde Bay E8-3							Flume sediment N`German harbour						
depth [cm]	k' [$10^{-3}s^{-1}$]	γ	Q_{LSV} [µC]	Q_{chrono} [µC]	Q_0 [µC]	Q_{chrono}/Q_{LSV}	depth [cm]	k' [$10^{-3}s^{-1}$]	γ	Q_{LSV} [µC]	Q_{chrono} [µC]	Q_0 [µC]	Q_{chrono}/Q_{LSV}
0,3	26,6	4,9	-6,7	-11,5	-18,2	1,72	0,1	10,8	1,2	-2,0	-136,1	-138,1	68,06
0,8	10,4	2,8	-5,1	-2,3	-7,4	0,45	0,2	12,4	1,2	-2,4	-290,9	-293,3	121,21
1,3	28,3	2,5	-1,3	-5,4	-6,6	4,31	0,4	9,2	1,1	-2,5	-286,7	-289,2	114,69
1,8	23,1	5,0	-4,4	-5,4	-9,8	1,23	0,6	13,7	1,3	-2,5	-229,9	-232,4	91,95
2,5	2,0	43,7	-23,0	-1,5	-24,5	0,06	0,8	10,5	1,2	-2,2	-116,2	-118,4	52,80
3,5	2,6	68,1	-33,0	-1,7	-34,7	0,05	1,0	11,0	1,2	-2,5	-442,3	-444,8	176,91
4,5	2,6	51,2	-38,0	-2,4	-40,4	0,06	1,1	15,9	1,5	-2,2	-263,9	-266,1	120,87
5,5	5,9	46,0	-27,3	-1,7	-29,0	0,06	1,3	8,9	7,5	-14,6	-7,7	-22,3	0,53
6,5	5,5	25,3	-39,5	-5,5	-45,0	0,14	1,8	7,5	11,0	-15,3	-5,5	-20,8	0,36
7,5	5,9	37,8	-23,0	-2,3	-25,3	0,10	2,5	5,9	11,7	-12,9	-4,1	-16,9	0,32
							3,5	7,3	11,8	-14,0	-4,6	-18,6	0,33
							4,5	5,3	10,1	-16,5	-6,0	-22,5	0,36
Weddewarden							**Wuemmewiesen**						
depth [cm]	k' [$10^{-3}s^{-1}$]	γ	Q_{LSV} [µC]	Q_{chrono} [µC]	Q_0 [µC]	Q_{chrono}/Q_{LSV}	depth [cm]	k' [$10^{-3}s^{-1}$]	γ	Q_{LSV} [µC]	Q_{chrono} [µC]	Q_0 [µC]	Q_{chrono}/Q_{LSV}
0,5	8,6	4,5	-15,0	-17,6	-32,6	1,17	0,5	39,9	2,5	-0,5	-23,6	-24,1	47,11
1,5	7,2	5,2	-22,0	-18,6	-40,6	0,84	1,5	53,3	2,5	-0,5	-28,3	-28,8	56,51
2,5	8,7	3,4	-13,3	-22,3	-35,6	1,67	2,5	9,0	1,3	-1,5	-49,8	-51,3	33,20
3,5	8,4	4,4	-21,0	-24,1	-45,1	1,15	3,5	7,5	1,3	-1,2	-75,7	-76,9	63,06
4,5	8,5	5,5	-17,0	-15,2	-32,2	0,89	4,5	22,2	1,9	-2,2	-19,6	-21,8	8,93
5,5	4,2	6,1	-22,0	-12,6	-34,6	0,57	5,5	7,8	1,1	-4,6	-76,5	-81,1	16,63
6,5	5,4	5,3	-28,0	-20,7	-48,7	0,74	6,5	10,5	1,2	-1,4	-56,8	-58,2	40,59
7,5	3,1	7,7	-23,0	-9,1	-32,1	0,39	7,5	16,1	1,5	-1,7	-35,4	-37,1	20,82

Table 4.2 illustrates that an increase in γ was the consequence of a low Q_{chrono}/Q_{LSV} ratio (Figure 8C). Q_{chrono}/Q_{LSV} decreased from above 1 to 0.06 below 2 cm dept corresponding to the strong increase of γ. Therefore, the amount of unreacted material in electrochemical studies affects dramatically the kinetic model parameter and lead to elevated γ values.

Flume sediment from a N´German harbor. DPV measurements showed the occurrence of reactive iron (oxyhydr)oxides in the upper 11mm. Typical voltammograms with and without reactive iron (oxyhydr)oxides are presented in Figure 4.9A. At 10 mm depth, two iron reduction peaks have been measured with peak potentials of 20 mV and –580 mV. In contrast, measurements further down showed two maxima at -580 mV and -800 mV indicating two different refractory iron compounds (i.e., 15 mm, Figure 4.9A). The coexistence of mackinawite, greigite, and pyrite was detected using CV, and was compared to voltammograms of standard minerals (Figure 4.9B). The metastable mineral greigite in

natural sediments is usually detected by magnetic susceptibility measurements at the sample location (Roberts and Turner 1993; Reynolds, Tuttle et al. 1994; Roberts 1995). The concomitant electrochemical detection of these three sulfide phases enables the direct observation of the transformation process from mackinawite to pyrite.

Free dissolved hydrogen sulfide could not be detected in the porewater of the sediment (not published data of the TREAD project) indicating fast precipitation and transformation of iron sulfide minerals.

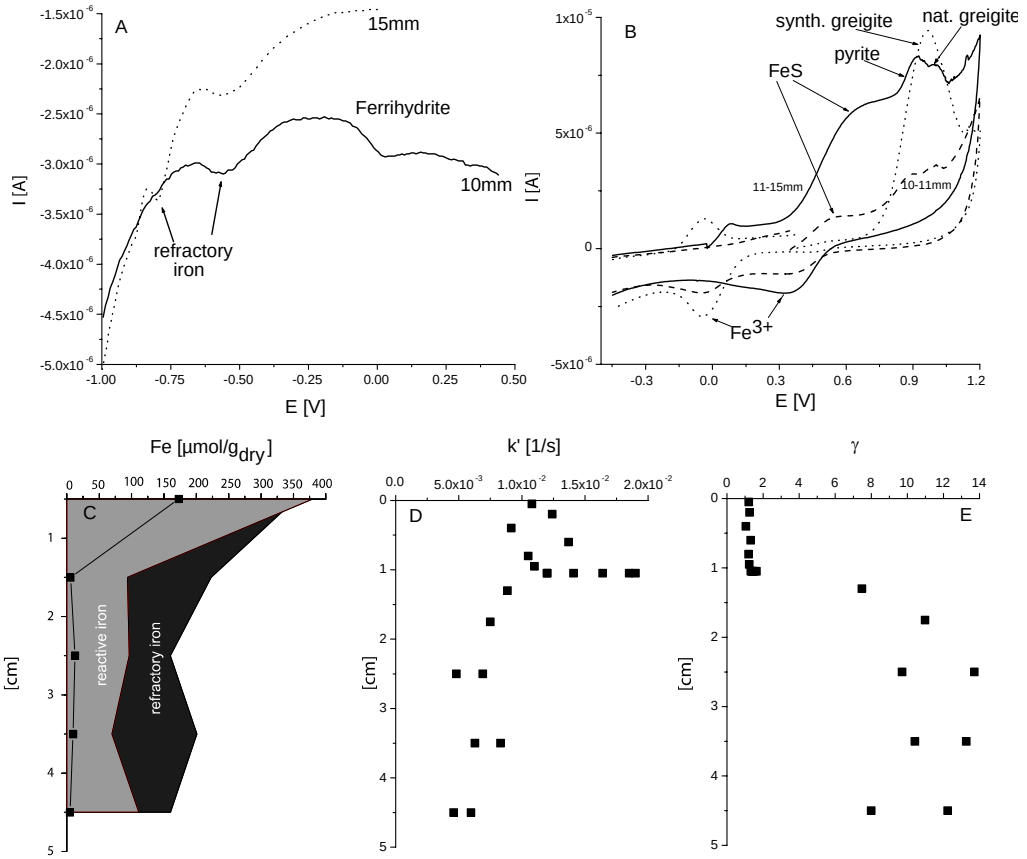

Figure 4.9 Flume sediment from a N´German harbor. A) Detection of different iron oxyhydroxide minerals at different depth intervals. B) Detection of different iron sulfide minerals (FeS, pyrite, greigite) at different depth intervals. C) Iron extraction depth profile. D, E) Reactivity profiles of k' and γ. Conditions used are the same as in Figures 7 and 8. The iron (oxyhydr) oxide reactivity decreases below 1 mm resulting in an increase of γ and a decrease of k'.

The occurrence of sulfide minerals and H_2S concentrations below detection level were supported by a high background level of reactive iron. The HCl extracted ferric iron decreased within the 1 cm from ~ 240 µmol/g_{dry} to almost zero (Figure 4.9C). A similar decrease could be observed for Fe_{acs}, but in contrast to HCl-Fe^{3+} the ascorbate extracted iron decreased from 380 µmol/g_{dry} to a background level of ~100 µmol/g_{dry} (Figure 4.9C). This high background level is an indication for the extraction of ferrous iron from iron sulfides minerals. Overall, the amount of extracted refractory and reactive iron is similar below 1cm.

Modeling of the reactivity changes resulted in increased *k'* values in a discrete zone between 10 mm to 11 mm depth. A high variability of the initial reactivity was observed by several chronoamperometric analyses at this depth interval (10 mm to 11 mm, Figure 4.9D). The increase in γ below 11 mm from values around 1.7 to ~10 and the simultaneously decrease of *k'* describe the decrease in the overall rate of reductive dissolution of the N´German harbor sediment (Figure 4.9E). The absolute increase in γ is lower as for the Eckernfoerde station E8-3. This is documented and supported by Table 4.2. The ratio of Q_{chrono} to Q_{LSV} decreased from values above 100 to values below 1. Comparing Q_{chrono}/Q_{LSV} *to* $Fe_{reactive}/Fe_{refractory}$ emphasizes that extracted ferrous iron was a major component of the reactive iron pool below 11 mm (Figure 4.9C, Table 4.2). The upper 11 mm were strongly regulated by reactive ferric minerals, while further down the refractory iron minerals dominated the biogeochemical processes.

Weddewarden. Figures 4.10A and 4.10B display the kinetic calculations for the bulk dissolution of ferric (oxyhydr)oxides. *k'* was constant from the surface to 5 cm depth while only a slight decrease was observed below this depth (Figure 4.10A). The variance of γ was small over the same depth interval (Figure 4.10B). In the upper 2 cm, the total iron pool consisted mostly of reactive iron. Further down an increase of refractory iron was observed (Figure 4.10C). Figure 4.10C shows also that the amount of ferric iron extracted by hydrochloric acid was stable (between 10 and 40 µmol/g_{dry}) with a minimum at 6 to 7 cm depth. The high reactive iron background concentration level was accompanied by the occurrence of pyrite and sulfide over the whole depth interval (i.e., voltammograms in Figure 4.10D). The comparison of Q_{chrono} to Q_{LSV} showed the highest value at 2.5 cm depth and a variance around 1 at all other depth intervals. Reactive iron (oxyhydr)oxides occurred over the entire investigated depth interval at Weddewarden, and this was reflecting in the small

change of k' and γ values. High organism activity is the reason for this high penetration depth of reactive (oxyhydr)oxides.

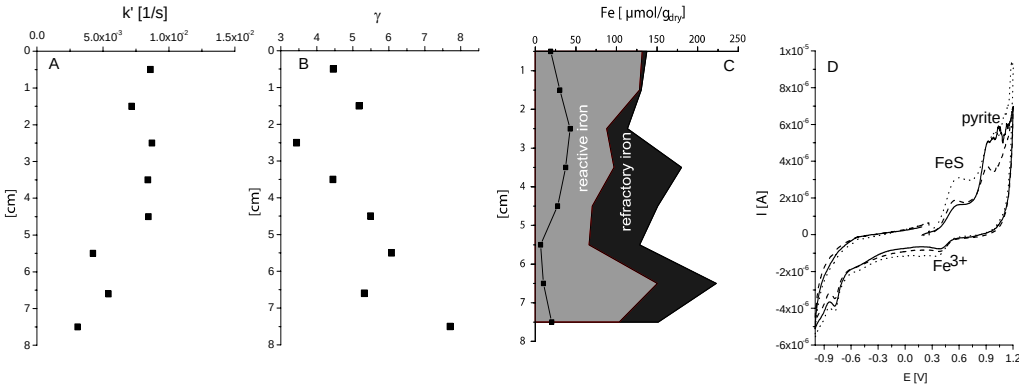

Figure 4.10 Weddewarden. A) Initial reactivity k' versus depth. B) γ versus depth. C) Solid phase characterization using different extraction protocols. D) Detection of different iron sulfide minerals (FeS, pyrite, greigite) at different depth intervals. Conditions used are the same as in Figures 7 and 8. The reactivity of the iron (oxyhydr)oxide pool changes slightly over depth.

Wuemmewiesen. The kinetic calculations for the freshwater station Wuemmewiesen showed a steeply decrease in k' from values of 0.006 s^{-1} to lower than 0.001 s^{-1} beneath 2 cm depth (Figure 4.11A). At the same depth, γ also decreases slightly (Figure 4.11B). The γ values comprise a range from ~1 to 2.5, which is similar to values calculated for synthetic reactive iron (oxyhydr)oxides reduced at –100 mV to –200 mV (Figure 4.2B, 4.3B). Chemical extractions methods showed a high background concentration of reactive iron, which varied within narrow borders over depth. Iron extracted by ascorbate was ~200 µmol/g_{dry} and HCl extracted ferric iron varied between 200 µmol/$g_{dry,}$ and 50 µmol/g_{dry}. The refractory proportion increases from ~20 µmol/g_{dry} to 100 µmol/g_{dry} over depth, but is always much lower than the reactive iron concentration (Figure 4.11C).

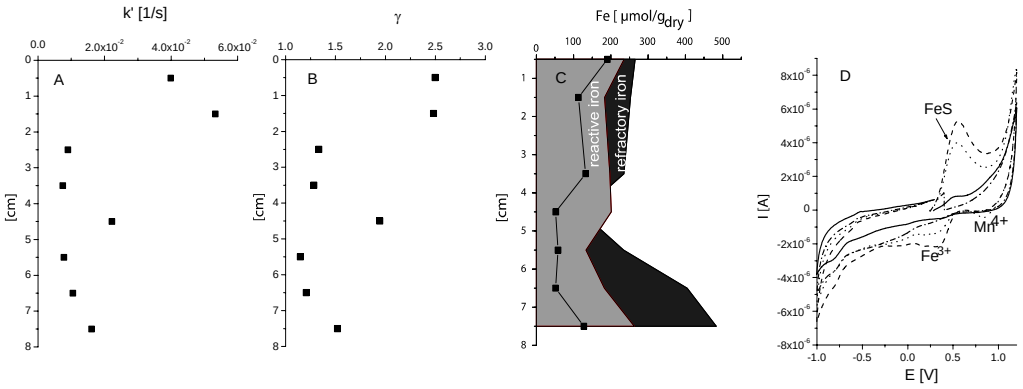

Figure 4.11 Wuemmewiesen. A) Initial reactivity k´ versus depth. B) γ versus depth. C) Solid phase characterization using different extraction protocols. D) Detection of different iron sulfide minerals (FeS, pyrite, greigite) at different depth intervals. Conditions used are the same as in figures 7 and 8. Less pronounced change in iron (oxyhydr)oxide reactivity over depth. The reactive iron background level is elevated in comparison to the described marine stations.

Q_{chrono}/Q_{LSV} also shows the dominance of the reactive iron fraction over the proportion of refractory iron minerals. This ratio varied in the range from 60 to 20 decreasing slightly with depth (Table 4.2). The level of this parameter indicate that most iron (oxyhydr)oxides were reduced at –100 mV to –200 mV, and therefore an effect of refractory iron on the γ value calculation is weak. In comparison to Eckernfoerde Bay E8-3, the N´German harbor sediment, and Weddewarden, a very strong FeS signal was detected at this unique freshwater station. No electrochemical signal was observed for pyrite or greigite (Figure 4.11 D). The large amount of precipitated FeS is unusual in a freshwater environment, but the wetland north of Bremen is fed by a subsurface salt deposit of the neighbor environment (Lilienthal, Germany). Sulfate reduction rate measurements of 1 µmol cm^{-3} d^{-1} and sulfate concentrations of 0.6 mM to 1.2 mM indicated high microbial activity and high sulfide reoxidation rates (unpublished data and personal communication: Dr. T. Ferdelman). Surprisingly, an electrochemical signal for Mn^{4+} reduction was detected by CSV in 2 cm to 4 cm depth. In cathodic experiments using LSV or DPV, a manganese signal was not observed. Therefore, it is unclear if the Mn^{4+} reduction signal results from anodic oxidation of Mn^{2+} during the anodic sweep of the cyclic measurements, or if the signal results from the direct reduction a natural Mn^{4+} compound.

By combining the results of solid state electrochemical (VIM) and classical extractions methods we have been able to identify the iron mineral composition of different environments and to describe the electrochemical bulk dissolution of the total iron pool treated as a reactive continuum. This discussion of four different environmental setting showed that the reactivity of iron oxides is strongly affected by the quality and diversity of the iron oxide pool. The comparison of the four environments (Eckernfoerde Bay E8-3, a N´German harbor sediment, Weddewarden, and Wuemmewiesen) showed significant differences in iron (oxyhydr)oxide reactivity with either dramatic (Eckernfoerde Bay E8-3) or only slightly (Weddewarden) reactivity changes over depth. Electrochemical detection of iron (oxyhydr)oxides or sulfide phases in combination with results of classical extraction protocols and other data allow a much better evaluation of the iron related biogeochemical processes. The electrochemical dissolution results are coherent with the classical extraction results and complement these by specific mineral detection.

A remarkable difference exists between wet chemical kinetic experiments using ascorbic acid and electrochemical kinetic experiments. The dissolution potential in electrochemical studies has always an effect on the overall reaction rate, while at high concentrations of ascorbic acid the reaction rate becomes independent of the concentration (Banwart, Davies et al. 1989; Postma 1993). The measured product of ascorbic dissolution experiments is the amount of dissolved ferrous iron. As the natural iron pool consists of ferric and ferrous iron minerals, the contribution of ferrous iron dissolution to the bulk mineral dissolution experiments has to be calculated, and subtracted for every time point of the kinetic experiment. Chronoamperometric experiments exclude a ferrous iron contribution, but the limit of the electrochemical approach is the calculation the total reduction charge Q_0, which is required for bulk reductive dissolution of the total ferric iron pool. Hence, a comparison of the two methods is only possible under defined conditions. In contrast to ascorbate experiments, the electrochemical dissolution experiments can be carried out within minutes while the bulk dissolution takes days to weeks using a wet chemical approach (Larsen and Postma 2001).

Further investigations have to be done using VIM to detect sulfide minerals in natural sediments. The mechanistic interpretation of the voltammetric oxidation of iron sulfide minerals is still not solved and has to be further investigated using a combination of VIM and spectroscopic methods to reveal the exact oxidation products. These first results show the potential to determine the presence of the intermediate greigite phase in the transforming process from FeS to pyrite. Comparative measurements with magnetic susceptibility analysis

have to be carried out to further evaluate to application of VIM to determine greigite in natural sediments.

VIM allows a better qualification of the iron phases in natural sediments in comparison to bulk extraction methods like classical extraction protocols of HCl, ascorbate or dithionite. In comparison to high-end analytical systems, like EXAFS and Mossbauer spectroscopy, VIM is a simple, inexpensive method allowing the screening of very complicate material compositions such as natural sediments.

Acknowledgements

We thank F. Scholz (University of Greifswald) for providing PIGE electrodes; T. Grygar for useful discussions of VIM, H. F. Passier (Netherlands Institute of Applied Geosciences, Utrecht, Netherlands) and M. Boetcher (MPI Bremen) for providing synthetic greigite. This research was supported by the Max Planck Society and the European Union (TREAD project, contract number: EVK-CT-2002-00081).

Chapter 5

Miniaturization of Voltammetric Microelectrodes for In-Situ Application in Natural Systems

Jochen Nuester and Ole Larsen*§*

*Max Planck Institute for Marine Microbiology, Celsiusstr. 1, D-28359 Bremen, Germany

DHI Water and Environment, Krusenberg 31, D-28857 Syke, Germany

In preparation

Abstract

Miniaturized iridium and silver based microelectrodes have been constructed and designed for laboratory and for in-situ studies. The construction, the advantages and disadvantages of different electrode materials (i.e., Ag, Ir) were discussed. This study gives an overview of the possibilities of microelectrodes and their limitations due to geometrical barriers. Miniaturized silver-based microelectrodes protected by a cellulose-acetate membrane can provide more information at submillimeter depth resolution in natural sediments, while iridium-based microelectrodes are most suitable for trace metal analysis in water column studies. Iridium-based microelectrodes showed good linearity with reasonable confidence intervals for the measurements of Pb and Cd. The used voltammetric parameters enabled a detection limit of 0.4 nM, but longer deposition times will allow lowering this limit. Silver-based microelectrodes showed good sensitivity and reproducibility for detection of O_2, Fe(II), Mn(II) and S(-II). The detection limits for Fe(II), Mn(II), and S(-II) are <12 µM, <4µM, and <0.8 µM, respectively. Finally, we demonstrate first depth profiling at millimeter resolution in a muddy N´German harbor sediment. The profiles observed are consistent with the known cycling of iron in this natural system.

5.1 Introduction

In-situ, real time measurements and speciation of transition elements in natural waters and sediments are strongly needed for quality monitoring purposes as well as to minimize artifacts such as contamination, losses by adsorption, or speciation changes which often occur during sampling, sample handling, and storage. In-situ measurements of transition elements like Pb, Cd, Cu, Mn, and Fe in natural environments represent a challenge for analytical and environmental sciences. The use of voltammetry is advantageous, because of the high sensitivity of this technique. Voltammetric electrodes are selective only to the mobile fraction of metals, i.e., free ions and small complexes, which diffuse quickly enough to be measured in the time scale of the voltammetric technique used, not to the total concentrations as with most other techniques.

In the last two decades, microelectrodes are developed for in-situ applications in natural waters, sediments, and biofilms (Revsbech, Joergensen et al. 1980; Jørgensen, Revsbech et al. 1983; Revsbech, Joergensen et al. 1983; Debeer, Sweerts et al. 1991; Brendel and Luther III 1995; Tercier, Parthasarathy et al. 1995). The development of voltammetric microsensors enabled the measurement of concomitant detection of different redox active species (Brendel and Luther III 1995; Tercier, Parthasarathy et al. 1995). These electrodes are most useful for water column studies, but unfortunately, none of these electrodes is entirely appropriate for applications to natural sediments. The interpretation of in-situ measurements in complex systems like natural sediments is highly dependent on the size of the used instrument. Natural sediments consist of different geochemical zones, which can vary horizontally and vertically within 50 µm distance (Joergensen 1977; Fenchel 1996; Shuttleworth, Davison et al. 1999). The use of existing voltammetric microsensors for sedimentary in-situ applications is consequently limited by the diameter of the electrode body (>200 µm)(Brendel and Luther III 1995; Tercier, Parthasarathy et al. 1995).

Fouling of the electrode surface by adsorption of macromolecular complexes of the sample remains one of the most serious limitations to the applicability of electroanalytical methods. To overcome this, studies have been done using different types of membranes based on size exclusion or electric charge repulsion (Hoyer and Florence 1987; Aldstadt and Dewald 1992; Lasalle, Limoges et al. 1994; Tercier and Buffle 1996; Belmont-Hebert, Tercier et al. 1998). A thick gel membrane, like an agarose gel, acts thereby as a dialysis membrane, i.e., allows diffusion of small metal ions and complexes, but retains colloids and macromolecules.

It was shown that these membranes are very inert and allow measurements of redox active species in the equilibrated membrane. The thickness of the membrane determines the equilibration time (Tercier and Buffle 1996; Belmont-Hebert, Tercier et al. 1998). Applications of agarose-membrane covered mercury-plated iridium-based microelectrodes and microelectrode arrays for direct speciation of Pb(II) and Cd(II) in synthetic water samples containing fulvic compounds, and natural waters have demonstrated the efficiency of these thick agarose gel membranes against electrode fouling (Tercier and Buffle 1996; Belmont-Hebert, Tercier et al. 1998). Cellulose acetate is another useful membrane material for this purpose. In test studies, it was shown that electrodes covered with such membranes offered a dramatic reduction of the adsorption interference with humic acids (Hoyer et al., 1999).

The voltammetric measurement of transition elements with microelectrodes was either done with mercury covered iridium microelectrodes, or with gold amalgam electrodes (Brendel and Luther III 1995; Tercier, Parthasarathy et al. 1995). Iridium based mercury microelectrodes were mainly applied to detect pico molar concentrations of heavy metals in aqueous systems, like cadmium or lead (Tercier, Parthasarathy et al. 1995; Tercier and Buffle 1996; Buffle, Tercier et al. 1997; Buffle, Wilkinson et al. 1997; Belmont-Hebert, Tercier et al. 1998), while gold amalgam microelectrodes were mostly applied to detect Fe(II), Mn(II), S(-II) and O_2 in sedimentary environments (Brendel and Luther III 1995; Luther, Brendel et al. 1998; Dollhopf, Nealson et al. 1999; Luther, Glazer et al. 2003).

The aim of this paper is to describe the miniaturization of iridium- and silver-based voltammetric microelectrodes, and to detect transition elements and other dissolved compounds in sedimentary or water column environments. Our major goal was to reduce dimensions of the electrode body allowing comparable measurements to other amperometric or potentiometric microsensors, and to minimize the disturbance of the sedimentary framework. In addition, agarose gel and cellulose acetate membranes were tested.

5.2 Experimental Section

5.2.1 Instrumental Set-Up

A μAutolab III, multimode polarograph with the software package GPES 4.9 (Ecochemie, Utrecht; Metrohm, Filderstadt) was used. Its small dimensions and high sensitivity makes it suitable for in-situ measurements. Unless specified, a three-electrode

system was used, with an Ag/AgCl/3 M KCl reference electrode (Metrohm, Germany), and a platinum rod as counter electrode. For sedimentary studies a homemade Ag/AgCl/ 3M KCl agarose reference electrode was used. Calibration and sediment profiling were carried out in a Faraday cage.

5.2.2 Voltammetric Procedures

All voltammetric measurements were carried out in the linear sweep (LSV) or the square wave mode (SWV), if not stated otherwise. Square wave anodic stripping analysis (SWASV) was recorded using the following instrumental settings: deposition potential, -1.1 V; deposition time, 30 s to 15 min; scan range, -1.1 V to –0.1 V; pulse height, 25 mV; step potential, 8 mV; conditioning potential, -0.1 V; conditioning time, 60 s; equilibration time, 5 s; frequency, 50 Hz. Linear sweep voltammetry to detect oxygen was carried out using the following instrumental settings: start potential, -0.1 V; final potential, -2 V; scan rate, 200 mV/s; conditioning potential, -0.1 V; conditioning time, 60 s; equilibration time, 5 s. LSV to detect sulfide was done under the following conditions: start potential: -0.1 V, final potential, -2 V; scan rate, 200 mV/s to 900 mV/s; conditioning potential, -0.8 V, conditioning time, 60 s, equilibration time, 5 s. Square wave voltammetry used to detect Fe(II) and Mn(II) was recorded using the following settings: start potential, -0.1 V; final potential, -2 V; frequency 50 Hz, amplitude potential, 25 mV; step potential, 2 mV; conditioning potential, -0.1 V; conditioning time, 60 s to 120 s; equilibration time, 5s.

5.2.3 Sediment Sampling and Core Analysis

The sampling site was a laboratory flume in which sediments of a north German harbor were studied. All samples were taken with Plexiglas core tubes approximately 10 cm long and 4 cm wide. Stoppers were placed in the bottoms of the tube, and the voltammetric analysis was started within two hours after sampling. Sediment profiles were measured by lowering the microelectrode into a core with a micromanipulator and taking measurements at millimeter intervals, usually in duplicate or triplicate to determine the reproducibility and response of the microelectrode. The reference, the counter, and the working electrode were arranged in a circle with 1 cm in diameter. The electrodes were allowed to equilibrate for 1 min at each depth prior to conditioning and application of the voltammetric mode.

5.2.4 Reagents

Analytical grade chemicals $Fe(NH_4)_2(SO_4)_2*6H_2O$, $MnCl_2*4H_2O$, H_2S (Flukka), and Milli-Q water were used to make standard calibrations. All calibrations were done using filtered Wadden Sea water (0.4 µm nuclepore filter). When iron calibration experiments are done at pH >5.5, sodium dithionite ($Na_2S_2O_4$) was added (final concentration: ~2 mM). Sodium dithionite was used to reduce any ferric iron so that Fe(II) calibrations can be made. Standard calibrations of Pb(II) and Cd(II) have been made by diluting 0.1 M AAS calibration solutions (Flukka).

5.3 Microelectrode Design

5.3.1 Iridium Wire Soldering

Owing to the high melting point of iridium (2453°C), soldering of an iridium wire to a shielded cable was found to be problematic (Tercier, Parthasarathy et al. 1995). In the study of Tercier, Parthasarathy et al. (1995) it was shown that electronic bombardment under vacuum results in an optimum contact between an iridium wire and a copper wire. In our study, we joined the irdium with a silver wire (Ø 300 µm, Allgemeine Gold- und Silberscheideanstalt AG, Germany) by direct brazing. During voltammetric measurements, the electrode was connected to a low noise shielded electronic cable using alligator clamps.

5.3.2 Etching Process of Iridium, Gold and Silver Wires

The etching process was carried out after the descriptions by Tercier et al. (1995). The end of an iridium wire (Ø 100 µm, Johnson Matthey, UK) was etched in a homemade Plexiglas cell against four titanium rod reference electrodes (Ø 5mm, Goodfellow, UK) in a saturated KCN solution. The etching process was controlled via a coupled homemade volt- and ampere-meter. The etching process was started by immersing 1cm of the iridium wire into the etching bath using a micromanipulator (Merzhäuser Wetzlar GmbH, Germany). The initial current was set to 1 A, and the cut off current was 200 mA. Sometimes a second etching process was carried out from 300 mA to 150 mA to obtain optimal iridium tip shapes. Optical microscope observations were carried out after each etching step. The etched iridium wires were cleaned in water and alcohol.

Silver wires (Ø 125 µm, Allgemeine Gold- und Silberscheideanstalt AG, Germany) were etched in a homemade Plexiglas cell with a graphite rod as counter electrode. The wires were carefully dipped into a saturated KCN solution, and manual up and downward movement of the wires resulted in a tip diameter of 5 µm to 10 µm. After finishing, the tip shape was microscopically inspected.

5.3.3 Internal Casing

The internal glass casing of the electrode was made of precleaned soda-lime glass capillaries, which are pulled and thinned over a heating flame (Figure 5.). The thinned glass section was formed by hanging vertically through an electrical heating loop (Fecralloy-Eisen/Chrom, Ø 1 mm, Goodfellow, UK) and pulled gravitationally down. The melting of the glass was stopped when the glass has diameter of 100 µm or less. The tip diameter of the internal glass casing was formed by a small heating loop of 25 µm thick platinum wire (Goodfellow, UK) (Ø 10µm to 20 µm). The whole process was controlled by a micromanipulator and a stereomicroscope (Zeiss, Germany). The etched wires (iridium, silver, gold) were inserted into the internal glass capillary under microscopic observation and fixed at the end of the casing by a quick drying epoxy, while the tip of the wire touches the tip of the glass body (Figure 5.1).

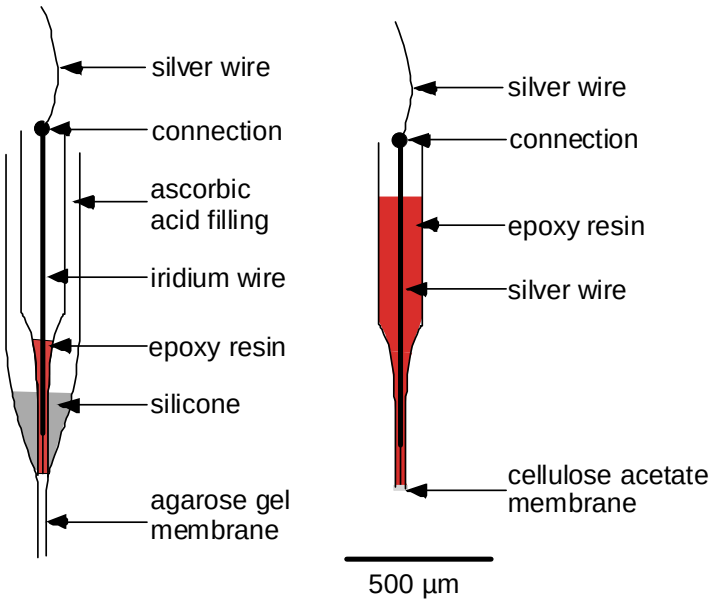

Figure 5.1 Drawing of an iridium based mercury electrode (A) and a silver based amalgam electrode (B).

5.3.4 Sealing

The sealing of the metal wire to the glass casing has to be tight, and no entrapped air bubbles should touch the metal wire. For application in marine environments, it is necessary to investigate the sealing material (i.e., the epoxy resin) concerning the stability in seawater. A further aspect is the viscosity of the sealing material, especially if irdium is used. The sealing material has to have a good sealing quality to the metal wire and the glass casing, but the viscosity of the material has to be low enough that the electrode will not break owing to an applied potential. The reason for this is unknown, but we assume that the iridium wire starts to vibrate by an imposed potential, especially if the potential is not swept linearly. Different types of sealing materials were studied such as crystal cement, silicone, and different types of epoxy resins. The crystal cement was too viscose, and the electrode broke during square wave voltammetric experiments. The polishing of electrodes filled with silicone showed poor results, and several applied epoxy resins were not stable in seawater. The epoxy resin of West Systems (105 epoxy resin and 206 hardener) showed the optimum characteristics (i.e., high purity, nonconductive, transparent), and no alteration was observed during use in seawater. In order to seal the electrode into the glass casing, the epoxy resin was injected with a syringe and an injection needle. The sufficient drying time of the epoxy resin was 48 hours.

5.3.5 Polishing

Once constructed, the electrode tip surface was polished. The disk morphology is a very important parameter in obtaining reproducible sensors. This parameter strongly depends on the polishing material and the procedure used. Different types of materials were tested such as diamond paste and aluminum powder dispersed on polishing pads. These materials appeared to be not appropriate, because the microelectrodes with a 10 µm to 30 µm tip diameter broke easily due to the strength of the fibers of the polishing pads. Optical controlling of some in this way polished electrodes showed scratches on the tip surface, and the aluminum powder could not completely be removed. The use of ultrasonification to clean the surfaces destroyed the microelectrode bodies. Best polishing results were received using diamond-lapping films (Ø 0.01 µm to 10 µm, Ultra prep diamond discs, Buehler, Germany).

Initially polishing was done by hand. It appeared that such procedure was not successful, because either the electrodes broke, or the time required to obtain a mirror like surface was very long (6 to 8 hours). In order to ensure a high quality of smooth electrode

surfaces, a homemade polishing setup was constructed. An essential requirement was optical control during the polishing process. Therefore, a polishing setup was developed consisting of of homemade polishing plate connected to a variable voltage source, a micromanipulator, and a stereomicroscope (Zeiss, Germany). The micromanipulator was used to hold the electrode in place, and to steer the electrodes movements. The whole polishing process was observed using the stereomicroscope. After finishing, the polish was inspected by an optical inverted microscope (Zeiss, Germany), and a normal optical microscope (Zeiss, Germany). Successful polishing results in a plain and mirror like electrode tip surface.

5.3.6 Electrode Plating and Polarization

Mercury was plated onto the Ir and Ag substrates at –400 mV (vs. Ag/AgCl/3 M KCl/1 M $NaNO_3$) in a deoxygenated 5 mM $Hg(CH_3COO)_2$ and 0.1 M $HClO_4$ solution (Tercier, Parthasarathy et al. 1995). Under these conditions, nucleation and growth of mercury nucleus were optimum (Figure 5.2). The iridium-based and the silver-based microelectrodes could be used at this stage of preparation for applications, but for the silver-based electrodes, it was necessary to add a polarization step to optimize the sensitivity and the reproducibility, and the iridium-based microelectrodes have to be covered with a membrane to avoid electrode fouling and to stabilize the mercury drop. The silver-based electrodes were placed in a 1.0 M $NaNO_3$ solution and polarized at –5.0 V for 30 seconds. During this time, the evolution of hydrogen gas can be observed from the reduction of water at the electrode surface. The evolution of hydrogen continues for some time after the potential is removed due to the reaction of sodium amalgam with water. In comparison to Brendel and Luther (1995), the polarization time was reduced to 30 seconds, because a longer polarization time destroyed the amalgam surface, and restricts the use of the electrode to potentials above -1.3 V. Hence, the detection of Mn(II) and Fe(II) was not possible.

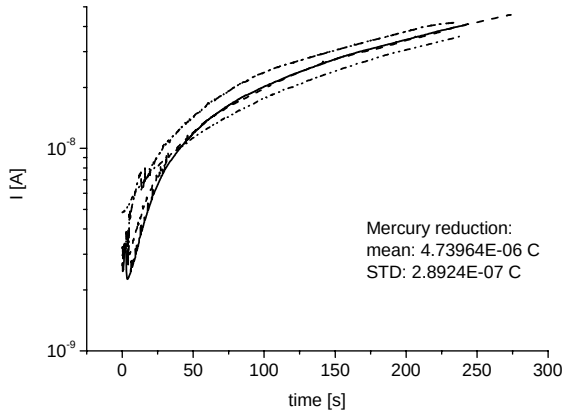

Figure 5.2 Mercury plating on iridium based microelectrodes: chronoamperometric potential: -0.4 V in 0.1 M $HclO_4$ and $5x10^{-3}$ M Hg^{2+}.

Miniaturized iridium-based mercury microelectrodes were renewed by reoxidizing the mercury droplet using linear sweep voltammetry from –300 mV to 300 mV at 5 mV/s in a deoxygenated solution of 1 M potassium thiocyanate (Tercier, Parthasarathy et al. 1995). A new mercury droplet was plated afterwards. This option was not possible for gold and silver amalgam microelectrodes. Thus, polishing of the electrode surface between each mercury deposition was necessary for gold and silver based mercury electrodes.

5.3.7 Surface Stabilization and Organic Fouling

Tercier and Buffle (1996) showed the application of iridium-based microelectrodes covered with a thick agarose membrane to protect against the electrode against fouling by organic molecules. The use of such membranes in front of iridium based miniaturized microelectrodes is more difficult. An additional external electrode body was necessary to attach an agarose gel membrane in front of the miniaturized microelectrodes. A Pasteur glass pipette was used as external electrode body, and was formed as described for the internal electrode casing. The tip of the external capillary was filled afterwards with an agarose membrane (1.5% Agarose LGL, Biofinex, Switzerland) by dipping the glass body in a warm agarose bath. The thickness of the membrane was between 200 µm and 500 µm, and was

dependent on the geometry of the glass body. Unfortunately, the membrane thickness could not be controlled.

The internal electrode casing was then immediately inserted in the external glass body. The internal casing was in place when it touched the agarose membrane, and was fixed by a quick drying epoxy resin at the upper end of the electrode body. After fixation, the lower end of the external electrode body containing the agarose gel membrane was inserted into a Pasteur pipette with Milli-Q water, allowed to equilibrate for at least 3 hours. The space between the internal casing and the external electrode body was filled with a low viscosity silicone (Sylgard 184, Dow Corning, Germany) to avoid dehydration of the membrane. After curing of the silicone, the external electrode body was filled with an ascorbate solution (20 % ascorbate in 3 M KCl and 0.1 M NaOH) to avoid internal oxygen penetration.

This construction allowed protection against electrode fouling and mercury drop stabilization. The mercury droplet was plated on the iridium substrate through the agarose membrane using voltammetric conditions as described above (Tercier and Buffle 1996). Unfortunately, the plating process was only successful in a few cases. The physical stability of the agarose gel membrane and the small agarose volume (volume, ~ $4*10^{-6}$ ml; thickness, 400 µm; diameter, 70 µm) may have a negative effect on the drop forming process. For microelectrodes with a an electrode body diameter of 1 mm, the agarose membrane volume is ~$1.25*10^{-3}$ ml (membrane thickness: 400 µm), and the mercury plating shows no limitations (Tercier and Buffle 1996).

Alternatively, cellulose acetate membranes were used to protect the iridium- and the silver-based microelectrodes. Therefore, the electrodes were dipped quickly in a solution consisting of 10 % cellulose acetate dissolved in acetone. A small and invisible cellulose acetate film covered the electrode surface. The iridium based electrodes were covered before mercury plating, and the gold and silver electrodes were covered after the amalgam formation.

Additionally, the electrodes were electrochemically protected against fouling by extending final potential to -1.8 V to -2.1 V in seawater (Brendel and Luther 1995). Ending the scans at this negative potential causes the reduction of sodium, the production of hydrogen, and the electroreduction of organic matter after each voltammetric sequence. This eliminates the continuous adsorption of organic matter onto the electrode after each measuring cycle. Accumulation of organic matter would result in a negative shift of the redox

potential of the analyzed redox active compounds, or suppress the signal of the measured species (Brendel and Luther III 1995).

5.4 Results and Discussions

5.4.1 Calibration of Miniaturized Mercury-Plated Iridium-Based Microelectrodes

Mercury-plated iridium-based microelectrodes protected by an agarose gel membrane were used for speciation of Pb and Cd without any sample pretreatment. These two metal species were chosen because these two elements belong to reversible redox systems, and they are important trace elements in environmental systems. Standard calibration experiments were carried out for both metals in deoxygenated seawater in the range of 10^{-9} M to 10^{-7} M (Figure 5.3). An average slope of 5.4 +/- 0.04 pA/nM for Pb(II) and 3.21 +/- 0.08 pA/nM for Cd(II) were obtained (Figure 5.3B). The background current of the electrode was shifting (Figure 5.3A), and a calculation of the peak heights was depending on background current shape. The addition of some suspended sediments to the last metal addition did not change the signal response. This preliminary test indicates that the miniaturized mercury-plated iridium-based microelectrodes covered with an agarose membrane can be used in complex environmental systems. Removing the electrode from the suspension showed that the outside of the electrode body was covered with a thin brownish sediment matrix, but this adsorption has no effect on the diffusion of Pb(II) and Cd(II) into the agarose membrane.

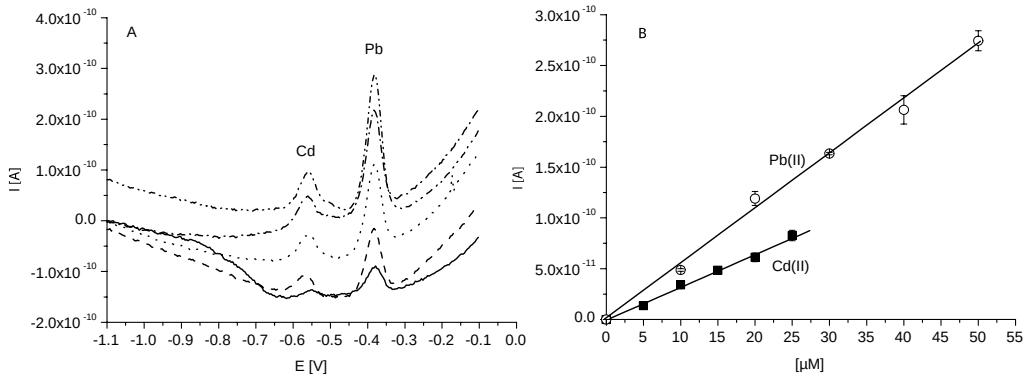

Figure 5.3 A: Standard addition of lead and cadmium and B) calibration plot in deoxygenated seawater. Square wave stripping voltammetry: deposition potential, -1.1 V; deposition time, 60 s; final potential, 0.1V; frequency, 50Hz; amplitude, 25mV; step potential, 8mV; conditioning potential, -0.1 V; conditioning time 60 s; equilibration time, 5 s.

The stability of the mercury droplet was tested in long time experiments. At three following days, square wave anodic stripping voltammograms were recorded using the same mercury droplet, but different concentrations of Pb (10 nM, 20 nM, and 10 µM) and different deposition potentials (Figure 5.4). The electrode was left in open circuit in the metal spiked seawater solution between the three days. Figure 5.4 displays the results of this experiment. The experiments with a Pb concentration of 10 nM and a deposition time of 100 s had a standard deviation of 6 %, the following experiment with 20 nM Pb and 300s deposition time showed a standard deviation of 1.5 %, and the last test with 10 µM Pb and 30 s deposition time had a standard deviation of 2.3 %. Either increasing the concentration and/or the deposition time reduced the measurement error. The results showed that reproducible analyses were obtained even after storing the electrodes in a seawater solution over night. A sensitivity change from one day to another was not experimentally tested. The application of such miniaturized mercury-plated iridium-based microelectrodes to detect Fe(II), Mn(II), and S(-II) was limited due to the instability of the electrode surface. Measurements with low concentrations of Fe(II) (50 to 80 µM) showed disturbances and very noisy voltammograms. Further increase of the Fe(II) concentrations resulted very broad and unspecified signals. The measurement of sulfide was also limited, only the detection of Mn(II) showed no complications. In-situ investigations in sediment cores showed that the agarose gel membrane was not stable in such environments. Therefore, the application of miniaturized mercury-plated iridium-based microelectrodes was not studied further.

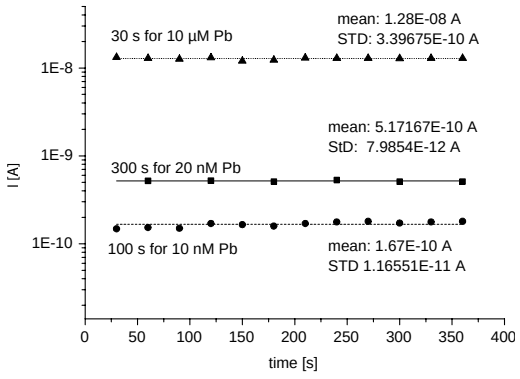

Figure 5.4 Long time measurement series for 20 nM Pb and 10 µM Pb for different deposition times: 100 s and 300 s for 20 nM Pb and 30 s for 10µM Pb. SQWV: frequency 50 Hz, amplitude 25mV, step potential 8mV, deposition potential 1 V, final potential –0.1 V.

5.4.2 Application of Silver Based Amalgam Miniaturized Microelectrodes

5.4.2.1 Conditioning

For marine sediments, the predominant electroactive species are O_2, H_2S, Fe(II), and Mn(II). To maintain reproducibility during the analysis, it is very important to condition the electrode at a potential, where the redox species is not active. We found out that a conditioning potential of -0.1 V for a period of 60 s is required to restore the electrode surface before measuring Fe(II) or Mn(II) in H_2S free environments. To optimize and to avoid any influence of H_2S, we used a standby potential of –0.8 V in SWV measurements to determine Fe(II) and Mn(II). At this potential H_2S, HS^-, and polysulfides (S_x^{2-}) do not undergo a redox reaction. This standby potential eliminates any influence of sulfide deposition at the electrode surface. Prior to any SWV measurements for Fe(II) and Mn(II) detection, the standby potential was reset to –0.1 V for 60 s. The conditioning and the standby potential were set to –0.8 V in LSV measurements to detect H_2S. For detection of oxygen using LSV, the standby potential and the conditioning potential were set to –0.1 V to avoid an oxygen depletion before sweeping the potential.

5.4.2.2 Oxygen Calibration

The advantage of voltammetry to detect concomitantly several electroactive species is presented in Figure 5.5. These voltammograms show the concomitant reduction of O_2, H_2O_2, and Mn(II) in the linear sweep and the square wave mode. Figure 5.5 illustrates that the reduction at the miniaturized silver amalgam fulfills the theoretical requirements that $E_{peak}(SWV) = E_{half\text{-}wave}(LSV)$. The uncatalyzed reaction of manganese with oxygen is low (Diem and Stumm 1984); therefore, a simultaneous electrochemical detection of both species is possible. According to Osteryoung and Osteryoung (1985), square wave voltammetry is the mode of choice for reversible electrode reactions due to increased scan rates and higher sensitivities. The square wave signal is a composite signal of the difference between a forward and a backward scan; hence, a sensitivity gain is not expected for irreversible electrode reactions. In fact, we noticed a decrease in sensitivity for oxygen in the SWV mode in comparison to the LSV mode (Figure 5.5).

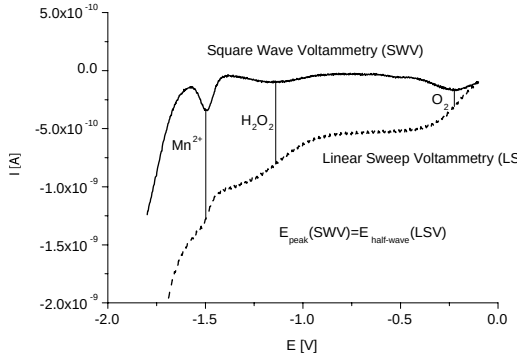

Figure 5.5 Detection of oxygen and manganese in SWV and LSV mode. Comparison of peak potentials of the square wave mode and the half-wave potential of the LSV mode. LSV: starting potential, -0.1 V; final potential, -1.8 V; scan rate, 200 mV/s; equilibration time, 5 s. SWV: start potential, -0.1 V; final potential, -1.8 V; frequency, 50 Hz; amplitude, 25 mV; step potential, 2 mV; conditioning potential, -0.1 V; conditioning time, 60s; equilibration potential, 5 s.

However, this was not true for the measurement of Mn(II) or Fe(II). Both reactions are not strict reversible, but the signal sensitivity was increased using SWV (Figure 5.5) (Brendel and Luther III 1995). H_2S was detected in the LSV mode, because it showed most promising results. Increasing the scan rate in the LSV mode and using microsensors result in an increased signal response and enables measurements at lower detection limits. We found it advantageously to use different voltammetric modes for the different interesting compounds. This minimizes electrode stability conflicts. Figure 5.6 shows the oxygen removal in seawater for standard calibration experiments. The comparison of different purging times with purified nitrogen gas illustrates the sensitivity of the miniaturized silver amalgam electrodes for the detection of oxygen. Due to the high sensitivity of this electrode reaction, a quantification of the partial pressure of oxygen is possible, but the changing background current level at –0.1 V sets limits to this calculation.

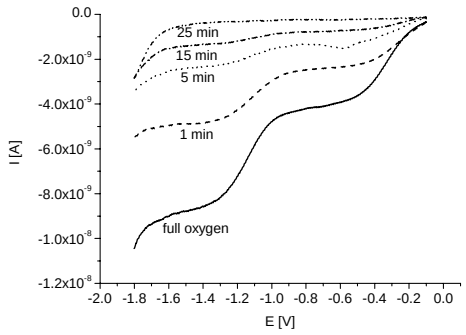

Figure 5.6 Oxygen removal of filtered seawater (31 ‰, pH 8) in a voltammetric cell. The duration of the purging time with purified nitrogen gas are given in the figure. LSV conditions: start potential, -0.1 V; final potential, -1.8 V; scan rate, 200 mV/s; equilibration time, 5 s.

Oxygen reduction is a two-step process. In the first step oxygen is reduced to hydrogen peroxide (E_{peak} (SWV) = ~ -0.3 V), and the produced hydrogen peroxide is further reduced to water (E_{peak} (SWV) = ~ -1.2 V) (Figure 5.5). The reduction of oxygen and H_2O_2 are each one electron transfer processes, and hence, the voltammetric reduction signal for both species is similar. Elevated signals for H_2O_2 are expected, if H_2O_2 is formed during the aerobic decomposition of organic matter compounds (Brendel and Luther III 1995).

5.4.2.3 Calibration of Mn(II)

Manganese is considered to be the easiest reducible ion at negative potentials below – 1.3 V. Figure 5.7B shows a calibration plot of Mn(II) reduction using a miniaturized silver amalgam microelectrode. The open circles represent reduction current peak heights of subsequent added Mn(II) into filtered seawater with a salinity of 31 ‰ in the concentration rage from 5 µM to 300 µM. Figure 5.7 shows typical voltammograms of a standard manganese reduction experiment (Figure 5.7A), and the corresponding calibration plot (Figure 5.7B). An average slope of 87 +/- 0.27 pA/µM for Mn(II) was obtained. The calculated minimum detection limit was lower than 4 µM.

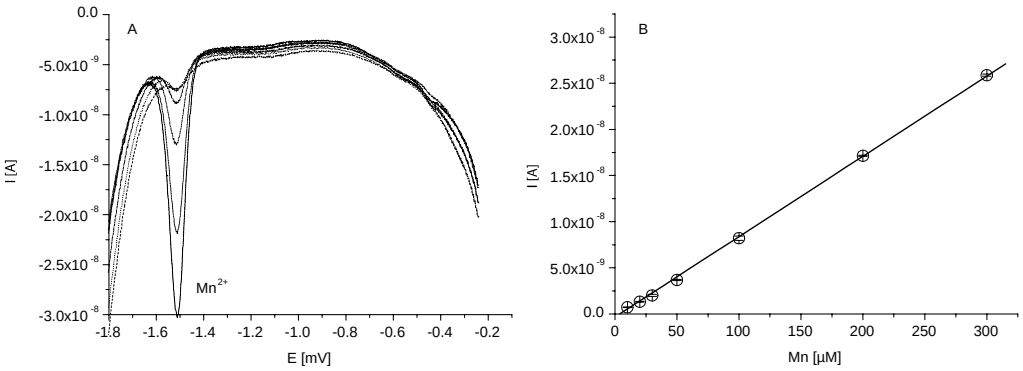

Figure 5.7 Calibrations of Mn(II) reduction in seawater (31 ‰, pH 8) using SWV: start potential, -0.1 V; final potential, -1.8 V; frequency, 50 Hz; amplitude, 25 mV; step amplitude, 2 mV, conditioning potential, -0.1 V, conditioning time, 60 s; equilibration time, 5 s.

As the oxidation of manganese by oxygen is very slow without catalysis, manganese calibrations can be used in principle as a "pilot ion method" to recalculate calibration plots of other elements of interest. It is assume that the ratio of the calibration slopes for each element should be stable. This would simplify the calibration procedures for the detection of all redox active elements in the potential window of the electrode. We found out that detailed calibrations for Mn(II), Fe(II), H_2S, and O_2 with one electrode results in a decrease of sensitivity with time. The calibrations of every element are very time consuming, but unfortunately, we observed that the pilot ion method is highly dependent on the quality of the electrode.

5.4.2.4 Calibrations of Fe(II)

The calibration curves for the reduction of Fe(II) showed a peak broadening, and the voltammograms were more scattered in comparison to Mn(II) reduction experiments (Figure 5.7). Figure 5.8 displays iron reduction voltammograms and standard calibration curves. The squares in Figure 5.8B represent reduction current peak heights of subsequent added Fe(II) ion into filtered seawater with a salinity of 31 % in the concentration rage from 20µM to 500 µM.

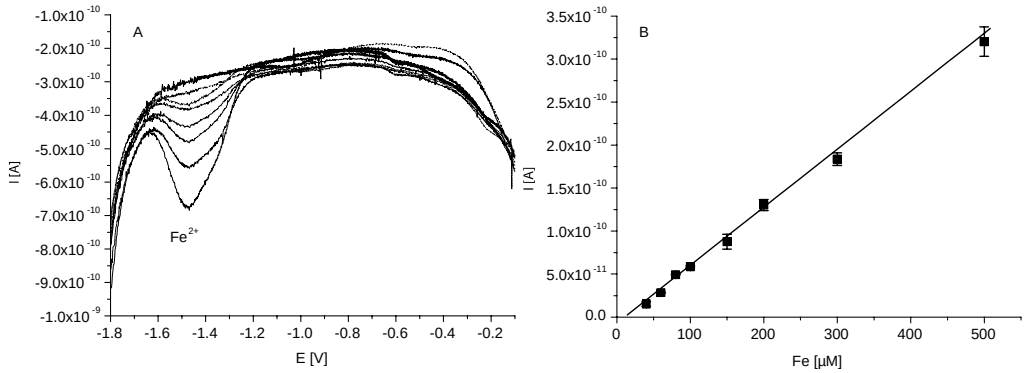

Figure 5.8 Standard addition of Fe^{2+} in seawater (31 ‰, pH 8). Square wave voltammetry: start potential, -0.1 V; final potential, -1.8 V; frequency, 50 Hz: amplitude, 25mV; step potential, 2mV; conditioning potential, -0.1 V; conditioning time, 60 s; equilibration time, 5 s. Peak broadening is characteristic for the reduction of Fe^{2+}.

An average slope of 0.67 +/- 0.011 pA/µM for Fe(II) was obtained. The calculated minimum detection limit was below 12 µM. The error bars for the standard deviation increases with increasing Fe(II) concentration. As metal iron does not react with mercury, and is also not wetted by liquid mercury, a deposition of metal iron at the electrode surface probably caused the change in sensitivity (Galus 1975; Galus 1984). Similar observations have been made by Ciszkowska et al. (1994) and Pizeta et al.(2003). Both studies concluded that silver amalgam electrodes are more appropriate for Fe(II) detection than gold amalgam electrodes. In contrast, the group of Luther (Brendel and Luther III 1995; Luther, Brendel et al. 1998; Dollhopf, Nealson et al. 1999; Dollhopf, Nealson et al. 2000; Taillefert, Bono et al. 2000; Luther, Glazer et al. 2003) showed reliable analytical results with gold amalgam electrodes. The electrodes used in these earlier studies are 100 µm in diameter(Brendel and Luther III 1995) or 30 µm in diameter (Pizeta, Billon et al. 2003), and therefore six to 20 times larger than the electrodes used in this study. The application of larger electrodes is probably advantageous in environments with higher Fe(II) concentration. However, most porewater of marine sediments do not show Fe(II) concentration above 600µM (Canfield, Joergensen et al. 1993; Canfield, Thamdrup et al. 1993; Thamdrup, Fossing et al. 1994; Thamdrup and Canfield 1996).

5.4.2.5 Calibrations of H_2S

Species of sulfur can be found in sediment porewater. The sulfur species have a large affinity to other metals (Fe, Cd, Cu, …..), and are important for biogeochemical and microbiological processes (Berner 1971; Joergensen and Fenchel 1974; Jørgensen 1990; Thamdrup, Finster et al. 1994; Schippers, Jozsa et al. 1996; Canfield, Boudreau et al. 1998; Habicht, Canfield et al. 1998; Canfield and Raiswell 1999; Canfield 2001; Schippers and Jørgensen 2002). The detection of sulfide is difficult due to the possible formation of thick HgS layers on the electrode surface. Figure 5.9 presents voltammograms of S(-II) standard additions in seawater in the range from 1µM to 100µM. With each standard addition the peak potential moved to more negative values (-0.63 V to 0.78 V), due to pH changes of the seawater electrolyte. The resulting signal of the voltammetric experiments is a composite signal of several processes. H_2S, HS^-, and polysulfides (S_x^{2-}) form HgS at potentials more positive than –0.5 V. Therefore the voltammetric signal actually represents the total sulfide concentration (ΣS(-II)).

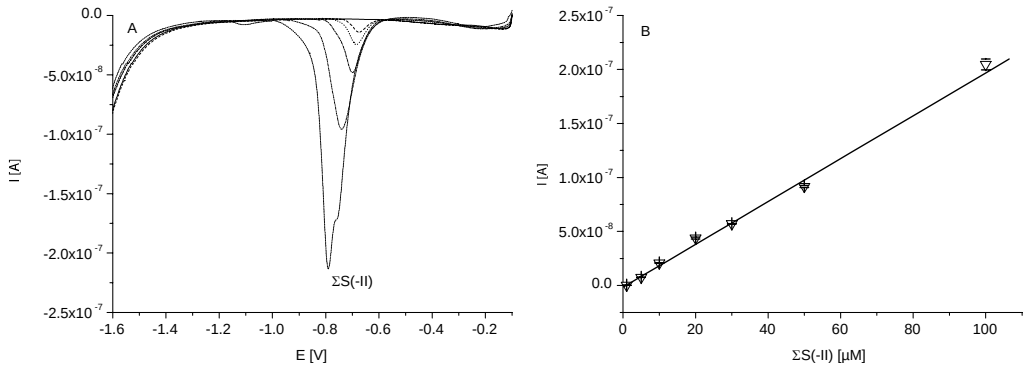

Figure 5.9 Standard addition of total S(-II) in seawater (31 ‰, pH 8). Square wave voltammetry: start potential, -0.1 V; final potential, -1.8 V; scan rate, 0.8 V/s; conditioning potential, -0.8 V; conditioning time, 60 s; equilibration time, 5s.

As described in part "*Conditioning*", the polarization time for potentials more positive than –0.5 V should be minimized to avoid the formation of thick HgS layers, which cannot be removed completely. Additional to the use of a conditioning potential of –0.8 V, the increase of the scan rate has a positive effect on the electrode conditions. Using scan rates above 800 mV/s allow cathodic measurements for sulfide concentrations above 100 µM. This is indicated in Figure 5.8, where a linear correlation is shown up to 100 µM. An average slope of 1.98 +/- 0.004 nA/µM for ΣS(-II) were obtained with a minimum detection level lower than 800 nM. To avoid the formation thick HgS layers on the electrode surface, it is possible to change the voltammetric sweep from –1.7 V to –0.1 V. This change results in an oxidation of the dissolved sulfide without any previous deposition step.

5.4.3 Environmental Applications

First in-situ applications to sediments were done in cores of muddy harbor sediment of N´German, which was used in a flume to study natural processes under laboratory conditions. The top layer of the sediment was reddish brown, and had a thickness of 1 cm to 1.5 cm. Oxygen was only studied qualitatively, because calibrations were limited to variation of the background signal (see *Oxygen calibrations*). No oxygen signal was observed below 5 mm (the qualitative data are not shown).

No manganese signal was recorded over the entire measured depth interval. Sulfide was only detected using a longer deposition potential (>30 s), but this preconcentration step destroyed the microelectrode and therefore only a qualitative evidence is given that sulfide occurs in low concentration below the reliable resolution of the voltammetric microsensor. This result was concurrent with the findings of H_2S amperometric microsensor measurements. Sulfide concentrations were therefore far below detection limit. Figure 5.10 shows the results of the first in-situ sediment core measurements. The distance of the three profiles was about 1 cm. Fe(II) was detected below 10 mm. The increase of dissolved ferrous iron is very strong to ~300 µM within 2 cm. Figure 5.10B shows typical voltammograms of these in-situ measurements. The voltammetric measurements showed a lot of noise, particular in the polarization range where iron reduction occurred. This noise is unlikely attributed to electrode shielding problems or electrode fouling, because there was no indication for measurement disturbances in the more positive polarization range. We assume that incomplete cleaning and metal iron deposition caused the rough voltammetric signals.

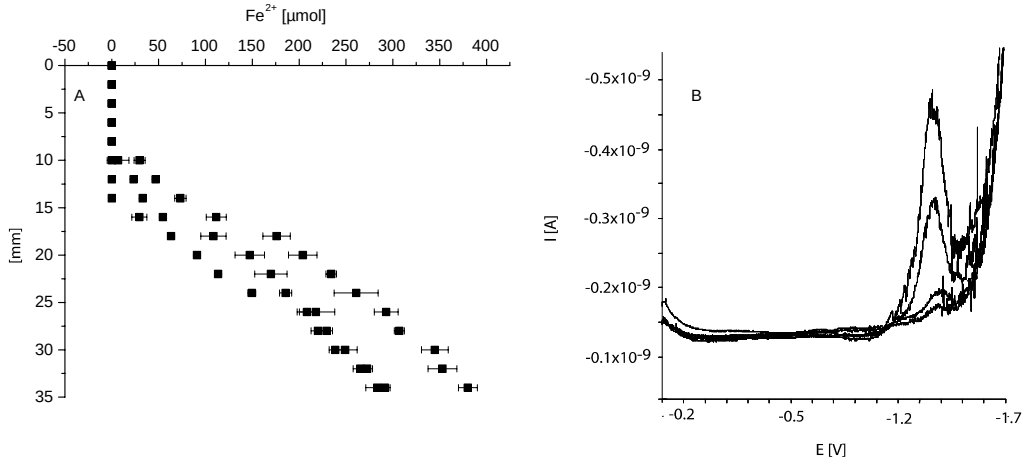

Figure 5.10 Sediment core measurements with a cellulose-acetate membrane covered miniaturized silver amalgam microelectrode in muddy sediment of a N´German harbor. A) Three profiles with 3 parallel measurements within a distance of 1 cm. B) Recorded typical voltammograms of these in-situ sediment measurements. Square wave voltammetry: start potential, -0.1 V; final potential, -1.8 V; scan rate, 0.8 V/s; conditioning potential, -0.1 V; conditioning time, 60 s; stand-by potential, -0.8 V; equilibration time, 5s.

The three profiles have a similar gradient, but in one profile, the ferrous iron concentration increased much faster than in the others, although the distance between the measurements was only 1 cm. In two profiles, a Fe(II) concentration up to ~250 µmol was measured, while the third profile hat a concentration of ~350 µmol. This 40 % elevated Fe(II) concentration illustrates the heterogeneity of the sediment. Especially, two profiles showed small measurement standard deviation, demonstrating reasonable reproducibility for in-situ applications. The miniaturized silver amalgam microelectrodes have a tip diameter of 20 to 50 µm. This diameter would allow higher resolution measurements in 100 µm to 200 µm steps. To test the applicability of those electrodes for sedimentary in-situ work, a 1 mm step interval was chosen. For flux calculation, profiles with higher resolution are necessary to evaluate small-scale changes over depth.

5.5 Conclusion

Miniaturized silver amalgam and mercury-plated iridium-based microsensors were designed and constructed for use in voltammetric cells and in-situ. The effort was put to the construction of these miniaturized electrodes. In a second step, attention was given to reproducibility and to first in-situ applications. We were faced with the problem of electrode surface stability, and the avoidance of electrode fouling. Especially, the use of thick membranes to iridium-based microelectrodes was limited. The mercury drop forming process was complicated in a small volume agarose gel membrane. Evaporation and drying of the agarose gel membrane made the handling and transfer of the electrodes extreme complicated. The stability of the mercury electrode surface, either as liquid droplet or as metal amalgam, limits the area of application. Iridium-based microelectrodes covered with a liquid mercury droplet need a second external electrode body filled with a membrane to assure the stability of the mercury droplet. This is especially necessary for application in sediments, but the handling of such agarose membrane covered electrodes is unfavorable for in-situ sediment studies. The use of such electrodes in water column studies is promising.

The solid nature of the silver amalgam electrode tip was advantageously to in-situ sediment work. These electrodes showed good reproducibility to measure Fe(II), Mn(II), S(-II) and O_2. To guarantee the right sensitivity for all measured ions, the use of a pilot ion method with manganese as the pilot ion should be avoided; otherwise, the results are only semi-quantitative. The detection of trace metals, like Cd and Pb, is favored using mercury-covered iridium-based microelectrodes, because the silver substrate of the silver amalgam electrode can undergo a reaction with these metals. Further experiments will be orientated towards more precise monitoring of sediment profiles while improving our knowledge on controlling the sensitivity and the stability of the electrode. The incorporation of the reference and the counter electrode in on a small combined electrode “chamber” will a further step to improve the sensitivity of these miniaturized electrodes.

Chapter 6

Determination of Metal Speciation by Reverse Titrations

Jochen Nuester[+] and Constant M.G. van den Berg[‡]

[+]Max Planck Institute Bremen, Celsiusstr. 1, 28359 Bremen, Germany

[‡]Department of Earth and Ocean Sciences, Liverpool University, Liverpool L69 3PG, UK.

Analytical Chemistry **77** (1): 11-19; 2005

Abstract

A new method is proposed to determine metal speciation by varying the concentration of a competing ligand at a constant metal concentration, with detection by cathodic stripping voltammetry. The free metal ion concentration is gradually lowered from its natural level while the method probes progressively deeper into the already complexed metal fraction: it is therefore a *reverse titration* rather than the *forward titration, which* is used for conventional complexing ligand titrations. The sensitivity is greatest at the lowest free metal ion concentration, where it matters most, and the method can be carried out in a single sample aliquot in the voltammetric cell. The method is applied here to copper speciation, but in principle, it can also be used for other metals. Modeling shows that this method has good sensitivity at ligand concentrations near the metal concentration (lower as well as greater). Comparative measurements of copper speciation using reverse and forward titrations of representative water samples of oceanic and coastal origin show good agreement; the data showed that these samples did not contain low levels of strong ligands in addition to the ligands detected by the forward titrations.

6.1 Introduction

The chemical speciation of copper, iron, cobalt, zinc, and several other metals in natural waters is controlled by organic metal binding ligands (Vandenberg 1984; Gledhill and Van den Berg 1994; Moffett 1995; Gordon, Codispoti et al. 2000; Ellwood and van den Berg 2001; Saito and Moffett 2001; Laglera and van den Berg 2003). For some metals, the speciation is complicated by redox reactions and the pH causing the formation of unstable, transient species. Copper has been extensively studied, and it has been suggested that relatively low Cu^{2+} concentrations in their hydrated form are toxic to many microorganisms, including bacteria (Hering, Sunda et al. 1987), phytoplankton (Brand, Sunda et al. 1986), and crab larvae (Sanders, Jenkins et al. 1983). In this work, we concentrate on copper, of which the speciation is known to be dominated by stable organic complexes in waters from oceanic, coastal, estuarine, and freshwater origin (van den Berg 1984; Xue and Sigg 1993; Moffett 1995; Laglera and van den Berg 2003).

The organic ligands participating in complexation of copper(II) fall in at least two major groups (L1 and L2). Several studies indicate that strong organic ligands (L1) dominate the copper complexation in open ocean surface waters, whereas the weaker ligands (L2) are involved in the complexation in coastal waters (Coale and Bruland 1988; Coale and Bruland 1990; Moffett, Zika et al. 1990; Donat and Van den Berg 1992; Kozelka and Bruland 1998). A third group has been determined in some cases (Kozelka and Bruland 1998).Little is known about the composition of the ligands. A recent study has shown that thiols are likely ligands for copper complexation in estuarine waters(Laglera and van den Berg 2003), but humic and fulvic acids are also thought to act as strong copper binding ligands (Kogut and Voelker 2001). In addition to organic ligands, sulfide clusters could also account for metal-binding ligands in fresh water (Rozan, Lassman et al. 2000), and sulfides are present in seawater at nanomolar concentration (Luther and Tsamakis 1989), Sulfhydryl-containing ligands, e.g. metallothionein-like proteins, could be present in colloids which could also act as complexing agents (Tang, Warnken et al. 2001).

The usual method to determine the concentration of natural complexing ligands (L) and their complex stability is by means of a titration with the metal while following the free (not complexed by L) concentration by cathodic stripping voltammetry (CSV) with competitive ligand equilibration (CLE) (Vandenberg 1984) by graphite furnance atomic adsorption spectroscopy of the extracted complex (Moffett and Zika 1987a; Moffett and Zika 1987b), by

anodic stripping voltammetry (Chau, Gachter et al. 1974), or by adsorption on MnO_2 (Vandenberg and Kramer 1979). Often more than one ligand is detected in natural waters. This tends to complicate the data interpretation (Buffle, Altmann et al. 1990; Filella, Buffle et al. 1990), when the detection method does not have the resolution to discriminate among more than 2 or 3 ligands (Vandenberg and Donat 1992).

The existing speciation methods titrate ligands one after the other by adding metal. Ligands with similar complex stability are titrated to some extent in parallel, which is what is causing problems with the interpretation of the data. For instance, it is well-known that starting a titration at a different detection window (which includes either using a different range of metal concentrations or a different concentration of the added competing ligand) tends to give different detected concentrations of natural ligands, with lower complexing stabilities for the ligands of higher concentrations detected at higher metal concentrations. Using CLE techniques, the titration starts below the original, free, metal ion concentration as the metal is distributed over the added and original ligands. During the titration with metal, the strong species are formed first, followed by the weaker species, which are less important with respect to the metal speciation in the original sample. For this reason, titrations should be carried out at a high detection window and at a realistic range of metal concentrations, unless it is the intention to detect the weaker ligands present at higher concentrations.

In this study, we propose a new procedure aimed specifically at the detection of the strong complexing ligands that may be present at concentrations similar to that of the metal (lower as well as higher), to get information on those ligands that are most important to the metal speciation in natural waters. This procedure is based on varying the detection window in CLE from low to high with detection by CSV (CLE/CSV) while keeping the metal concentration constant. The detection window is varied by gradually increasing the concentration of the added competing ligand. By lowering the free metal ion concentration, the method probes progressively deeper into the metal species originally present in the water, as if by a reverse metal titration. The ligand concentration is estimated by either curve-fitting or data linearization. Here, we use copper for the first application and testing of this method. The copper speciation was determined by following the peak height of the copper salicylaldoxime ($CuSA_2$) complex during titrations with SA. In this study, we present the theory, testing against EDTA, and titrations on bulk oceanic samples and coastal waters; the titrations are compared against the usual forward complexing ligand titrations.

6.2 Materials and Methods

6.2.1 Equipment

The voltammetric system consisted of a Metrohm VA-Stand (663 VA-Stand, Metrohm, Switzerland) connected via an IME 663 module to a computer-controlled voltammeter (PGSTAT 10, Eco Chemie, Netherlands). The working electrode was a hanging mercury drop electrode (HDME, drop surface area 0.38 mm^2). The reference electrode was a double-junction Ag/AgCl (3 M KCl) electrode, and the counter electrode was a platinum wire. The solutions were stirred by a rotating PTFE rod during the deposition step of the measurements. Sample bottles (LDPE, Nalgene) were cleaned by soaking 1 week in 50% HCl, followed by at least 1 week in 10% HCl, and were subsequently stored partially filled with 0.01 M HCl. The voltammetric measurements were performed in a glass cell cleaned with 2 M HCl and 0.01 M HCl.

6.2.2 Reagents

Water was purified by reverse osmosis (Milli-RO, Millipore) followed by ion-exchange (Milli-Q). Ammonia and hydrochloric acid (Analar grade, Merck) were further purified by subboiling quartz-distillation. Solutions of copper were prepared by dilution of an atomic adsorption spectrometry standard solution (BDH, SpectrosoL grade) in 0.01 M HCl. A pH buffer containing 1 M boric acid (Analar grade) and 0.35 M ammonia was UV-digested for 1 h to remove organic matter. An addition of 150 µL of this buffer to 10 mL of seawater resulted in a pH of 8.35. A 0.1 M solution of salicylaldoxime (SA) (BDH) stock solution was prepared in 0.1 M HCl.

6.2.3 Sample Collection and Storage

Seawater from the North Atlantic Ocean was collected from various depths, filtered (0.1 µm filtration cartridge), and mixed during cruises with the RV Pelagia (MERLIM cruise 1999, and COMET cruise, 2001) and stored as bulk seawater in 50 L HDPE containers. These samples are called here MERLIM and COMET, respectively. This water was stored at room temperature in the dark. For some experiments, this water was digested with UV-light (1 h, 125 W high-pressure mercury vapor lamp) to remove any organic ligands and was then indicated as UV-seawater (UV-SW). The water of Venice Lagoon was collected November

2002 using a peristaltic pump from a depth of 0.5 m; it was filtered on-line through a 0.1 μm filtration cartridge and stored frozen.

6.2.4 Procedure to Determine Total Dissolved Copper Using CSV

Total copper was determined by CSV after 45 min of UV digestion of samples in silica tubes at the original pH (pH 8). The silica tubes were conditioned with each sample before use to minimize the loss of copper due to adsorption onto the tube walls. A15 ml portion of the samples was pipetted into the voltammetric cell; mixed with 150 μL of borate buffer and 37.5 μL of SA; and then deaerated for 5 min using oxygen-free, water-saturated, nitrogen gas; then the solution was left to equilibrate for 10 min. The measurement parameters were: deposition potential of -0.15 V; deposition time 60 s while stirring; a quiescence period of 15 s; CSV scan in the square-wave mode from -0.15 to -0.6 V with a modulation frequency of 10 Hz; step height 2.5 mV, pulse height 25 mV. The measurements were repeated after addition of copper standard to calibrate the sensitivity. Between measurements, the deaeration time was 15s.

6.2.5 The Reverse Titration Procedure to Determine Copper Complexation

A 15 ml portion of seawater was transferred to a voltammetric cell and, 150 μL of borate buffer was added. The concentration of SA was increased stepwise from 0.01 to 70 μM. Thus, the entire titration was performed in a single, small, sample aliquot in a voltammetric cell. The start and final SA concentrations can be varied from those used here, depending somewhat on the original copper and natural ligand concentration (for instance, lower SA concentrations could be used for higher copper concentrations). The titration was halted when the increase in the peak height for the copper/SA complex leveled off. Each SA addition was equilibrated for 30 min, and a purging time of 10 s was allowed after each addition; the solution was blanketed with nitrogen at all times. The concentration of the $Cu(SA)_2$ complex was determined by CSV using the square-wave modulation with a frequency of 10 Hz and a step potential of 2.5 mV; the deposition potential was -0.15 V for 60 s, the quiescence period was 15 s, and the potential scan was from -0.15 to -0.6 V. A titration of UV-digested seawater was used as the control, and a UV-digested aliquot with added EDTA was used for comparative purposes.

6.2.6 Forward Copper Complexing Ligand Titrations

Comparative copper-complexing ligand titrations were carried out using the conventional metal-titration technique in which the ligands are titrated with metal additions to 28 mL capped, polystyrene, tubes (Sterilin) (Campos and Van den Berg 1994). Approximately 150 mL of sample water was transferred to a PTFE bottle, borate buffer was added to a concentration of 0.01 M, and 5-10 μM SA. The copper concentration was varied between 0 and 400 nM in 10 Sterilin tubes, and 10 mL of the seawater was added to each tube. The samples were equilibrated at least 8 h or overnight at room temperature (~20 °C). The Sterilin tubes were conditioned three times as described above. The samples were transferred to the voltammetric cell, and the concentration of the copper/SA complex ($Cu(SA)_2$) was determined using CSV as before.

6.2.7 Data Analysis

Data-fitting was carried out using the EXCEL plug-in Solver. The measured data (ratio of maximum current to the actual current) were subtracted from data modeled using estimated values for K'_{CuL} and C_L. The differences were squared and summed; the sum was minimized by Solver by adjusting the values for K'_{CuL} and C_L by least-squares regression. Where necessary, values for a second ligand and for the maximum current (i_{pmax}) were fitted simultaneously.

6.3 Theory

6.3.1 Modeling of the CSV Response during a Reverse Titration of Seawater with and without Natural Ligands

In a reverse titration, the dissolved metal is bound progressively by additions of the ligand used to give the CSV response. During the titration, the CSV response increases until all metal is bound as the electroactive species; at this point, the peak height is maximal (i_{pmax}). Because the response is directly related to the concentration of the electroactive, adsorptive, species, the CSV response can be modeled by calculation of the abundance of this species during the titration. There are two models possible because there are two species, CuSA and $CuSA_2$ (Campos and Van den Berg 1994), which can adsorb. The previous work suggested that the $CuSA_2$ species adsorbs, and this was confirmed by the modeling here, so the relevant model will be discussed in detail, whereas the 1:1 CuSA model will be treated more briefly.

Rather than modeling absolute peak heights, ratios of peak heights were used; this way, there is no need to know the sensitivity (response/metal concentration), as is required for the usual forward titrations. The plot of relative peak height, *X,* as a function of the SA concentration was modeled using:

$$X = [CuSA_2] / C_{Cu} \quad (1)$$

where C_{Cu} is the dissolved copper concentration. X is the ratio of the actual over the maximum current: $X = i_p/i_{pmax}$; and $0 < X < 1$ at concentrations of SA from low to high. The CSV response (i_p) is maximal ($i_p = i_{pmax}$) when all copper occurs as $CuSA_2$. The relationship between the CSV response and $[CuSA_2]$ depends on the sensitivity, $S = i_p/[CuSA_2]$. The sensitivity changes with the concentration of SA, and this is varied continuously during the titrations. Fortunately, there is no need to know the sensitivity for these titrations because it cancels out of the equation for X. Instead, it is necessary to have a good estimate for i_{pmax}, which is optimized through fitting of the titrations to the model. Substitution of the mass balance for copper,

$$C_{Cu} = [Cu'] + [CuSA] + [CuSA_2] + [CuL_n] \quad (2)$$

into Eq. 1, the following more detailed ratio is obtained, more useful for data fitting

$$X = [CuSA_2]/([Cu'] + [CuSA] + [CuSA_2] + [CuL_n]) \quad (3)$$

where CuL_n is one of the complexes with natural organic ligands of type L, and [Cu´] is the concentration of inorganic copper (not complexed by any organic ligand). The concentration of each species is related to that of Cu^{2+} through an α-coefficient, e.g.:

$[Cu'] = \alpha_{Cu}[Cu^{2+}]$

$[CuSA] = \alpha_{CuSA}[Cu^{2+}]$

$[CuSA_2] = \alpha_{CuSA2}[Cu^{2+}]$.

A value for α_{Cu} of 35 was calculated from an ion-pairing model as before (Campos and Van den Berg 1994). Values for the α-coefficients of Cu^{2+} and SA were calculated using

$\alpha_{CuSA} = K'_{CuSA}C_{SA}$

$\alpha_{CuSA2} = B'_{CuSA}C_{SA}$

where K' and B′ are the conditional stability constants valid for seawater of the same salinity. The total concentration of SA (C_{SA}) was used here because it was much greater than the concentration of copper. This was not done for the unknown ligands, L, which was present at much lower concentrations, so a correction had to be made for the amount of ligand tied up by copper. For species of the type CuL (CuL_1 and CuL_2), the following relationship was used.

$$[CuL] = K'_{CuL}[Cu^{2+}]C_L/(1 + K'_{CuL}[Cu^{2+}]) \quad (4)$$

By substitution of the concentration terms in Eq. 3, the following relationship was obtained for the case of adsorption of $CuSA_2$.

$$X = \alpha_{CuSA2}/(\alpha_{Cu'}+\alpha_{CuSA}+\alpha_{CuSA2}+ K'_{CuL}C_L/(1+K'_{CuL}C_L[Cu^{2+}])) \quad (5)$$

Values for K'_{CuL} and C_L were calculated by nonlinear least squares regression of *experimental* values of X (from i_p/i_{pmax}) to the *modeled* values of X using Eq. 5 with optimization of initial estimates for the ligand concentration and conditional stability constant.

If two ligands of type L (L_1 and L_2) are present, this equation changes to

$$X = \frac{\alpha_{CuSA_2}}{\left(\alpha_{Cu'} + \alpha_{CuSA} + \alpha_{CuSA_2} + \frac{K'_{CuL_1}C_{L_1}}{\left(1+K'_{CuL_1}[Cu^{2+}]\right)} + \frac{K'_{CuL_2}C_{L_2}}{\left(1+K'_{CuL_2}[Cu^{2+}]\right)}\right)} \quad (6)$$

More terms for additional ligands can be added to the denominator as required, but in practicality, it may be difficult to fit more than two ligands as the number of parameters increases. The complexing stability constants (K'_{CuL1} and K'_{CuL2}) and ligand concentrations (C_{L1} and C_{L2}) of the natural organic ligands were calculated by least-squares regression of experimental X values to those calculated using Eq. 6. Free concentrations of Cu^{2+} for Eq. 5 and 6 were calculated (see below) using the fitted values for C_{Ln} and K'_{CuLn} and were part of the optimization process.

6.3.2 Calibration of the Conditional Stability Constants for CuSA and $CuSA_2$

Values for B'_{CuSA2} and K'_{CuSA} (the conditional stability constants for $CuSA_2$ and CuSA, respectively) were calculated by curve-fitting of experimental values of $X=i_p/i_{pmax}$ (obtained in UV-SW in the absence of natural ligands) to the modeled values. The following equation was used for X, which is derived by setting the concentration C_L in Eq. 5 to 0.

$$X=\alpha_{CuSA2}/(\alpha_{Cu'}+\alpha_{CuSA}+\alpha_{CuSA2}) \quad (7)$$

After substitution of the α-coefficients, this is changed to

$$X= B'_{CuSA2}[SA]^2/(\alpha_{Cu'}+K'_{CuSA}[SA]+ B'_{CuSA2}[SA]^2) \quad (7')$$

This equation is valid for adsorption of $CuSA_2$. In the case of adsorption of CuSA but in the presence of $CuSA_2$ at high concentrations of SA, the following equation is valid:

$$X = \alpha_{CuSA}/(\alpha_{Cu'}+ \alpha_{CuSA}+\alpha_{CuSA2}) \quad (8)$$

And in the case of CuSA adsorption without the presence of $CuSA_2$,

$$X=\alpha_{CuSA}/(\alpha_{Cu'}+\alpha_{CuSA}) \quad (9)$$

The three relationships were compared to see which best described reverse titrations of UV-SW and were used to calibrate the complex stability of Cu with SA and confirm the identity of the adsorbing species.

We attempted to fit the stability constants for the two expected species (CuSA and $CuSA_2$) using the relative peak height as a function of the concentration of SA in Eq. 7. Preliminary calculation showed that it was not possible to fit both constants using Eq. 7 because both constants occur in the denominator and one in the numerator. A number of good fits could be obtained, all having a constant ratio for the complex stabilities of CuSA and $CuSA_2$. Therefore, a second relationship was obtained from the sum of the α-coefficients for copper complexation by SA determined by competition against EDTA at 25 μM SA (Campos and van den Berg, 1994): $(\alpha_{CuSA} + \alpha_{CuSA2}) = 10^{5.83}$ for seawater. One of the two constants was then eliminated in Eq. 7 (and similarly in Eq. 8 and 9) using

$$K'_{CuSA}[SA] = (\alpha_{CuSA} + \alpha_{CuSA2}) - B'_{CuSA2}[SA]^2$$

This meant that only one parameter (e.g. B'_{CuSA2}) remained to be fitted by the least squares regression and could be used to calculate a value for K'_{CuSA}.

6.3.3 [Cu^{2+}] Calculation

In UV-SW (used for calibration), values for the concentration of Cu^{2+} were calculated from

$$[Cu^{2+}] = C_{Cu}/(\alpha_{Cu} + \alpha_{CuSA} + \alpha_{CuSA2})$$

In the presence of a single natural ligand of type L, the following quadratic equation was obtained by substitution of the concentration terms of the individual species in the mass balance of the metal concentration (Eq. 2).

$$[Cu^{2+}]^2 K'_{CuL}(\alpha_{Cu}+\alpha_{CuSA}+a_{CuSA2}) + [Cu^{2+}](\alpha_{Cu}+\alpha_{CuSA}+\alpha_{CuSA2}-K'_{CuL}C_{Cu})+K'_{CuL}C_L = 0 \quad (10)$$

Concentrations of Cu^{2+} were calculated with the usual solution for this quadratic equation. Values for K'_{CuL} and C_L were initially estimated and then optimized during the iterative least-squares fitting process; these values were used to calculate values for [Cu^{2+}] at every SA concentration during the reverse titration. The calculated concentrations of Cu^{2+} were then used to model the X ratio at each SA concentration in Eq. 5 for one ligand of type L.

In the presence of two ligands of type L, the following equation was obtained by substitution of Eq. 2.

$$[Cu^{2+}]^2 K'_{CuL}(\alpha_{Cu'} + \alpha_{CuSA} + \alpha_{CuSA2} + \alpha_{CuL2})$$
$$+ [Cu^{2+}](\alpha_{Cu'} + \alpha_{CuSA} + \alpha_{CuSA2}-K'_{CuL1}C_{cu} + K'_{CuL1}C_{L1}) - C_{Cu} = 0 \quad (11)$$

This equation was not fully resolved because α_{CuL2} occurred within the bracketed part. Values for this were calculated using Eq. 12 and using estimated values for [Cu^{2+}].

$$\alpha_{CuL2} = (C_{L2} - C_{Cu} + C_{L1})K'_{CuL2} \quad (12)$$

6.3.4 Linearization Method to Fit Natural Ligands

Although the curve-fitting procedure was effective to fit the reverse titrations, we evaluated whether it is possible to use a linear procedure, as commonly used in the forward titrations. For this reason, the van den Berg-Ruzic linearization method (Vandenberg and Kramer 1979; Ruzic 1982; Vandenberg 1982; Vandenberg 1982) was used to evaluate the complexing ligand concentration (C_L) and the conditional stability constant K'_{CuL}.

$$[Cu^{2+}]/[CuL] = [Cu^{2+}]/C_L + 1/(C_L K'_{CuL}) \quad (13)$$

A plot of $[Cu^{2+}]/[CuL]$ as a function of $[Cu^{2+}]$ is linear if only one ligand of type L is present and curved if there are two or more (e.g., van den Berg, 1982); this is convenient for checking whether the data can be fitted to a one-ligand model because this is not immediately apparent from the nonlinear methods.

Experimental values for the concentration of Cu^{2+} were obtained using the following relationship, which assumes that only $CuSA_2$ adsorbed during the voltammetric measurement,

$$[Cu^{2+}] = XC_{Cu}/\alpha_{CuSA2} \quad (14)$$

and the concentration of CuL was obtained from the mass balance of copper.

$$[CuL] = C_{Cu} - [CuSA] - [CuSA_2] - [Cu'] = C_{Cu} - [Cu^{2+}](a_{Cu}+a_{CuSA}+a_{CuSA2}) \quad (15)$$

The experimental X values in Eq. 14 were used to obtain values for $[Cu^{2+}]$ and the ratio $[Cu^{2+}]/[CuL]$. Values for K'_{CuL} and C_L were calculated from the slope and the Y-axis intercept of the plot of $[Cu^{2+}]/[CuL]$ as a function of $[Cu^{2+}]$ by linear least-squares regression according to Eq. 13. These values for C_L and K'_{CuL} were then used to model values for X using Eq. 5 to allow comparison of modeled and experimental X values.

6.4 Results and Discussion

6.4.1 Model Calculations Showing the Response Expected for Reverse Titrations of Copper Complexes with SA

Free ionic copper concentration and the relative CSV response (X values) were calculated as a function of the SA concentration, using Eq. 10 and 5, for given values of B'_{CuSA2}, K'_{CuSA}, K'_{CuL}, C_{Cu}, and C_L. Values for these parameters were taken from Campos and van den Berg (1994)(1994). Previously (Campos and Van den Berg 1994), it was demonstrated that either of two copper(II)-SA complexes can adsorb at the electrode, the CuSA or the $CuSA_2$ species, but it was considered more likely that the $CuSA_2$ species adsorbed. It will be demonstrated below that, indeed, the $CuSA_2$ species best fits the adsorption model, so in this model calculation, it is assumed for now that only the $CuSA_2$ is electroactive. The modeled X values (representing the relative CSV response) are summarized in Figure 1, showing the expected S-shaped CSV response as a function of log[SA]. This

means that the response first increases and subsequently levels off in a symmetric and predictable fashion.

6.4.2 Modeling of Effects of Variations in Analytical Parameters: Natural Ligand Concentration, Salinity, and the Copper Concentration, on the Shape of the Reverse Titration

At a given complex stability, K'_{CuL} the modeled CSV response is very sensitive to variations in the concentration of the natural ligand (C_L) also when this is less than the copper concentration C_{Cu} (Figure 6.1A). This is important, because this means that it should be possible to detect low ligand concentrations using reverse titrations. With the usual complexing ligand titrations, it is difficult to determine ligand concentrations less than, or only slightly greater than, the metal concentration. The natural ligand is then nearly metal-saturated, causing a titration with little or no curvature and making it difficult to establish the titration endpoint. Also in the usual complexing ligand titrations, a ligand (L1) at a concentration less than metal would be missed in the presence of another ligand (L2) at higher concentration, even if ligand L1 binds the metal more strongly.

The modeling suggests that the reverse titration method would be more suitable to detect low ligand concentrations because the method works by removing previously complexed copper. It therefore detects the ligand(s) actually binding the metal in the original sample condition, rather than detecting the excess ligand, as is done in the forward CC titrations. The modeling showed that the CSV response is diminished more at low SA than at higher SA concentrations when the concentration of ligand L is increased from less than to greater than the copper concentration, causing the S-shape to become steeper (Figure 6.1A).

Furthermore, the modeling showed (Figure 6.1A) that titrations with SA have to be in the range of 10^{-7}-$10^{-3.5}$ M SA to cover expected complexes for copper. The influence of variations in the salinity was modeled by varying the values for the stability constants for the CuSA and $CuSA_2$ species using the known salinity relationship for these constants), log B'_{CuSA2} =15.78-0.53 log(salinity) and log K'_{CuSA} = 10.12-0.37log(salinity) (Campos and van den Berg, 1994).

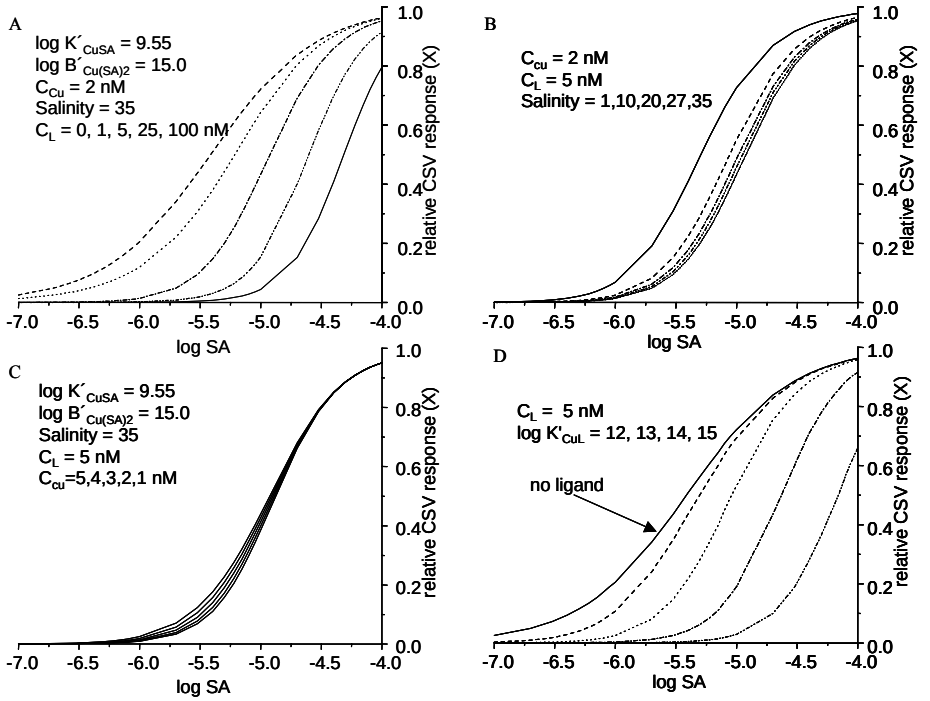

Figure 6.1 Modeling of the effect of variations in analytical parameters on the CSV response (the X-ratio) during the reverse titrations: A) as a function of CCu; B) as a function of salinity; C) as a function of changes in CCu at CCu < CL; and D) as a function of changes in CL at CCu < CL.

The salinity effect on the reverse titration response (Figure 6.1B) is most pronounced at low salinities: a change in the salinity from 35 to 15 (i.e. from normal seawater to brackish water) caused only a minor change in the CSV response, but a salinity change to freshwater conditions affected the modeled CSV response more dramatically. This is in line with expectation because the change in ionic concentrations is orders of magnitude in the low salinity range and varies by only a factor of 2 in the higher range. It shows that repeat calibrations of the Cu/SA complex stability on UV-SW are not necessary at salinities encountered in normal seawater, but it may be necessary to refine the published data for low salinities.

The effect of variations in the background copper concentration is shown in Figure 6.1C. Because the data are plotted as a ratio of i_p/i_{pmax}, the effect of the variations in the copper concentration is small although the effect on i_p and i_{pmax} individually would be directly related to the copper concentration and could be large. The ratio of the ligand over the copper

concentration is affected by the changes in the copper concentration, and it can be seen that the titration curve flattens somewhat when the copper concentration is similar to or greater than the ligand concentration. The reason for this is that then, some of the copper is "free" (not bound by L), and this fraction, therefore, gives a peak at lower SA concentrations than does the complexed copper. The effect is not apparent at higher SA concentrations because then the change in the *X* ratio is controlled by CuL.

Increasing the stability of the CuL complexes at constant concentration of L causes a shift of the S-shaped titrations to higher SA concentration, because more SA has to be added to dissociate stronger complexes (Figure 6.1D). To a first approximation, the complex stability of the Cu-SA complexes is exactly balanced by that of the CuL species when $X = 0.5$. This means that the shift in the titrations must exactly balance any changes in the stability of CuL species. The shift is approximately one decade in SA for each 2 decades change in α_{CuL} because the stability of the Cu/SA species is dominated by that of $CuSA_2$.

6.4.3 Kinetic and Sensitivity Aspects

Kinetic aspects were tested in preliminary experiments by following the CSV peak height as a function of time at various concentration points throughout a titration with SA. The data showed that the solutions reached equilibrium after 20-30 minutes; longer equilibration times of up to 8 h did not change the analytical signal in a systematic manner. For this reason, a 30 min equilibration time was used after each SA addition. This way, a titration in a single sample aliquot took ~8 h. This is a longer measuring time than would be required (3-4 h) if the sample had been subdivided into 10-15 aliquots, allowing these to equilibrate, and then these had been measured in quick succession. However, advantages of the single voltammetric cell titration are that a much (10-15 times) smaller sample size (10 - 15 mL for the titration) can be used and that the entire titration can, in principle, be automated by using an autoburet for the additions of the competing ligand (SA).

6.4.4 I_{pmax} Correction

There is a practical problem related to establishing the maximum peak current (i_{pmax}) of the titration. The peak current continues to increase to high SA concentration because of the presence of α_{CuSA} as well as α_{CuSA2} in the denominator of Eq. 5 and 6. For this reason, the modeled value for *X* is 0.96 (i.e., 4 % less than unity) for 100 µM SA in the absence of competing natural ligands. In the presence of a competing ligand, *X* is slightly less again: for

instance, X is 0.95 in the presence of 5 nM type L ligand with a log K'_{CuL} = 13.3. It is, therefore, not correct to simply equate the current obtained at the highest SA concentration with $i_{pmax,}$ because X then would be overestimated by ~5%.

Modeling showed that the nonlinear method of data-fitting is sensitive to the value of i_{pmax}. Model fitting with hypothetical data showed a large variation in calculated values for K'_{CuL} and C_L at values for i_{pmax} varying by between 5 and 10% of the correct value, as shown in Table 6.1. For instance, at an actual ligand concentration of 5 nM, the calculated ligand concentration would increase to 43 nM if the value for i_{pmax} was underestimated by 5%, but it would drop to 2 nM if it was overestimated by 5%.

Table 6.1 Model Calculations to Evaluate the Sensitivity of Data Fits to Selection of an Incorrect Value for i_{pmax} on the Calculated Values for C_L and K'_{CuL}[a].

i_{pmax} (nA) used in model	found C_L (nM)	found logK'_{CuL}	log α_{CuL}
90	915	10.8	4.76
95	43	12.2	4.83
100	**5**	**13.3**	**5.00**
105	2.4	13.8	5.18
110	1.9	14.1	5.38

[a]Modeled seawater composition: C_L = 5 nM, logK'_{CuL} = 13.3, i_{pmax} = 100 nA. Corrected values are shown in bold.

This shows that the ligand concentration calculated by this curve fitting method is very sensitive to establishing the correct value for i_{pmax}. However, an error of 5% is readily spotted visually by plotting modeled values for X (calculated using the fitted values for C_L and K'_{CuL}) on top of the actual X values. Furthermore, i_{pmax} can be fitted to the data along with C_L and K'_{CuL}. Modeling showed that this worked well in the case of a single ligand, but poor fits (errors in i_{pmax}) were obtained for a 2-ligand model because the number of parameters including i_{pmax} increased to 5. In our data fits (below), the value of i_{pmax} was initially based on the highest peak height obtained during the titration, and this was subsequently corrected by modeling of the titration curves using the fitted parameters.

6.4.5 Reverse Titrations of Copper in UV-Digested Seawater with and without EDTA

Additions of SA to seawater caused the peak height for copper to increase in accordance with the model calculations and with previous work (Campos and Van den Berg 1994). In UV-digested seawater, the reduction signal could be recorded from SA concentrations starting from 0.1 μM. The peak height increase with increasing SA concentrations was accompanied by a shift of the copper peak potential in line with expectation because of the increased complex stability.

The titration curve was shifted to higher SA concentrations in the presence of 30 and 65 μM EDTA (Figure 6.2). The data points of titrations with and without added EDTA are shown in this diagram along with modeled titrations for various EDTA concentrations showing that the modeled response agrees with the data. It can be seen that the shift in the curve was in accordance with the complex stability, with a greater shift for higher EDTA concentration. Data fits gave values of 9.5 and 9.6 for $\log K'_{CuEDTA}$, slightly below that estimated for CuEDTA in seawater ($\log K'_{CuEDTA}$=10.1). The stability constants for the Cu-SA complexes have themselves been calibrated against EDTA (Campos and Van den Berg 1994), suggesting that it may be necessary to recalibrate the stability of the Cu/SA complexes.

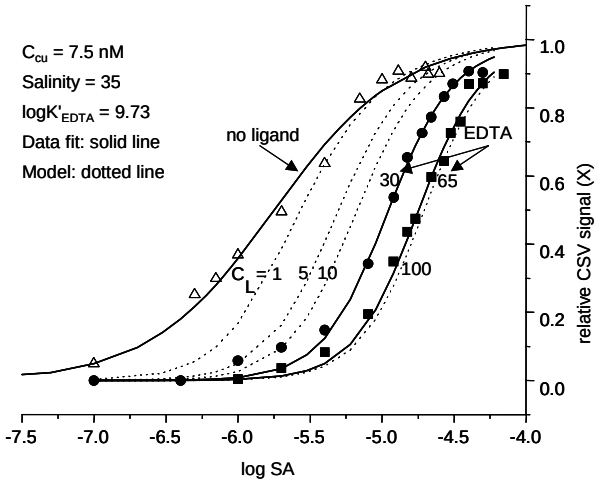

Figure 6.2 Reverse titrations of UV-SW with and without EDTA (30 and 65 µM). The plot shows the titrations as data points, with modeled data fits as solid curves going through the points; modeled titrations for additional EDTA concentrations (1, 5, 10, 100µM EDTA) are shown as dotted curves.

6.4.6 Reverse Titrations of Seawater Samples

Two samples of the Atlantic (bulked filtered seawater, collected during different cruises), and one from near-shore waters (Venice lagoon) were selected to test the reverse titration method because they represented both open oceanic and near-shore waters, with the expectation that the lagoon waters might present a special challenge due to probably containing higher levels of organic matter. Two of the samples were also analyzed by the conventional method to determine the complexing ligand concentration by titration with copper (Campos and Van den Berg 1994). The reverse copper titrations of the samples are shown next to that for UV-SW in Figure 6.3. The sample titrations were shifted to much higher SA concentrations than in the UV-digested seawater, and large differences were apparent between the samples.

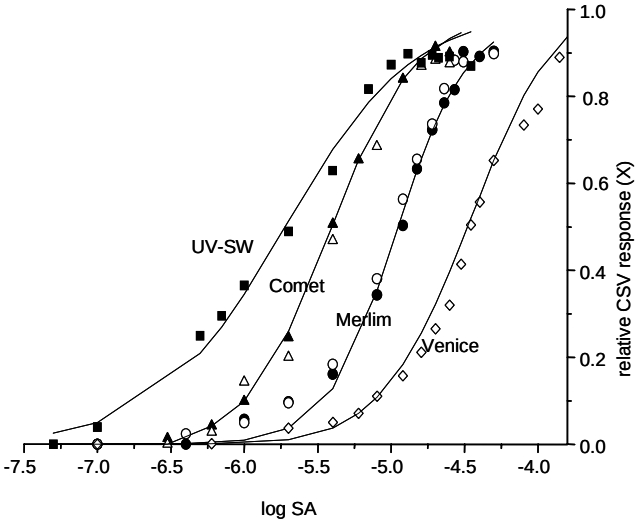

Figure 6.3 Reverse titrations of copper complexes in UV-SW and three seawater samples from differing environments. The curves represent model fits to the experimental data, which are shown as data points.

Determination of the copper concentration by copper additions at the end of the reverse titrations, at SA concentrations where the CSV signal response had approximately leveled off, resulted in calculated copper concentrations ~10 % lower than obtained with a SA concentration of 25 µM after UV digestion. This suggests that at the end of these titrations, for instance, at a SA concentration of 30 µM with a value for α_{CuSA} of 10^6, 10% of the copper was still complexed by the natural ligands. It is likely that this was an inert fraction that was not resolved by these titrations; possibly this could be resolved by using overnight equilibration of the entire titration, but this was not further investigated.

6.4.7 Determination of K'_{CuL} and C_L and Comparison of Different Fitting Methods

Curve fitting was used to fit values for K'_{CuL} and C_L to the reverse titrations. This was done by matching the experimental X values to model values (Eq. 5) by varying K'_{CuL} and C_L with optimization by least squares-regression (Figure 6.4).

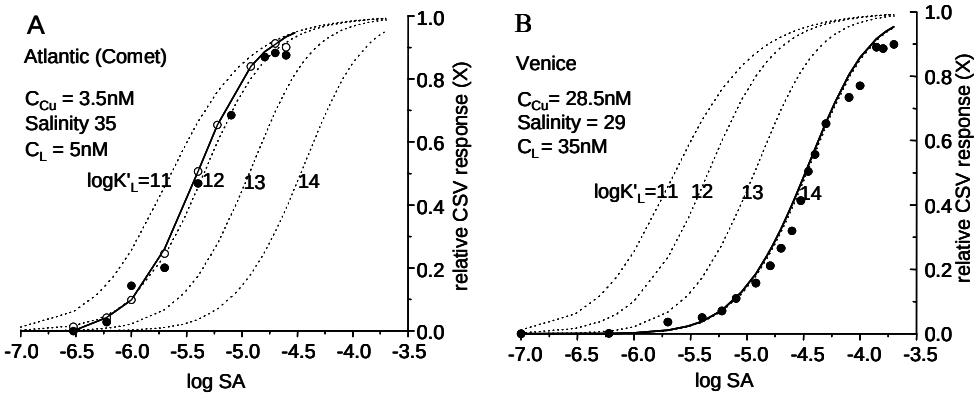

Figure 6.4 Effect of varying the values for complex stability in the model fits to the data sample from the North Atlantic (Comet 2001) (A) and one of the Venice lagoon (B). The fits to the experimental data points are shown as solid curves, whereas the dotted curves represent modeled data for different complex stabilities.

The results are shown in Table 6.2, where they can be compared to values obtained by fitting to two ligands of type L (eq. 6) instead of one, to values obtained by linearization of the data according to eq. 12, and to values obtained by the conventional complexing ligand titrations. All samples could be modeled by a single ligand and to two ligands. The two-ligand model described the data better, but the improvement was small. The concentration of the second ligand was smaller, and the complex stability was weaker than the first ligand and, therefore, not relevant to the copper speciation. We will therefore discuss the single ligand fit in more detail.

The detected ligand concentrations varied between 3 nM for the Merlim Atlantic sample and 35 nM for the lagoon sample. The complex stabilities varied between 12.5 and 13.6 for logK'_{CuL}. The complex stability was greater in the Merlim Atlantic sample (logK'_{CuL1}=13.71) than in the other Atlantic sample (logK'_{CuL1}=12.82), but no conclusions should be drawn from this because these were stored and bulked samples, of use only to test the method. Comparison of the reverse titrations to the usual forward complexing ligand titrations showed that the same ligand concentration was found by both methods for the lagoon sample (both 35 nM), but a lower ligand concentration (4 instead of 6 nM) was found in the Comet Atlantic sample.

Table 6.2 Fitting of Ligand Concentrations and Conditional Stability Constants to the Sample Titrations Shown in Figure 6.3, and Comparison to Results from Forward Complexing Ligand Titrations.

	direct fit one ligand nM	direct fit two ligands nM	linearization one ligand nM	linearization one ligand nM
	Reverse titration			Forward titration
		Venice Lagoon		
C_{L1}	34.5	34.2	34.8 ± 5.0	35.4 ± 2.8
C_{L2}		0.7		
logK'_{CL1}	13.8	13.5	13.7 ± 0.1	13.3 ± 0.8
logK'_{CL2}		11.9		
		North Atlantic, Comet Sample		
C_{L1}	4.1	4.4	4.4 ± 0.3	6.1 ± 0.2
C_{L2}		0.4		
logK'_{CL1}	13.1	12.5	12.55 ± 0.05	13.1 ± 0.3
logK'_{CL2}		11.3		
		North Atlantic, Merlim Sample		
C_{L1}	2.7	2.5	2.7 ± 0.5	not analyzed
C_{L2}		0.8		
logK'_{CL1}	13.9	13.6	13.6 ± 0.1	not analyzed
logK'_{CL2}		11.8		

The detected complex stability was the same by the two methods. On the whole, the agreement between the reverse and forward titrations was good. A detailed study of copper speciation using forward complexing ligand titrations in the presence of either SA (as used here) or tropolone (Achterberg and van den Berg) found two ligands of significantly differing complex stability: L1 at concentrations of 3.5 ± 1.0 nM with log K'_{CuL1} =13.2 ± 0.3 and a weaker ligands at a lower detection window. The copper species found here using the reverse titrations (and the CC titrations) are in the same range as the L1 ligands detected in that study, suggesting that there is general agreement between the values obtained by the reverse method and the conventional forward titrations technique.

6.5 General Discussion

The modeling suggests that the method of reverse titrations proposed and tested here may be especially useful to detect low ligand concentrations. Experimentally, similar ligand concentrations were found in comparative titrations by the reverse and the forward CC titrations, indicating that the reverse method can be used to successfully determine copper

speciation. The data also showed that in these samples there was no evidence of an additional ligand-binding copper at lower ligand concentration than that found with the conventional, forward, titrations. Although this finding is very preliminary (for only a few stored samples), this could be good news for the forward complexing ligand titrations, because it suggests that no ligands of importance to copper speciation are being missed by that method.

The curve-fitting method, based on a least-squares regression and using a readily accessible spreadsheet, was used to fit speciation parameters (ligand concentrations and stability constants) to the experimental *X* values (peak heights/maximum peak height) to model parameters: this approach appeared to work well and could also be used to optimize the value estimated for i_{pmax}. Comparison to the linearization method showed that similar results were obtained using the two methods. The linearization procedure has the added advantage of making it easy to spot whether a second ligand is present; furthermore, the more simple statistics make it possible to get values for the standard deviation of the ligand concentration and the complex stability from internal consistency within a single titration, which was not possible using the curve-fitting method. Standard deviations in this case, therefore, have to be estimated from repeated titrations, although the residual error of the least squares regression could be reported and could be compared between titrations.

In the reverse titration method, the shift of the experimental CSV response compared to an UV-SW titration is a direct measure of the complex stability (α_{CuL}); in the forward titration method, on the other hand, the shift in the response is a measure of the ligand concentration. An advantage of the reverse titrations method is that low ligand concentrations at levels equal to or less than that of the metal can be detected. An advantage of the forward titrations is that the position of the curvature in the titration data is a direct measure of the ligand concentration and gives a visual estimate of the concentration of the first and strongest ligand. So each method has advantages: for samples with ligand concentrations > metal concentration, the more intuitive output of the forward ligand titration may be more convenient, whereas at lower ligand concentrations, the reverse procedure will give more accurate results and shows better the complex stability of CuL.

During the reverse metal titration, the free metal concentration is progressively reduced with increasing concentration of the added ligand (SA in this study). At the highest concentration of the added ligand (SA), the sensitivity for the metal is greatest (see Figure 6.1) when also the free metal concentration is at its lowest. So rather unexpectedly, greatest sensitivity is obtained at the lowest free metal ion concentration. During the titration the free

metal ion concentration is lowered by 5 decades in UV-SW (from an α value of 35 for inorganic complexation to 10^6 at 30 μM SA), and by 1-2 decades when the copper is already complexed by natural ligands, as occurring in seawater.

For this method to work, it is essential to be able to accurately model the CSV response as a function of the added ligand concentration. This worked well for copper and SA, in which the response appeared to be exactly related to the formation of the $CuSA_2$ species. Preliminary experiments using iron and zinc have indicated that the CSV response with their adsorptive ligands may be more complicated and less easy to model.

The usual forward ligand titrations require conditioning of the titration vessels with the titrated samples to eliminate the problem of variable results that commonly occur for the first two or three titrations. In this work, each entire titration was carried out in the voltammetric cell. The vessel could, therefore, not be conditioned for each concentration of SA, though it could be conditioned for the copper concentration. Relatively stable peaks indicated that there were no major adsorption problems during these titrations; however, it was found that the titrations improved after the first one, indicating that a general conditioning of the voltammetric cell took place during the titrations.

Acknowledgements

The stay of J. Nuester in the laboratory of the Marine Electrochemistry research group at Liverpool University was funded by a Marie Curie Host Fellowship (Contract No. HPMT-CT-2001-00218). The samples from the Atlantic were collected during cruises with support of the PIs (de Baar and Timmermans) and officers and crew of the RV Pelagia (NIOZ, Netherlands).

Chapter 7

Iron(III) Oxide Heterogeneity and Bacterial Iron(III) Oxide Reduction

Ole Larsen[1], Jochen Nuester[1], and Dieke Postma[2]*

[1]Max Planck Institute for Marine Microbiology, Celsiusstr. 1, D-28359 Bremen, Germany

[2]Environment and Resources, Technical University of Denmark, 2800 Lyngby, Denmark

[*]DHI Water and Environment, Krusenberg 31, D-28857 Syke, Germany

prepared for submission to Aquatic Geochemistry

Abstract

The reactivity of Fe-oxides towards abiotic and bacterial dissolution was assessed and evaluated. The variation in Fe-oxide reactivity was investigated by studying the kinetics of bulk reductive dissolution of a suite of synthetic Fe-oxides in 10 mM ascorbic acid at pH=3 and including literature data. Furthermore, the importance of Fe-oxide mineralogy for bacterial Fe-oxide reduction was studied by quantifying the initial dissolution rate of the Fe-oxides by *Shewanella putrefaciens* strain CN32. Previous published data on bacterial reduction was included in order to elucidate the effects of Fe-oxide mineralogy. Abiotic initial dissolution rates form a consistent mechanistical basis. Initial abiotic and bacterial dissolution rates do not correlate indicating that the dissolution mechanisms are fundamentally different. For the different iron oxides, the abiotic initial rate was independent of the specific surface area, emphasizing the importance of the crystal structure for the dissolution rate. For bacterial dissolution the initial rates correlate with the gross surface area indicating a marginal importance of Fe-oxide mineralogy.

7.1 Introduction

The occurrence of iron(III) oxides (hereafter iron oxides) in the environment has been comprehensively reviewed by Cornell and Schwertmann (1996). A wide range of iron oxide minerals is found in natural sediments, comprising ferrihydrite, lepidocrocite, goethite and hematite as the most common ones. In natural sediment the minerals occur in heterogeneous assemblages, which in addition include intergrowths with clays and organic matter. Apparently it is the reactivity of the iron oxides in the sediment that to a large extent determines their reduction (Raiswell and Canfield, 1996).

The role of microbes in the reduction of iron oxides is also well recognized (Lovley et al, 1993). During the last decade pure cultures of dissimilatory iron oxide reducers have been isolated and the characteristics of these organisms have been studied (Ghiorse (1988); Lovley, (1991;1993b;1995) and Thamdrup, (2000)). Pure culture experiments have been carried out with various synthetic iron oxide minerals and the results show that the microbial iron oxide reduction rate also depends on the reactivity of the iron oxide minerals (Munch and Ottow, 1980). In addition, Roden and Zachara (1996) have shown that the available surface area has a much larger influence on the rate of iron reduction than the mineralogy.

In natural sediments, the reduction of iron oxides is the terminal electron accepting step in the total process of organic matter degradation. The first step is extracellular hydrolysis and fermentation of organic matter. The proportion of electron flow that proceeds via the different pathways, iron oxide, sulfate reduction, and methanogenesis depends on their abundance and energy gains of the terminal electron accepting reaction (Lovley and Phillips, 1987a). In most cases, it is the reactivity of the organic matter that determines the overall rate of organic matter degradation. However, in the case of iron oxide reduction the dissolution rate, and thereby the reactivity of the iron oxides, constitutes an additional potentially rate limiting step. When the reactivity of the organic matter is high then the kinetics of iron oxide reduction may become rate limiting for the overall process of iron reduction. Reversibly, when the reactivity of organic matter is low then it is unlikely that dissolution of iron oxides would becomes overall rate limiting.

In this contribution, we aim at collecting the knowledge on the influence of iron oxide heterogeneity on bacterial iron oxide reduction and abiotic dissolution. At first, we establish a framework where the reactivity of iron oxide minerals in abiotic systems is assessed and quantified, and in the second part, the importance of iron oxide reactivity for bacterial iron

oxide reduction is evaluated and discussed. Aiming at bridging applied chemistry with microbiology, already numerous variables are in focus, and in order to simplify the discussion it is focused on experimental systems rather than the nature.

7.2 Materials and Methods

7.2.1 Oxide Synthesis and Characterization

A variety of synthetic iron oxides (listed in Table 1) was synthesized according to the procedures described in Schwertmann and Cornell (1991). The suite of oxides included a series of goethites with differing crystallinity and surface area synthesized from $Fe(NO_3)_3$ at different temperatures as described in (Schwertmann et al, 1985), together with a high surface area goethite produced by air oxidation of $FeCl_2$ in $NaHCO_3$ buffer. A commercial hematite preparation purchased from Fisher Scientific was included in the experiments. All oxides were washed free of anions by centrifugation, freeze-dried (with the exception of freshly precipitated ferrihydrite), and passed through a 100 μm sieve prior to use in experiments. The iron oxides presented in Larsen and Postma (2001) were not freeze dried but dial. The crystallographic identity of the oxide phases was verified by XRD (Phillips APD 3600 automated X-ray Powder diffractometer). The surface area of the synthetic iron oxides and oxide-coated sand was determined by multi-point BET analysis (Micromeritics Model Gemini). The hydroxylamine-HCl extractable Fe(III) content of the oxides was determined by shaking (250 rpm) 0.025-0.1 g of material in 5 mL of 0.25M NH_2OH/0.25M HCl for 1 hr followed by Ferrozine analysis of the Fe(II) content of the extract (Stookey, 1970).

The total reactive iron oxide content of three previously studied (Roden and Zachara, 1996) (Roden and Urrutia, 1999) iron oxide-bearing subsurface materials (HC and CP subsoils and Oyster coastal plain sediment) was determined by citrate-dithionite extraction as previously described (Roden and Zachara, 1996). The natural materials were air dried and passed through a 2-mm sieve prior to analysis. The surface area and hydroxylamine HCl-extractable iron content of the natural materials were determined as described above. Selected properties of the synthetic iron oxide-coated sand and natural iron oxide-bearing materials are listed in Table 2. Additional properties of these materials are reported elsewhere (Rai et al, 1996;Zachara et al, 1989;Zachara et al, 1995).

7.2.2 Initial Rates of Synthetic Iron Oxide Reductive Dissolution by Ascorbate

Experiments were carried out in 1.3 L glass reaction vessels immersed in a thermostated bath (25^{o}C) with a stirring propeller fitted through the top of the vessel. The stirring rate was kept constant for all the experiments. Purified and water-saturated N_2 was continuously passed through the vessel to maintain anoxic conditions. Each experiment was started by filling the reaction vessel with 1.1 L of a anoxic 10 mM ascorbic acid solution, adjusted to pH=3.000±0.005, followed by addition of stock suspensions of synthetic iron oxides washed free of salts by dialysis and kept in suspension. Measuring the concentration of released Fe^{2+}, which in acid solution is unlikely to form any precipitate, the reaction of ascorbic acid with iron oxides was followed. The samples were in-line filtered through a 0.2 μm cellulose acetate membrane filter and injected directly into ferrozine. Then a Na-acetate buffer solution was added to the vials and subsequently Fe^{2+} was determined spectrophotometrically (Stookey, 1970). Preliminary experiments performed in the dark demonstrated that light had no influence on the results.

The synthetic iron oxides that were dissolved both chemically and bacterially were analyzed in a slightly different way. Here the freeze dried iron oxides were suspended at a concentration of 5 mmol Fe(III) L^{-1} in 100 mL of N_2-bubbled 10 mM ascorbic acid (pH 3) contained in 120-mL serum bottles (capped with a thick rubber stopper and crimp sealed). The oxide suspensions were incubated at room temperature on a rotary shaker over a 1 to 2-d (except for freshly-precipitated ferrihydrite) incubation period, during which samples for dissolved Fe(II) analysis were removed periodically with a N_2-flushed plastic syringe and filtered through a 0.2 μm syringe filter into Ferrozine. Accumulation of Fe(II) was linear during the incubation period. A maximum of ca. 20% of the iron oxide content of the oxide suspensions was reduced during the incubation period, except for lepidocrocites, which was reduced 65% of a 22-hr period. Initial rates of oxide reduction were computed by linear regression analysis of Fe(II) vs. time data. Analysis of freshly-precipitated ferrihydrite reduction by ascorbate was conducted over a 1-hr incubation period, during which time Fe(II) accumulated in a hyperbolic manner. The initial rate of ferrihydrite reduction was computed from the first derivative of a nonlinear curve fit of Fe(II) vs. time data to an equation depicting the accumulation of end-product from a first-order reaction.

7.2.3 Initial Rates of Bacterial Synthetic Iron Oxide Reduction

Synthetic iron oxides were suspended at a concentration of 10 mmol Fe(III) L^{-1} in 10 mL of Pipes (piperazine-N, N'-bis {2-ethanesulfonic acid}, dipotassium salt) buffer (10 mM, pH 6.8) in 25-mL anaerobic pressure tubes (Bellco, Inc.). Triplicate tubes were prepared for each oxide, and the tubes were bubbled for 5-10 min with O_2-free N_2 prior to being capped with thick rubber stoppers and crimp sealed. The oxide suspensions were not autoclaved so as to avoid the possible influence of heating on their surface properties and crystallinity. The tubes were inoculated with ca. 2×10^8 cells mL^{-1} of the dissimilatory iron oxide reducing bacterium *Shewanella putrefaciens* strain CN32 (Fredrickson et al, 1999). Strain CN32 was isolated from anaerobic groundwater and is capable of carrying out dissimilatory iron oxide reduction with either lactate or H_2 as an electron donor. As previously described (Fredrickson et al, 1999), the cells were grown aerobically for 16 hr on tryptic soy broth and then washed twice with sterile anaerobic Pipes buffer prior to use in iron oxide reduction experiments. After inoculation, 10 mL of headspace gas was removed from the tubes and replaced with 100% H_2. The tubes were incubated at room temperature on a rotary shaker (150 rpm) over a 3-d incubation period. Subsamples were removed periodically with a N_2-flushed plastic syringe and 18G needle and analyzed for dissolved (0.2 μm-filtered) and total (0.5M HCl-extractable) Fe(II) content by Ferrozine analysis. Accumulation of both dissolved and total Fe(II) was linear over the incubation period for all oxide phases. Initial rates of oxide reduction were therefore computed by linear regression analysis of total Fe(II) vs. time data; r^2 values were ≥ 0.9 for all experiments.

7.3 Kinetics of Dissolution – The Concept

The kinetics of iron oxide dissolution has been studied in a large number of experimental studies using various reactants and/or different iron oxide minerals. The resulting information is difficult to overview since there are many variables involved. To assess the kinetics of iron oxide dissolution in a more systematic way, Postma (1993) applied the general rate law for mineral dissolution of Christoffersen and Christoffersen (1976) to the interpretation of dissolution of iron oxides:

$$J_B = \frac{d\frac{m}{m_0}}{dt} = k \cdot m_0 \cdot f\left(\frac{m}{m_0}\right) \cdot g(C) \qquad (1)$$

In this rate law J_B is the overall (bulk) dissolution rate ($mol \cdot s^{-1}$), m_0 the initial mass of crystals and m the mass of crystals at time t and k the rate constant (s^{-1}). $f(m/m_0)$ is a function of the undissolved crystal fraction often approximated by an exponential function: $(m/m_0)^{\gamma}$. The function g(C) is a function of the reactant such as the solution composition (type and concentration of reactant and pH) for chemical experiments and microbial activity for biological experiments. A different experimental design must be used to assess the functions f and g. To investigate the effect of the reactant on iron oxide dissolution $f(m/m_0)$ should be kept constant in the course of the experiment. In initial rate dissolution experiments, only a negligible fraction of the iron oxide dissolves and therefore $f(m/m_0)$ remains constant. The use of different iron oxides in initial rate experiments will result in different values of k, the rate constant. On the other hand, when the effect of bulk dissolution of iron oxide on the reaction rate is studied then it would be an advantage to keep function g(C) constant. In addition, the experiments must now be designed to last a period of time that allows the iron oxide to dissolves quantitatively. By using a high concentration of the reactant and only a little iron oxide, the solution composition changes only marginally and g(C) is constant. When g (C) is constant, Eq. 1 can be rewritten to:

$$\frac{J_B}{m_0} = k' \cdot \left(\frac{m}{m_0}\right)^{\gamma} \qquad (2)$$

Here, k' contains both the rate constant and g(C). The γ-value expresses the change in rate, J_B, during dissolution. Different processes may alter the surface properties of the iron

oxide and thereby decrease the dissolution rate. The dissolution of a crystal at high-energy sites like dislocations or corners proceeds at a rate that is much higher than at basal crystal surfaces (Cornell and Schwertmann, 1996). The quantity of the high-energy sites is however very low in comparison to the basal surfaces. Consequently, a decrease in dissolution rate can be due to the consumption of high-energy surface sites. When dissolution at basal surfaces dominates then the rate becomes proportional to the instantaneous surface area. If the particles are approximated by uniform spheres (or another 3-dimensional body), then the γ-parameter takes a value of 2/3. The change in dissolution rate is also related to changes in particle size distribution, and the dissolution of a skewed polydisperse mineral preparation can yield a γ-value higher than 2 (Larsen and Postma, 2001).

7.4 Initial Dissolution Rate - The Effect of the Reagent

According to the overall model the effect of reagent on the rate of iron oxide dissolution is best investigated in initial rate experiments with $f(m/m_0)$ being a constant. Surface fluxes, i.e. the initial dissolution rate normalized to surface area, for various reagents reacting with goethite are compiled in Figure 7.1 (see also Table 7.1) and show a variation covering more than four orders of magnitude.

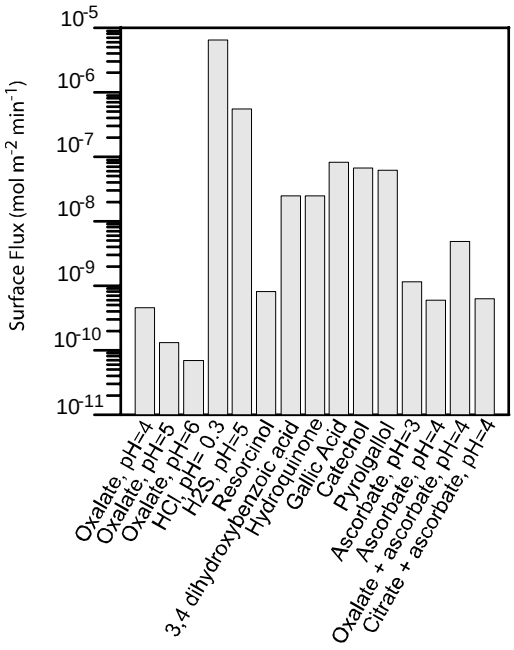

Figure 7.1 A presentation of initial dissolution rates of goethite by various reactants. Data from: Zinder et al., 1986; Sidhu et al., 1981; dos Santos Afonso and Stumm, 1994; LaKind and Stone, 1989; Reyes and Torrent, 1997.

A low surface flux is found for complexing agents like oxalate while the highest surface flux is recorded for H_2S. Different organic reductants like pyrogallol and catechol give a surface flux that is only an order of magnitude lower. A word of caution is appropriate in the comparison of the surface fluxes since the goethite employed in the different experiments may have had different surface properties. In general, the differences in rate illustrate the difference in mechanisms of iron oxide dissolution.

The different mechanisms for iron oxide dissolution are outlined for hematite at pH 3 in Figure 7.2 (Banwart et al, 1989). The presence of only protons gives a very low initial dissolution rate, a ligand like oxalate increases the rate somewhat, but substantial higher rates are found in the presence of a reductant like ascorbate and the highest rates are observed in the presence of both a ligand and a reductant. The initial dissolution rate also depends on the concentration of ascorbate. At a low ascorbate concentration, the effect is large while at high ascorbate concentrations the effect becomes small. This was interpreted as reflecting saturation of the hematite surface by ascorbate (Banwart et al, 1989).

At a molecular level, the dissolution of iron oxides involves either an electrophilic attack on the oxobonds (proton induced) or a nucleophilic attack on the Fe atom (ligand promoted). These steps are accompanied by hydration and release of the Fe-atom. Zinder et al. (1986) showed the rate limiting step of iron oxide dissolution to be the detachment of Fe from the surface. The transfer of charge to the Fe-atom increases the dissolution rate by easing the nucleophilic/electrophilic attack. Hence, e^--transfer precede detachment of Fe by reductive dissolution but does *puncto strickto* not lead to dissolution by itself. Below the different mechanisms are discussed in some more detail.

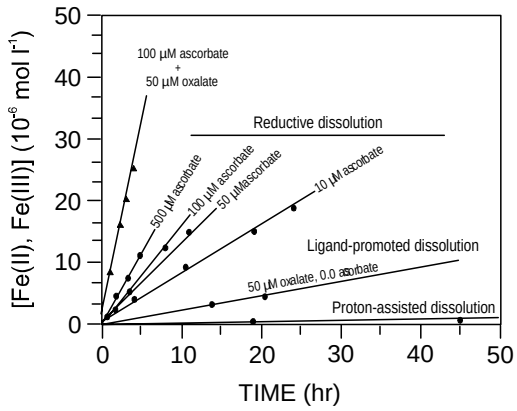

Figure 7.2 Dissolution of hematite in the presence or absence of ascorbate and or oxalate at pH=3. The dissolution rate is for proton assisted dissolution $0.028 \cdot 10^{-9}$ mol m^{-2} min^{-1}, for ligand promoted dissolution $0.35 \cdot 10^{-9}$ mol m^{-2} min^{-1}, for reductive dissolution $2.47 \cdot 10^{-9}$ mol m^{-2} min^{-1} and for ligand promoted reductive dissolution $9.95 \cdot 10^{-9}$ mol m^{-2} min^{-1} (Banwart et al., 1989, with permission).

7.4.1 Proton Assisted Dissolution of Iron Oxides

Table 7.1 compiles experimental results for proton assisted dissolution of iron oxides. A general mechanism for proton assisted dissolution of oxides was proposed by Furrer and Stumm (1986) and Stumm and Furrer (1987). Initially a proton is adsorbed by a surface OH group forming a $Fe(OH_2)_2^+$ surface complex. Adsorption of additional protons weakens the Fe-O bond by strong polarization and lead ultimately to dissolution. A rate law for proton assisted dissolution is

$$J_P = k \cdot (C_P^s)^n \qquad (3)$$

where J_P is the rate ($mol \cdot m^{-2} \cdot s^{-1}$), k the reaction constant, and C^s_P the surface concentration of protons. The number of protons required for weakening of the Fe-O bond is given by the exponent n. Equation 3 may be extended to include anion effects, anions as Cl^- may replace surface OH groups and assist in the release of Fe. Surface protonation is strongly pH dependent, and results presented in Table 7.1 show that the dissolution rate of hematite increases by five orders of magnitude when the pH decreased from 3 to 1.

Table 7.1 (A) Initial abiotic dissolution rate normalized to surface area, the so-called Surface flux of iron oxides by different reactants. The ferrihydrite marked with an "a" was freeze-dried prior to the dissolution experiment.

	Oxide	Reactant Conc. M	Temp. / pH (^{o}C)	Surface flux $mol \cdot m^{-2} \cdot min^{-1}$	Reference
Ligand Promoted dissolution					
Citrate	Fh	$9.5 \cdot 10^{-4}$	25 / 4	$2.7 \cdot 10^{-8}$	Liang et al. (2000)
Citrate	Fh	$9.5 \cdot 10^{-4}$	25 / 6.5	$4.2 \cdot 10^{-9}$	Liang et al. (2000)
EDTA	L	10^{-3}	20 / 7	$3.3 \cdot 10^{-8}$	Biber et al. (1994)
Oxalate	Gt	10^{-3}	25 / 4	$4.6 \cdot 10^{-10}$	Zinder et al. (1986)
Oxalate	Gt	10^{-3}	25 / 5	$1.3 \cdot 10^{-10}$	Zinder et al. (1986)
Oxalate	Gt	10^{-3}	25 / 6	$6.9 \cdot 10^{-11}$	Zinder et al. (1986)
Oxalate	Hm	$5 \cdot 10^{-5}$	25 / 3	$3.5 \cdot 10^{-10}$	Banwart et al. (1999)
Proton assisted dissolution					
HCl	A	0.5	25 / 0.3	$1.5 \cdot 10^{-4}$	Sidhu et al.(1981)
HCl	Fh	0.5	20 / 0.3	$7.1 \cdot 10^{-4}$	Cornell et al. (1974)
HCl	Gt	0.5	25 / 0.3	$6.5 \cdot 10^{-6}$	Sidhu et al.(1981)
HCl	Gt	0.5	20 / 0.3	$7.6 \cdot 10^{-6}$	Cornell et al. (1976)
HCl	Gt	0.5	20 / 0.3	$7.5 \cdot 10^{-5}$	Cornell et al. 1976 (1976)
HCl	Hm	0.5	25 / 0.3	$1.4 \cdot 10^{-5}$	Sidhu et al.(1981)
HCl	Hm	0.5	20 / 0.3	$1.0 \cdot 10^{-6}$	Cornell et al. (1974)
HCl	L	0.5	25 / 0.3	$7.0 \cdot 10^{-3}$	Sidhu et al.(1981)
HCl	Mh	0.5	25 / 0.3	$1.0 \cdot 10^{-4}$	Sidhu et al.(1981)
HCl	Mt	0.5	25 / 0.3	$3.7 \cdot 10^{-4}$	Sidhu et al.(1981)
HNO_3	Hm	0.001	25 / 3	$2.8 \cdot 10^{-11}$	Banwart et al. (1999)
HNO_3	Hm	0.1	22 / 1	$1.2 \cdot 10^{-6}$	Samson and Eggleston (2000) Samson et al. (2000)
HNO_3	Hm	0.1	22 / 1	$1.9 \cdot 10^{-6}$	Samson and Eggleston (2000) Samson et al. (2000)
Reductive dissolution					
3,4 DHB*	Gt	10^{-3}	30 / 4.2	$2.5 \cdot 10^{-8}$	LaKind and Stone (1989)
Ascorbate/Citrate	Gt	$5 \cdot 10^{-2}$+0.2	25 / 6	$6.3 \cdot 10^{-10}$	Reyes and Torrent 1997
Ascorbate/Citrate	Gt	$5 \cdot 10^{-2}$+0.2	25 / 6	$1.7 \cdot 10^{-9}$	Reyes and Torrent 1997

Table 7.1 (B) Initial abiotic dissolution rate normalized to surface area, the so-called Surface flux of iron oxides by different reactants. The ferrihydrite marked with an "a" was freeze-dried prior to the dissolution experiment.

	Oxide	Reactant Conc. M	Temp. / pH (^{o}C)	Surface flux mol·m^{-2}·min^{-1}	Reference
Reductive dissolution					
3,4 DHB*	Gt	10^{-3}	30 / 4.2	$2.5 \cdot 10^{-8}$	LaKind and Stone (1989)
Ascorbate/Citrate	Gt	$5 \cdot 10^{-2}$+0.2	25 / 6	$6.3 \cdot 10^{-10}$	Reyes and Torrent 1997
Ascorbate/Citrate	Gt	$5 \cdot 10^{-2}$+0.2	25 / 6	$1.7 \cdot 10^{-9}$	Reyes and Torrent 1997
Ascorbate/Citrate	Hm	$5 \cdot 10^{-2}$+0.2	25 / 6	$3.7 \cdot 10^{-10}$	Reyes and Torrent 1997
Ascorbate/Citrate	Hm	$5 \cdot 10^{-2}$+0.2	25 / 6	$6.4 \cdot 10^{-9}$	Reyes and Torrent 1997
Ascorbate/oxalate	Gt	10^{-3}+10^{-3}	25 / 4	$4.8 \cdot 10^{-9}$	Zinder et al. (1986)
Ascorbate/oxalate	Hm	0.1/$5 \cdot 10^{-5}$	25 / 3	$9.9 \cdot 10^{-9}$	Banwart et al. (1999)
Ascorbate	Fh	10^{-2}	20 / 3	$6,0 \cdot 10^{-7}$	This study
Ascorbate	Fh^{a}	10^{-2}	20 / 3	$1.0 \cdot 10^{-8}$	This study
Ascorbate	Fh	$4.8 \cdot 10^{-2}$	20 / 7.5	$2 \cdot 10^{-6}$	Deng and Stumm (1994)
Ascorbate	Fh	10^{-3}	25 / 4	$4.1 \cdot 10^{-6}$	Liang et al. (2000)
Ascorbate	Fh	10^{-3}	25 / 6	$2.5 \cdot 10^{-9}$	Liang et al. (2000)
Ascorbate	Fh	10^{-2}	20 / 3	$2.5 \cdot 10^{-6}$	Larsen and Postma (2001)
Ascorbate	Fh	10^{-2}	20 / 3	$2.0 \cdot 10^{-6}$	Larsen and Postma (2001)
Ascorbate	Fh6	10^{-2}	20 / 3	$2.7 \cdot 10^{-7}$	Larsen and Postma (2001)
Ascorbate	Fox	10^{-2}	20 / 3	$4.5 \cdot 10^{-9}$	This study
Ascorbate	Gt	10^{-2}	20 / 3	$4.9 \cdot 10^{-9}$	This study
Ascorbate	Gt	10^{-2}	20 / 3	$1.0 \cdot 10^{-9}$	This study
Ascorbate	Gt	10^{-2}	20 / 3	$9.4 \cdot 10^{-10}$	This study
Ascorbate	Gt	10^{-2}	20 / 3	$6.7 \cdot 10^{-10}$	This study
Ascorbate	Gt	10^{-2}	20 / 3	$2.3 \cdot 10^{-10}$	This study
Ascorbate	Gt	10^{-3}	25 / 3	$1.1 \cdot 10^{-9}$	Zinder et al. (1986)
Ascorbate	Gt	10^{-3}	25 / 4	$6.0 \cdot 10^{-10}$	Zinder et al. (1986)
Ascorbate	Gt	10^{-2}	20 / 3	$2.8 \cdot 10^{-8}$	Larsen and Postma (2001)
Ascorbate	Hm	10^{-4}	25 / 3	$2.5 \cdot 10^{-9}$	Banwart et al. (1999)
Ascorbate	Hm	10^{-2}	20 / 3	$4.4 \cdot 10^{-9}$	This study
Ascorbate	Hm	10^{-2}	20 / 3	$4.5 \cdot 10^{-9}$	This study
Ascorbate	L	10^{-2}	20 / 3	$9.2 \cdot 10^{-8}$	This study
Ascorbate	L	$4.8 \cdot 10^{-2}$	20 / 7	$1.9 \cdot 10^{-5}$	Deng and Stumm (1994)
Ascorbate	L	10^{-2}	20 / 3	$2.8 \cdot 10^{-7}$	Larsen and Postma (2001)
Ascorbate	L	10^{-2}	20 / 3	$4.4 \cdot 10^{-7}$	Larsen and Postma (2001)

Table 7.1 (C) Initial abiotic dissolution rate normalized to surface area, the so-called Surface flux of iron oxides by different reactants. The ferrihydrite marked with an "a" was freeze-dried prior to the dissolution experiment.

	Oxide	Reactant Conc. M	Temp. / pH (^{o}C)	Surface flux $mol \cdot m^{-2} \cdot min^{-1}$	Reference
Reductive dissolution					
Catechol	Gt	10^{-3}	30 / 4	$6.7 \cdot 10^{-8}$	LaKind and Stone (1989)
Cysteine	Fh	$5 \cdot 10^{-3}$	25 / 6	$7.1 \cdot 10^{-7}$	Amirbahman et al. (1997)
Cysteine	Fh	$5 \cdot 10^{-3}$	25 / 8.3	$1.9 \cdot 10^{-6}$	Amirbahman et al. (1997)
Gallic acid	Gt	10^{-3}	30 / 3.1	$8.1 \cdot 10^{-8}$	LaKind and Stone (1989)
H_2S	Gt	10^{-3*}	20 / 5	$2.2 \cdot 10^{-3}$	Biber et al. (1994)
H_2S	Gt	10^{-3*}	25 / 5	$5.5 \cdot 10^{-7}$	Afonso and Stumm (1992)
H_2S	Hm	10^{-3*}	25 / 5	$9.9 \cdot 10^{-8}$	Afonso and Stumm (1992)
H_2S	Hm	10^{-2*}	20 / 4	$2.1 \cdot 10^{-2}$	Biber et al. (1994)
H_2S	L	10^{-3*}	25 / 5	$2.0 \cdot 10^{-6}$	Afonso and Stumm (1992)
H_2S	Mt	10^{-3*}	25 / 5	$1.4 \cdot 10^{-6}$	Afonso and Stumm (1992)
HQS*	Fh	$5 \cdot 10^{-4}$	20 / 7.4	$1.1 \cdot 10^{-5}$	Deng and Stumm (1994)
HQS*	L	$5 \cdot 10^{-4}$	20 / 7.3	$4.8 \cdot 10^{-5}$	Deng and Stumm (1994)
HQS* + humus	L	$5 \cdot 10^{-4*}$	20 / 7.3	$4.3 \cdot 10^{-4}$	Deng and Stumm (1994)
Hydroquinone	Gt	10^{-3}	30 / 3.5	$2.5 \cdot 10^{-8}$	LaKind and Stone(1989)
I^-	Hm	1.2	20 / 2.7	$6.0 \cdot 10^{-8}$	Ali et al.(1996)
I^-	Hm	1.2	20 / 2	$2.5 \cdot 10^{-7}$	Ali et al (1996)
Oxalate/Fe^{2+}	Gt	$10^{-3}/5 \cdot 10^{-3}$	25 / 3	$3.5 \cdot 10^{-8}$	Suter et al. (1991)
Photoreductive	L		20 / 4	$7.9 \cdot 10^{-7}$	Waite and Morel (1994)
Photoreductive	L		20 / 6.5	$4.5 \cdot 10^{-7}$	Waite and Morel (1994)
Photoreductive	L		20 / 8.2	$1.6.10^{-7}$	Waite and Morel (1994)
Pyrogallol	Gt	10^{-3}	30 / 3.4	$6.1 \cdot 10^{-8}$	LaKind and Stone (1989)
Resorcinol	Gt	10^{-3}	30 / 4	$8.0 \cdot 10^{-10}$	LaKind and Stone (1989)
SO_3^{2-} + Light	Hm	10^{-3}	25 / 3.9	$6.8 \cdot 10^{-3}$	Ansari et al. (1995)
SO_3^{2-} + Light	Hm	10^{-3}	25 / 3.95	$1.9 \cdot 10^{-2}$	Ansari et al. (1995)
SO_3^{2-} + Light	Hm	10^{-3}	25 / 4	$1.6 \cdot 10^{-2}$	Ansari et al. (1995)

DHB: Dihydroxybenzoic acid; HQS: 8-hydroxyquinoline-5-sulfonic acid, + humus indicate the addition of 5 ppm humus; Photoreductive: 300 $\mu E/cm^{-2}min^{-1}$ in a 10^{-4} M citrate solution.

7.4.2 Ligand Promoted Dissolution of Iron Oxides

As illustrated in Figure 7.2 for oxalate, the adsorption of a ligand to the surface of an iron oxide may increase the rate of dissolution. A general mechanism for ligand promoted dissolution can be written as

$$\equiv Fe^{III}\text{-}OH_2^+ + L^- \rightarrow \equiv Fe^{III}L + H_2O \rightarrow Fe^{III}L_{(aq)} + H_2O \quad (4)$$

In extension to proton assisted dissolution, the rate equation including ligand promoted dissolution becomes:

$$J_L = k_L \cdot (C_L^s) \cdot (C_P^s)^n \quad (5)$$

where J_L is the dissolution rate, k_L is the reaction constant and C^s_L is the surface concentration of the ligand. A ligand promoting dissolution forms a mononuclear surface complex that weakens the Fe-O bonds to the neighboring atoms in contrast to ligands forming bi- or trinuclear surface complexes that stabilize the surface and thereby retard the dissolution process. In addition to the surface concentration of the ligand, also the concentration of protons influences the dissolution rate (Eq. 5). Both the surface charge of the oxide and the speciation of the ligand in solution are affected by the pH. Optimal adsorption requires the surface to be positively charged, while the concentration of the negatively charged uncomplexed ligand is maximal. Therefore, ligand promoted dissolution of iron oxides is most effective in a narrow pH window. For citrate, this pH window ranges from 4 to 5 whilst for oxalate/oxalic acid the maximal dissolution rate is at pH 2-4 and for EDTA at pH 9-11 (Cornell and Schwertmann, 1996).

7.4.3 Reductive Dissolution of Iron Oxides

Reductive dissolution of iron oxides is the most important dissolution mechanism in natural sediments. Figure 7.1 and Table 7.1 also shows that reductive dissolution of iron oxide by dissolved sulfide and various organics is faster than by other mechanisms. As mentioned earlier reduction of structural Fe(III) to Fe(II) weakens the bonds in iron oxides and ease hereby the proton assisted or ligand promoted dissolution. The reductive dissolution of

hematite by ascorbate was already illustrated in Figure 2. The dissolution rate could be expressed as:

$$J_{RD} = k\left[> Fe^{III} HA\ \right] \quad (6)$$

where $>Fe^{III}HA$ is the surface ascorbate complex and k the first-order rate constant (Banwart et al., 1989). In the experiment with hematite, the proton assisted dissolution rate of iron oxides increased about 100 fold by addition of ascorbate (Figure 7.2). For the dissolution of goethite by ascorbate, Zinder et al. (1986) found the dissolution rate to increase with the surface protonation in an exponential of three. The data compiled for reductive dissolution in Table 1 indicates also for other iron oxides a strong increase in dissolution rate with decreasing pH, implying increasing surface protonation. For ligand promoted reductive dissolution, the mechanism can be exemplified by:

$$>FeOH_2^+ + L^- \leftrightarrows >FeL + H_2O \quad (7a)$$

$$>FeL + e^- \leftrightarrows >Fe^{II}L^- \quad (7b)$$

$$>Fe^{II}L^- + nH_2O \leftrightarrows \text{new surface site} + FeL_{(aq)} \quad (7c)$$

Here the >FeL complex acts as an electron shuttle, since ligand complexes with Fe^{2+} are generally less strong than with Fe^{3+}, the Fe^{2+}-complexes decompose and the ligand reattaches to the surface of iron oxides dissolution (Suter et al, 1988). In analogy to ligand promoted dissolution, ligand promoted reductive dissolution is a function of the surface concentration of the ligand-iron surface complex and the pH determining surface charge and ligand speciation (Zinder et al., 1986).

7.5. The Reactivity of Iron Oxides

Using a constant g(C) (Eq. 1) the initial rate approach is also suitable to compare the reactivity of different iron oxides as reactivity resides in the rate constant k. Figure 7.3 compares the initial rates for different iron oxides in ascorbate under conditions where the surface is saturated with ascorbate. The results show ferrihydrites and lepidocrocite to be the most reactive iron oxides while goethite and hematite have reactivity that is orders of magnitude lower.

In natural environments often a substantial part of the available pool of iron oxides becomes reduced. For example in marine sediment high in reactive organic matter, nearly all the iron oxide present at the surface becomes reduced within the upper 5 centimeter (Canfield, 1989). Furthermore, in many prolonged microbial experiments 40-60% of the iron oxide is turned-over (Lovley and Phillips, 1987b). When a significant part of the iron oxides is reduced, the pool of iron will change due to preferential dissolution of the most reactive material and the rate of iron oxide reduction will decrease over time. Eq. 2 can describe this change in reactivity over time, given that g(C) is kept constant.

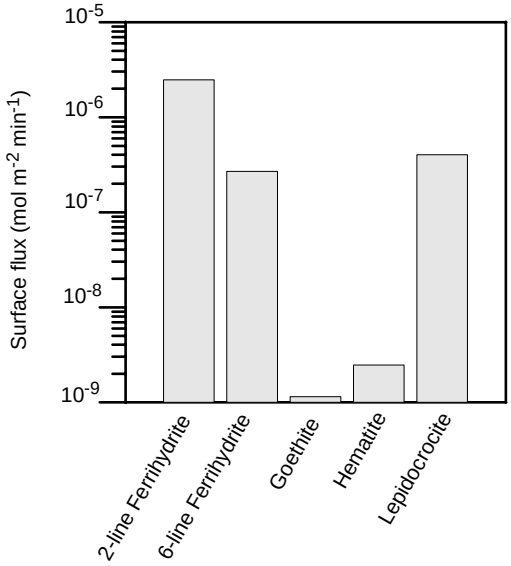

Figure 7.3 Initial dissolution rates of various iron oxides by proton assisted reductive dissolution. In all experiments the iron oxide surfaces were saturated with ascorbate at pH=3. Goethite data from Zinder et al. (1986), hematite from Banwart et al. (1989), the rest from Larsen and Postma (2001).

The results of bulk dissolution experiments with goethite, lepidocrocite, and ferrihydrite at pH 3 and in the presence of excess ascorbate are shown in Figure 7.4 and the included lines are fits of Eq. 2. The initial rates are consistent with those shown in Figure 7.3, ferrihydrite dissolution being faster than lepidocrocite, which again is faster than goethite. However, the decrease in reaction rate when most of the crystal mass has been dissolved is quite different. For ferrihydrite and lepidocrocite, the rate decelerates strongly when about 20 % of the crystal mass is left but for goethite the rate remains about the same. The rate equations based on Eq.

2 for different iron oxides can be compared in a plot of $-\log(J_B/m_0)$ vs. $-\log(m/m_0)$ (Figure 7.5). In this plot the slope of the lines equals the exponent (γ in Eq. 2) and the intersection with the y-axis is the rate constant (k' in Eq. 2). The γ ranges from 1.0 for goethite over close to 1.4 for lepidocrocites to 2.3 for akaganéite and 2.5 for 6-line ferrihydrite.

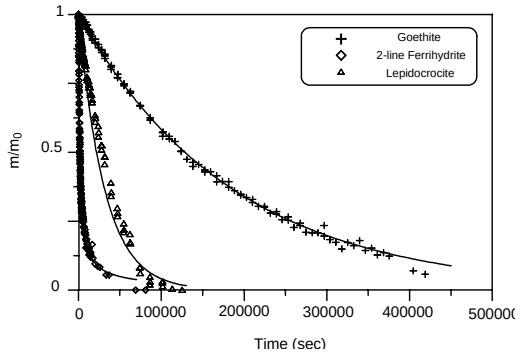

Figure 7.4 Proton assisted reductive dissolution of 2-line ferrihydrite, lepidocrocite and goethite by 10 mM ascorbate at pH=3.0. m/m_0 is the fraction of undissolved mineral. The lines represent the rate law shown in Eq. (2).

The implication is that when 10 % of the akaganéite crystal mass is left, then the reaction rate is only 0.5 % of the initial rate. Identical preparations of ferrihydrite were found to yield γ-values of respectively 1.0 and 2.3 indicating substantial heterogeneity for ferrihydrites. The general conclusion is that the consideration of bulk dissolution of iron oxides produces a very large range in iron oxide reactivity. In Figure 7.5 the range in reaction rate going from the initial rate of a 2-line ferrihydrite to 90 % of dissolved akaganéite is four orders of magnitude and here the better crystalline goethites and hematites are not even included.

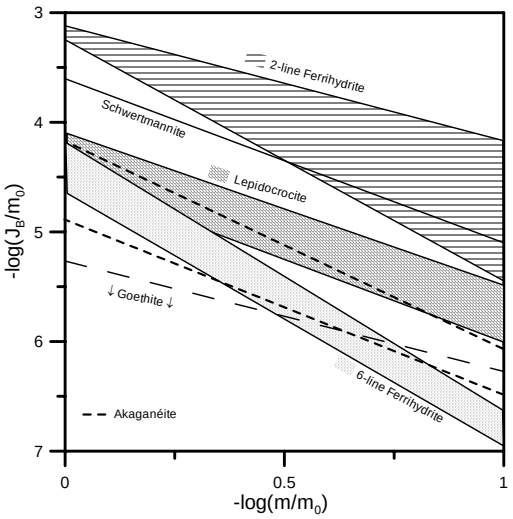

Figure 7.5 Comparison of iron oxide reduction rates, normalized over initial mass (J_B/m_0) versus the undissolved mineral fraction (m/m_0). The shaded areas represent the average of 5 lepidocrocite, 8 2-line and 5 6-line ferrihydrites as well as 6 akaganéite preparations.

7.6. Microbial Iron Oxide Reduction: Dependence on Iron Oxide mineralogy

During an initial rate measurement the reactivity of the iron oxide present remains constant (constant $f(m/m_0)$) allowing the simplification of the generalized rate law for mineral dissolution (1) to:

$$J / m_0 = k'' \cdot g(C) \tag{8}$$

where k'' is the product of the rate constant and $f(m/m_0)$ and g(C) is a function of the solution composition that may also comprise microbial activity. Hence, it is possible to draw an analogy between abiotic initial rates, where in 10 mM ascorbic acid also g(C) is a constant, and a microbial initial rate determination where g(C) still may vary.

Table 7.2 shows a compilation of initial rates derived from microbial reduction experiments. The initial rates are expressed as surface fluxes and the experiments cover a wide variation in substrate, reducing organism and iron oxide mineralogy and specific surface area. A summary

of the ranges in initial surface flux for different iron oxides is given in Fig. 7.6. The initial surface fluxes vary within 1 order of magnitude and the lowest initial rate was found for a ferrihydrite preparation that was dehydrated by freeze drying prior to the dissolution experiment. Table 7.2 also contains a number of new experiments carried out in this study to shed further light on the issue of how iron oxide reactivity controls bacterial iron oxide reduction rates. Experiments to determine initial rates (3 d incubation period) of reduction were carried out for 11 different synthetic iron oxides by a groundwater dissimilatory iron oxide reducing bacteria.

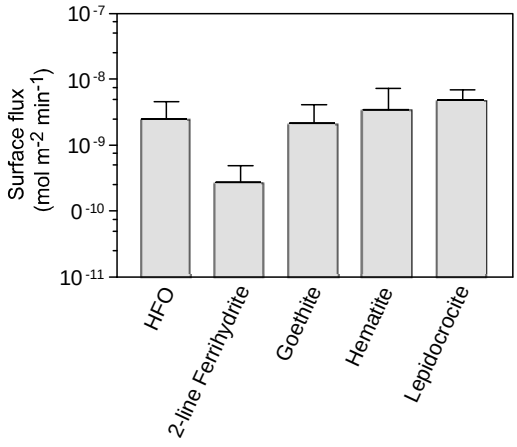

Figure 7.6 Initial surface area-normalized rates of bacterial iron oxide reduction for several different Fe(III) oxides minerals. The ferrihydrite preparation marked with an asterisk was freeze dried prior to bacterial reduction. Values plotted represent the mean ± SD of 3-18 different experiments for a given mineral phase. Data were obtained from the literature compilation presented in Table 2.

The organism used (*S. putrefaciens* strain CN32) has been employed in several recent studies of iron biomineralization and trace metal behavior during bacterial iron oxide reduction (Fredrickson et al, 1999; Fredrickson et al, 2000; Fredrickson et al, 2001; Roden et al, 2001; Zachara et al, 1998; Zachara et al, 2001b; Zachara et al, 2001a). The experiments were conducted under non-growth conditions in Pipes buffer with H_2 as the electron donor to maintain constant biological and simplified aqueous geochemical conditions. Parallel determinations of initial rates of oxide reduction by ascorbate at pH 3 were conducted in order

to directly compare the kinetics of biotic vs. abiotic oxide reduction as a function of iron oxide properties. It is important to stress that it was the initial rate of oxide reduction that was of interest in these experiments, rather than the long-term extent of reduction.

Table 7.2 (A) Initial microbial dissolution rate normalized to surface area, the so-called Surface flux of iron oxides by different microorganisms. The ferrihydrite marked with an "a" was freeze dried prior to the dissolution experiment. The surface areas marked with an asterisk have not been measured but is estimated. Abbreviations G and NG in the electron donor column stands for growth and non-growth respectively.

Organism	Oxide	Cell density	Electron donor	Surface area m^2/g	Surface flux $mol \cdot m^{-2} \cdot min^{-1}$	Reference
G. metallireducens	Fh	$1.5 \cdot 10^9$	Acetate / G	600*	$4.4 \cdot 10^{-10}$	Nevin and Lovley (2000)
G. metallireducens	Gt	$2.0 \cdot 10^8$	Acetate / G	55	$7.8 \cdot 10^{-10}$	Roden and Urrutia (1999)
G. sulfurreducens	Fh	$2.0 \cdot 10^8$	Acetate / NG	600*	$6.4 \cdot 10^{-9}$	Roden and Wetzel (2002)
S. alga BrY	Fh	$2.0 \cdot 10^8$	Lactate / G	600*	$2.4 \cdot 10^{-9}$	Roden and Zachara (1996)
S. alga BrY	Fh	$1.5 \cdot 10^9$	H_2 / NG	600*	$1.3 \cdot 10^{-9}$	Das and Caccavo (2000)
S. alga BrY	Fh[a]	$2.0 \cdot 10^8$	Lactate / G	241	$4.2 \cdot 10^{-10}$	This study
S. alga BrY	Gt	$1.5 \cdot 10^9$	Lactate / G	153	$3.9 \cdot 10^{-9}$	Roden and Zachara (1996)
S. alga BrY	Gt	$2.0 \cdot 10^8$	Lactate / G	55	$2.0 \cdot 10^{-9}$	Roden and Zachara (1996)
S. alga BrY	Gt	$2.0 \cdot 10^8$	Lactate / G	55	$2.5 \cdot 10^{-9}$	Roden and Zachara (1996)
S. alga BrY	Gt	$2.0 \cdot 10^8$	Lactate / G	55	$3.5 \cdot 10^{-9}$	Roden and Zachara (1996)
S. alga BrY	Gt	$2.0 \cdot 10^8$	Lactate / G	55	$9.5 \cdot 10^{-10}$	Roden and Urrutia (1999)
S. alga BrY	Gt	$2.0 \cdot 10^8$	Lactate / G	23	$8.7 \cdot 10^{-9}$	Arnold et al. (1988)
S. alga BrY	Gt	$4.0 \cdot 10^7$	Lactate / NG	19	$3.9 \cdot 10^{-10}$	This study
S. alga BrY	Hm	$2.0 \cdot 10^8$	Lactate / G	10	$2.6 \cdot 10^{-9}$	Roden and Zachara (1996)
S. putrefaciens CN32	Fh	$2.0 \cdot 10^8$	Lactate / G	600*	$6.7 \cdot 10^{-10}$	Roden et al. (2002)
S. putrefaciens CN32	Fh	$2.0 \cdot 10^8$	Lactate / G	600*	$4.0 \cdot 10^{-9}$	This study
S. putrefaciens CN32	Fh[a]	$2.0 \cdot 10^8$	H_2 / NG	290	$1.2 \cdot 10^{-9}$	This study
S. putrefaciens CN32	Fox	$2.0 \cdot 10^8$	H_2 / NG	176	$2.4 \cdot 10^{-10}$	This study
S. putrefaciens CN32	L	$2.0 \cdot 10^8$	H_2 / NG	64	$2.8 \cdot 10^{-9}$	This study

Table 7.2 (B) Initial microbial dissolution rate normalized to surface area, the so-called Surface flux of iron oxides by different microorganisms. The ferrihydrite marked with an "a" was freeze dried prior to the dissolution experiment. The surface areas marked with an asterisk have not been measured but is estimated. Abbreviations G and NG in the electron donor column stands for growth and non-growth respectively.

Organism	Oxide	Cell density	Electron donor	Surface area m^2/g	Surface flux $mol \cdot m^{-2} \cdot min^{-1}$	Reference
S. putrefaciens CN32	Gt	$2.0 \cdot 10^8$	H_2 / NG	211	$1.2 \cdot 10^{-9}$	This study
S. putrefaciens CN32	Gt	$2.0 \cdot 10^8$	H_2 / NG	96	$1.4 \cdot 10^{-9}$	This study
S. putrefaciens CN32	Gt	$2.0 \cdot 10^8$	H_2 / NG	73	$1.3 \cdot 10^{-9}$	This study
S. putrefaciens CN32	Gt	$2.0 \cdot 10^8$	H_2 / NG	62	$1.6 \cdot 10^{-9}$	This study
S. putrefaciens CN32	Gt	$2.0 \cdot 10^8$	Lactate / G	60	$4.1 \cdot 10^{-10}$	Liu et al. (2001)
S. putrefaciens CN32	Gt	$2.0 \cdot 10^8$	Lactate / G	55	$3.5 \cdot 10^{-10}$	This study
S. putrefaciens CN32	Gt	$2.0 \cdot 10^8$	H_2 / NG	38	$2.5 \cdot 10^{-9}$	This study
S. putrefaciens CN32	Gt	$2.0 \cdot 10^9$	Lactate / G	23	$8.8 \cdot 10^{-9}$	Arnold et al. (1988)
S. putrefaciens CN32	Hm	$2.0 \cdot 10^8$	H_2 / NG	19	$3.9 \cdot 10^{-10}$	This study
S. putrefaciens CN32	Hm	$2.0 \cdot 10^8$	H_2 / NG	10	$1.9 \cdot 10^{-9}$	This study
S. putrefaciens 200	L	$2.0 \cdot 10^6$	Lactate / G	110	$4.8 \cdot 10^{-9}$	Cooper et al. (2000)
S. putrefaciens 200	L	$2.0 \cdot 10^9$	Lactate / G	26	$7.0 \cdot 10^{-9}$	Arnold et al. (1988)
S. putrefaciens 200	Gt	$2.0 \cdot 10^6$	H_2 / NG	165	$2.0 \cdot 10^{-9}$	Cooper et al. (2000)
S. putrefaciens 200	Gt	$2.0 \cdot 10^9$	Lactate / G	15	$1.4 \cdot 10^{-9}$	Arnold et al. (1988)
S. putrefaciens 200	Hm	$2.0 \cdot 10^9$	Lactate / G	11	$9.0 \cdot 10^{-9}$	Arnold et al. (1988)

The results of the microbial and abiotic experiments are shown in Fig. 7.7 and listed in Table 7.2. The surface fluxes determined are well in line with earlier studies. A strong linear correlation is observed between initial microbial dissolution rates of iron oxide reduction and oxide surface area (Fig. 7.7). Three oxides that were strongly aggregated (as evidenced very rapid particle settling after mixing) were reduced at much lower rates than the other 8 oxides. Although a linear correlation between surface area and initial dissolution rate was observed for the aggregated oxides, this may be fortuitous since there is no a priori reason to suspect that the nature of particle aggregation would be the same for hematite, feroxyhite, and 2-line ferrihydrite. Generally, however, the results confirm the linear dependence of initial bacterial iron oxide reduction rate on the oxide surface area previously described by Roden and Zachara (1996).

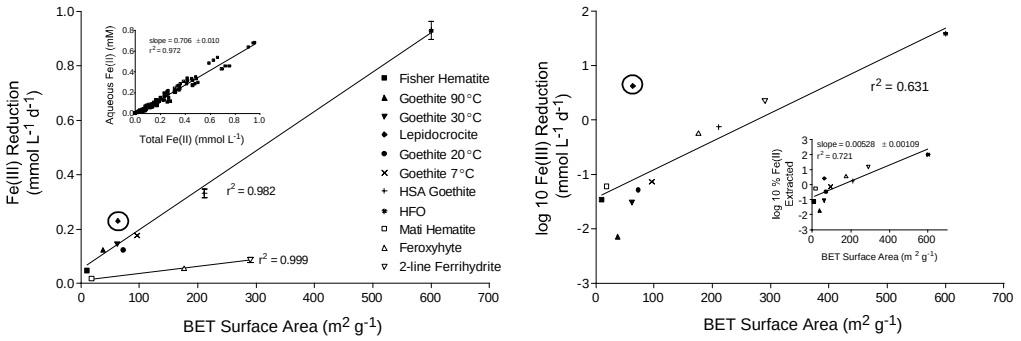

Figure 7.7 Relationship between oxide surface area and initial rate of reduction of various iron oxides by strain CN32 (2×10^8 cells mL^{-1}) (A) vs. ascorbate (10 mM, pH 3) (B). Starting Fe(III) concentrations in the biotic and abiotic reduction experiments were 10 mmol L^{-1} and 5 mmol L^{-1}, respectively. Rates shown in panel A are the results of linear regression analysis of Fe(II) vs. time data for triplicate 10-mL cultures; error bars show standard error of the slope parameter. Rates shown in panel B are the results of linear regression analysis of Fe(II) vs. time data for a single 100-mL suspension of oxide in ascorbate; error bars are omitted due to log-transformation. Open symbols represent oxides that demonstrated strong particle aggregation; solid symbols represent oxides, which showed no such aggregation. Inset in panel A shows the relative accumulation of dissolved vs. total Fe(II) during the bacterial iron oxide reduction experiments. Inset in panel B shows relationship between HA-extractable Fe(III) and oxide surface area. Solid lines show results of linear least-squares regression analyses.

As expected from section 5, the initial rates in ascorbic acid, here included in Fig. 7.7 to enable direct comparison with the microbial rates, vary by many orders of magnitude. Accordingly, there is no linear dependence on the surface area either. And in consequence, there is no simple correlation between the initial surface fluxes in chemical and in microbial dissolution rates.

7.7 Microbial Iron Reduction Mechanisms

A range of different processes sketched in Fig. 7.8 can limit microbial activity and cause a decrease in the iron oxide reduction rate. Transport of electrons from bacteria to the iron oxides, the reactivity of the iron oxides, and the inhibition of the reduction process due to changes in the chemical environment and accessibility of electron donor are the most important of these processes. The rate-limiting step for the microbial reaction has not yet been determined since the actual reaction mechanism basically remains unknown.

Several electron transfer pathways between the organisms and iron oxides have been proposed and two of these seem particularly feasible. One proposed mechanism involves the reductive dissolution of the iron oxides by an extra cellular electron shuttle (ligand promoted reductive dissolution) that in oxidized form serves as an electron acceptor (discussed in details elsewhere in this volume); the other mechanism involves a direct interaction between cell membrane and iron oxide.

Iron reducing bacteria such as *Shewanella* can produce extracellular electron shuttling compounds (quinone-like molecules) that may be involved in enzymatic iron oxide reduction. Newman and Kolter (Newman and Kolter, 2000) demonstrated the excretion of quinone compounds by *S. putrefaciens*, and suggested that release of such compounds might be involved in the transfer of electrons between *S. putrefaciens* and solid-phase iron oxides. An analogous suggestion had been made previously for *Geobacter sulfurreducens*, although subsequent studies demonstrated that the putative electron shuttling compound, a 9.6 kDa *c*-type cytochrome, does not actually function as an electron shuttle to Fe(III) (Lloyd et al, 1999).

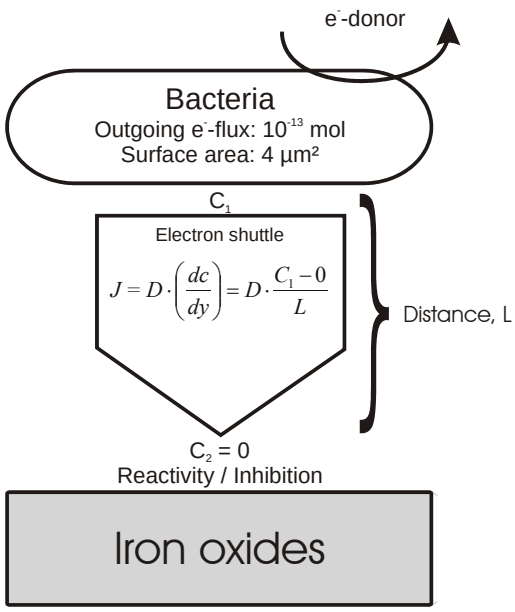

Figure 7.8 Schematic view of the bacteria iron oxide interface. The big arrow indicates the transport of electrons from bacteria to iron oxide and includes the expression for diffusional flux. C_1 and C_2 are the concentrations of reductant at the bacteria and iron oxide respectively. The reactivity of iron oxides and an eventual inhibition of the surface reactivity can be rate limiting when the e^--donor and transport conditions are satisfactorily supplied.

Nevin and Lovley (2002) (this issue) provide explicit evidence that *Shewanella* alga strain BrY produces and excretes electron shuttling compounds (very likely quinone-like compounds with a molecular weight of ca. 10 kDa or less), which allow the organism to reduce solid-phase iron oxides that they cannot directly contact. These findings are, however, in direct contrast to those obtained with *G. metallireducens*, which clearly does not produce extracellular electron shuttles during growth on insoluble iron oxides (Nevin and Lovley, 2000).

At a microscopic level, iron oxide reducers live in a world where transport is controlled by diffusion. Diffusion is a fast processes over small distances but sluggish when the distance increase. The amount of iron oxide required in one bacterial life cycle (defined as one doubling time) by one *Geobacter metallireducens* could be estimated from the data supplied by Lovley and Phillips (1988). Here, $3 \cdot 10^{10}$ cells oxidized 0.8 mmol acetate to CO_2 while they produced 3.2 mmol Fe^{2+}, in accordance with the theoretical 1:4 ratio. Hence, an iron oxide

reducing bacteria require a volume of iron oxide (10^{-13} mol Fe), which correspond to the volume of the organism. Assuming that iron oxides readily react with the electron shuttles and consume all reactant at the surface, the maximal distance between the iron oxide surface and a cell can be calculated for linear diffusion sketched in Figure 7.8. This distance depends on the time and concentration of intermediates. Seeliger et al. (Seelinger et al, 1998) found $9 \cdot 10^{-8}$ M of a c-type cytochrome capable of reducing iron oxides in a *Geobacter sulfurreducens* culture, which was proposed to support a kind of extracellular respiration. Lovley et al. (1996;1998), showed that *Geobacter metallireducens* are capable of using humic substances as electron acceptor and that this reaction is coupled to the reduction of iron oxides. The maximal distances were calculated using quinone as a model component for organic matter and cytochrome. The results of these calculations are shown in Table 7.3. The diffusion coefficient for quinone was estimated using the Wilke-Chang technique (Perry et al, 1984) and the diffusion coefficient for cytochrome was provided by Sealing et al. (1998). The concentration of cytochrome was multiplied with 3 since it transports 3 electrons per molecule. The quinone concentration was set to 10^{-5} M, which was supposed to be the maximal concentration one can find in natural environments.

The fluxes presented in Table 7.3 are considerably higher than the fluxes measured in the incubation experiments (Table 7.2), but in these experiments the coverage of iron oxides by microorganisms were actually low. After accounting for the "excess" surface area the aqueous electron shuttles can only support the high metabolic activity found in a culture experiment if the distance between iron oxide and bacteria is very small, in contrast to the conclusions drawn by Seelinger et al. (1998). Our calculations suggest that cytochrome only can be a key player when the bacteria adhere to the surface of iron oxides since at larger distances the reaction rate will be completely determined by the transport rate.

Table 7.3 The maximal distance between iron oxides and an iron oxide reducing organism based on a flux of 10^{-13} mol electrons supported by two electron shuttles. The metabolic activity was given by the doubling time seen in the first column. A bacterium was supposed to have a surface area of 2 µm² towards the iron oxide.

		Electron Shuttle	
Doubling time, hours	Required Flux per cell, mol m^{-2} s^{-1}	**Quinone** $D=1.08 \cdot 10^{-9}$ m²/s C_1= 0.01 mol/m³	**Cytochrome** $D=1.2 \cdot 10^{-10}$ m²/s $C_1=6 \cdot 10^{-4}$ mol/m³
		Max. distance, µm	***Max. distance, µm***
4	$3.5 \cdot 10^{-6}$	2.9	0.02
12	$1.2 \cdot 10^{-6}$	8.6	0.06
48	$2.9 \cdot 10^{-7}$	34.6	0.25
192	$7.2 \cdot 10^{-8}$	138.2	1.0

The contradiction to Seelinger et al. (1998) could be explained if well-fed organisms in cultures leak some of their cytochrome. Molecules that diffuse faster and occur at higher concentrations (like quinone) are actually able to support a satisfying electron flux at distances approaching microniches. A long life cycle will also increase the required electron flux as calculated in Table 7.2, since the consumption for a maintenance metabolism will increase. Taking a 2-8 day generation time for the bacteria the dissolution rate of iron oxides must exceed about $2 \cdot 10^{-5}$ mol/m²/min not to limit the reduction rate.

The isolation of iron oxide reducing bacteria from iron oxide surface mostly inhibits the reduction process, which has been taken as evidence for the need of direct contact between bacteria and iron oxides. The calculations presented above show that the separation of the bacteria from the surface by a few hundred µm effectively obstructs microbial iron oxide reduction. Grantham and Dove (1996) found that *Shewanella* dissolve iron oxides leaving bacteria shaped holes in the iron oxides documenting that a short reaction distance was involved. A direct reaction between the cell membranes and the iron oxides reducers was proposed and described by Myers and Myers (1992) and Munch and Ottow (1993a). Such a mechanism relieves the transport limitations, as only the electron donor would have to diffuse through the aquatic media.

7.8 Discussion

The data presented in this paper demonstrates some major differences in the behavior of abiotic reductive dissolution of iron oxides and bacterial reduction of iron oxides. For abiotic reduction, the effect of the iron oxide mineralogy is strong and yields a variation in initial surface flux covering three orders of magnitude (Fig. 7.1). In addition, the reactant (Fig. 7.2) is important and different reactants add four orders of magnitude in variation to the initial surface flux.

In enzymatic reduction of iron oxides the mineralogy still has influence on the initial surface flux but the effect is far less than would be predicted based on their relative susceptibility to abiotic reductive dissolution (Fig.7.6). This contrasting behavior is further illustrated by comparing the compilation of surface area-normalized initial rates of abiotic oxide reductive dissolution (Table 7.1) vs. bacterial reduction (Table 7.2). Also, the enzymatic reduction rate values are near the lower end of the range for abiotic reduction rate, closest a ligand like oxalate. The most striking aspect is, however, that enzymatic reduction rates are much more uniform than abiotic reduction rates. They fall mostly within a single order of magnitude regardless of the fact that apart from different iron oxides also different organisms, substrate etc. are employed.

A tentative conclusion would be that during enzymatic iron oxide reduction in cultures the mechanism is fundamentally different from abiotic reductive dissolution. As seen in section 7.7 the transport distance may exert control over enzymatic reduction while in abiotic reductive dissolution experiments this factor generally is relieved. As discussed in section 7.4, in abiotic reduction of iron oxide it is the detachment of a metal ion from the oxide surface site that is generally viewed as the rate-limiting step in iron oxide dissolution (Zinder et al., 1986). Considering the tendency for Fe(II) to reassociate (or never become detached in the first place) with oxide surfaces during enzymatic reduction at circumneutral pH (discussed extensively in Roden and Urrutia (2002), the kinetics of bacterial iron reduction may not be controlled by a leaving group. The most obvious explanation is that the rate of electron transfer, rather than Fe(II) detachment, is the rate-limiting step during enzymatic reduction. This suggestion is consistent with the much lower surface area-normalized rates of enzymatic vs. ascorbate-catalyzed iron oxide reduction (Fig. 7.1 and 7.6; Tables 7.1 and 7.2). Several processes may exert control over the electron transfer rate (Fig. 7.8). The transport processes and their dependence on distance to iron oxide dealt with by Nevin and Lovley (2002)

The question arises as to whether electron shuttling was involved in the iron oxide reduction activity of *S. putrefaciens* strain CN32 in this study. This is an important consideration, since the presence of such compounds might be expected to alter the response of enzymatic reduction activity to oxide surface and crystallographic properties. For example, one might expect that the presence of a soluble electron shuttling compound acting as a major reductant for iron oxides would make the enzymatic reduction system behave more like an abiotic reduction system in which the kinetics of electron transfer would be influenced by thermodynamic factors such as oxide crystal order vis-à-vis an effect on Fe(II) detachment energy. While we cannot rule out the possibility that electron shuttling compounds were present in our synthetic iron oxide reduction experiments (since we did not test for their presence), the fact that the oxide reduction experiments were conducted under non-growth conditions and in the absence of an organic carbon source suggests that biosynthesis of such compounds was not likely to have occurred. In addition, the cells used for the experiments were grown in the absence of Fe(III), so that production and storage of large quantities of electron shuttling compounds would not have been expected. Together these considerations suggest that soluble electron shuttling compounds were not likely to have been involved in controlling the initial rates of synthetic iron oxide shown in Fig. 7.6A. Nevertheless, the influence, which such compounds may have on the relative importance of surface area vs. crystal structure control on enzymatic iron oxide reduction, is a fruitful topic for future study. The same applies to the recent (Nevin and Lovley, 2001b) demonstration that some iron reducing bacteria (e.g. *Geothrix fermentans*; (Coates et al., 1999)) produce organic ligands that solubilize iron oxides. Iron oxide solubilization by such ligands might be expected to both significantly enhance rates of enzymatic oxide reduction (Lovley and Woodward, 1996), and to amplify the influence of the crystal structure on the kinetics of enzymatic reduction, in this case as a result of the influence of oxide crystal order on the rate of iron oxide dissolution by the ligands (Cornell and Schwertmann 1996).

A recent study by Lower et al. (2001) demonstrated (through the use of atomic force microscopy) apparent molecular recognition of iron oxide surface sites by a putative ca. 150 kDa outer membrane protein of the dissimilatory FeRB *Shewanella oneidensis* (formerly *S. putrefaciens* strain MR-1), a close relative of the organism employed in this study. These findings suggest the possibility that the direct linear relationship between enzymatic iron oxide reduction rate and oxide surface area shown in Fig. 7.7A (and by analogy, the similarity of surface area-normalized electron transfer rates across a broad range of oxide minerals; Fig.

7.2) results from the fact that dissimilatory iron reducing bacteria "recognize" iron oxide surfaces equally, independent of the underlying crystal structure, such initial rates of electron transfer subsequent to recognition proceed independent of crystal structure. This suggestion is consistent with the ability of *Shewanella* species to adhere equally well to both amorphous and crystalline iron oxides (Das and Caccavo, 2000), and may provide a mechanistic explanation for the fundamentally different behavior of enzymatic vs. abiotic oxide reduction with respect to the relationship between initial reduction rate and oxide surface area . It remains; however; somewhat unclear why enzymatic reduction rate is proportional to the available surface area but independent of the ratio of cell number over surface area. Particularly because the available surface area of the iron oxides in all experiments exceeded the surface area of the studied microorganisms by 3-5 orders of magnitude.

A final comment is on the implications for iron reduction in natural sediments. In marine sediments it is normally observed that more reactive iron oxides are reduced before less reactive iron oxides as determined by various chemical extractions (1993;1994). Reactivity is here the summed effect of both surface area and iron oxide mineralogy and it would be difficult to distinguish between the two parameters. However, in the competition between microbial and abiotic iron reduction, e.g. by dissolved sulfide, the latter process must be expected to be much faster.

7.9 Conclusions

Inorganic reductive dissolution experiments show different forms of iron oxides to have an initial reactivity ranging over 3 orders of magnitude and an internal heterogeneity covering 2-3 orders of magnitude. The experiments consistently show the reactivity to decrease from ferrihydrite to goethite/hematite. In general, the more crystalline iron oxides are more homogeneous and less reactive. Generally it is the detachment of the iron atom from the crystal lattice that is rate determining for the overall dissolution processes while it is accelerated by the presence of ligands and reductants.

Available evidence from bacterial cultures suggests on the other hand that enzymatic reduction does not respond strongly to the crystal structure of the iron oxide being reduced. Although variations in oxide crystal structure may alter rates of enzymatic reduction to some extent, the primary controlling factor appears to be the collective oxide surface area. In addition, the surface fluxes for enzymatic reduction in bacterial cultures vary within a

remarkable narrow range. Tentatively it is concluded that here the electron transfer step is overall rate controlling. The relative importance of the individual processes remain, however, still unclear.

Chapter 8

Concluding Remarks and Perspectives

This study presents new electrochemical methods to describe and to identify biogeochemical systems. Special emphasis was put on the detection and kinetic description of solid state particles and on the detection of free and complexed transition metals. New insights were gained in the application of new electrochemical methods, which allow a much faster environmental analysis and offer the potential for further in-situ and on-site studies.

Chapter 4 shows the promising results of Voltammetry of Immobilized Microparticles (VIM) to describe the solid state compounds of natural environments. This method enabled the distinction between refractory and reactive iron (oxyhydr)oxides, and between different iron sulfide minerals. This method had the advantage of being able to describe the reactivity change imposed by the composition change of the total iron pool without knowing the exact mineral composition, and additionally the possibility to detect the different iron compounds of which the iron pool was composed. The application to four natural environments shows the sensitivity to changing iron mineral composition. The electrochemical differentiation between iron sulfide minerals opens a new way to study the transformation of FeS to pyrite via greigite in sedimentary environments. In further applications, the electrochemical measurements could be combined to spectroscopic methods for a more detailed analysis of the electrochemical oxidation products. A combination of magnetic susceptibility measurements, more specific greigite extractions, and VIM offers a more exact determination of greigite in natural sediments, and probably suggests the suitability of VIM as a routine analysis of iron minerals in natural ecosystems.

Chapter 5 describes the possibilities using miniaturized microelectrodes for the determination of O2, S(-II), Fe(II), Mn(II) and transition metals. It describes detailed the construction of miniaturized microelectrodes, and evaluates different microsensor setups for different analytical purposes. These first test measurements show the applicability for in-situ studies, but also define the limitations of such devices. The use of solid amalgam miniaturized microelectrodes is most useful for measurements in sedimentary environments, where a solid electrode tip is advantageous. Iridium microsensors covered with a mercury droplet are more useful in aqueous systems to study nanomolar concentrations of transition metals, where the tip stability is less important.

The future application of such microsensors is strongly dependent on the construction and the polishing of such micro-devices. The incorporation of such microsensor devices in autonomous Lander systems is possible. To avoid the work with mercury, new studies should be done using bismuth as detector metal, because bismuth also offers the possibility to measure at very negative potentials due to a high overpotential. The use of lithography and nanoelectrodes may also be advantageous for the application to natural systems. Nanoelectrodes would reduce the background current, so that lower detection limits would be possible.

Chapter 6 describes the new method of *reverse titrations*. This new method allows the detection of different complexing ligands, and the calculation of their stability constants. An advantage of this new method is the reduction of the required sample volume. This method has been developed using copper, as a model compound, but future application to other ligand metal systems seem to be possible.

Chapter 7 is directly connected to chapter 4 using a continuum reactivity model to asses the abiotic and the bacterial dissolution of iron (oxyhydr)oxides. The comparison of initial abiotic and bacterial dissolution rates indicates that the dissolution mechanisms are fundamentally different. These experiments showed that abiotic dissolution experiments are strongly dependent on the crystal structure, while the bacterial initial dissolution rate correlates with the gross surface area. This study illustrates clearly that microbiological experiments have to be used very carefully to estimate microbial dissolution rates. The number of bacteria and the concentration of iron (oxyhydr)oxides in a dissolution experiment have to be adjusted to avoid artifacts caused by a growing bacterial population and to assure the all ferric iron is reduced within the timeframe of the experiment.

Future Projects.

Future projects are directly linked to the processes described in this thesis:

- bulk dissolution experiments in ascorbate can be combined to iron isotope fractionation analysis to investigate early diagenetic process
- redesigning of bacterial dissolution approaches, so that a comparison to wet chemical approaches is possible
- use of biological force microscopy to investigate different microbial dissolution mechanisms, and combining these force measurements to molecular biological techniques to investigate involved membrane proteins
- search for new electrode materials, which are not toxic, and allow measurements a very negative potentials to detect biogeochemistry related redox species.
- combining voltammetric microsensor systems to self controlled profiling systems
- Combining VIM with spectroscopic studies to evaluate the electrochemical reduction mechanisms of sulfide minerals

The overall goal behind all these future interests is to improve the understanding of coupled biogeochemical iron-sulfur cycle and the differentiation between biotic and abiotic processes involved.

Reference List

Abram, J. W. and D. B. Nedwell (1978). "Hydrogen as a substrate for methanogenesis and sulphate reduction in anaerobic saltmarsh sediement." Archives of Microbiology **117**: 93-97.

Achterberg, E. P. and C. M. G. van den Berg Deep Sea Res. **submitted**.

Afonso, M. D. and W. Stumm (1992). "Reductive Dissolution of Iron(III) (Hydr)Oxides by Hydrogen-Sulfide." Langmuir **8**(6): 1671-1675.

Aldstadt, J. H. and H. D. Dewald (1992). "Determination of Heavy-Metals by Thin-Layer Chromatography Square-Wave Anodic-Stripping Voltammetry." Analytical Chemistry **64**(24): 3176-3179.

Ali, S. P., M. A. Blesa, et al. (1996). "Reductive dissolution of hematite in acidic iodide solutions." Langmuir **12**(20): 4934-4939.

Aller, R. C. (1980). "Quantifying solute distributions in the bioturbated zone of marine sediments by defining an average microenvironment." Geochimica et Cosmochmica Acta **44**: 1955-1965.

Aller, R. C. (1984). "The importance of relict burrow structures and burrow irrigation in controlling sedimentary solute distributions." Geochimica et Cosmochmica Acta **48**: 1929-1934.

Aller, R. C. (1990). "Bioturbation and Manganese Cycling in Hemipelagic Sediments." Philosophical Transactions of the Royal Society of London. Series A, Mathematical and Physical Sciences **331**(1616): 51-68.

Aller, R. C. (1994). "Bioturbation and remineralization of sedimentary organic matter: effects of redox oscillation." Cemical Geology **114**: 331-345.

Aller, R. C. and P. D. Rude (1988). "Complete oxidation of solid phase sulfides by manganese and bacteria in anoxic marine sediments." Geochimica et Cosmochmica Acta **52**: 751-765.

Amirbahman, A., L. Sigg, et al. (1997). "Reductive dissolution of Fe(III) (hydr)oxides by cysteine: Kinetics and mechanism." Journal of Colloid and Interface Science **194**(1): 194-206.

Ansari, A., J. Peral, et al. (1995). "Photooxidation of Sulfite Ions in the Presence of Some Iron-Oxides." Journal of Photochemistry and Photobiology A-Chemistry **87**(2): 121-125.

Anshutz, P., C. Hyacinthe, et al. (1999). "The distribution of inorganic phosphorus in modern sediments of the Bay of Biscay." Comptes Rendus De L Academie Des Sciences Serie II Fascicule a-Sciences De La Terre Et Des Planetes **328**(11): 765-771.

Arnold, R. G., T. J. Dichristina, et al. (1988). "Reductive Dissolution of Fe(III) Oxides by Pseudomonas Sp 200." Biotechnology and Bioengineering **32**(9): 1081-1096.

Banfield, J. F. and K. H. Nealson (1997). Geomicrobiology: Interactions Between Microbes and Minerals. Washington, D.C., Mineralogical society of America.

Banfield, J. F., S. A. Welch, et al. (2000). "Aggregation-based crystal growth and microstructure development in natural iron oxyhydroxide biomineralization products." Science **289**(5480): 751-754.

Banwart, S., S. Davies, et al. (1989). "The Role of Oxalate in Accelerating the Reductive Dissolution of Hematite (Alpha-Fe2o3) by Ascorbate." Colloids and Surfaces **39**(4): 303-309.

Banwart, S. A. (1999). "Reduction of iron(III) minerals by natural organic matter in groundwater." Geochimica et Cosmochmica Acta **63**(19-20): 2919-2928.

Barbeau, K., E. L. Rue, et al. (2001). "Photochemical cycling of iron in the surface ocean mediated by microbial iron(III)-binding ligands." Nature **413**(6854): 409-413.

Bard, A. J. and L. R. Faulkner (2001). Electrochemical Methods - Fundamentals and applications. New York, Wiley.

Barker, G. C. and A. W. Gardner (1960). "Pulse Polarography." Fresenius Zeitschrift Fur Analytische Chemie **173**(1): 79-83.

Barker, G. C. and I. L. Jenkins (1992). "Square-Wave Polarography (Reprinted from the Analyst, Vol 77, Pg 685-695, 1952)." Analyst **117**(12): R1-R11.

Belmont, C., M. L. Tercier, et al. (1996). "Mercury-plated iridium-based microelectrode arrays for trace metals detection by voltammetry: Optimum conditions and reliability." Analytica Chimica Acta **329**(3): 203-214.

Belmont-Hebert, C., M. L. Tercier, et al. (1998). "Gel-integrated microelectrode arrays for direct voltammetric measurements of heavy metals in natural waters and other complex media." Analytical Chemistry **70**(14): 2949-2956.

Benning, L. G., R. T. Wilkin, et al. (2000). "Reaction pathways in the Fe-S system below 100 degrees C." Chemical Geology **167**(1-2): 25-51.

Berner, R. A. (1969). "Synthesis of Framboidal Pyrite." Economic Geology **64**(4): 383-&.

Berner, R. A. (1970). "Sedimentary pyrite formation." American Journal of Science **268**: 1-23.

Berner, R. A. (1971). "Sulfate reduction, pyrite formation, and the oceanic sulfur budget." Nobel Symposium **20**: 347-361.

Berner, R. A. (1980). Early Diagenesis. Princeton, Princeton University Press.

Berner, R. A. (1984). "Sedimentary pyrite formation: An update." Geochimica et Cosmochmica Acta **48**: 605-615.

Berner, R. A. (1989). "Biogeochemical cycles of carbon and sulfur and their effect on atmospheric oxygen over phanerozoic time." Palaeogeography, Palaeoclimatology, Palaeoecology **75**: 97-122.

Biber, M. V., M. D. Afonso, et al. (1994). "The Coordination Chemistry of Weathering .4. Inhibition of the Dissolution of Oxide Minerals." Geochimica et Cosmochmica Acta **58**(9): 1999-2010.

Bixler, J. W., M. Fifield, et al. (1989). "An Evaluation of Ultrathin Ring and Band Microelectrodes as Amperometric Sensors in Electrochemical Flow Cells." Electroanalysis **1**(1): 23-33.

Blakeney, M. D., T. Moulaei, et al. (2000). "Fe(III) reduction activity and cytochrome content of Shewanella putrefaciens grown on ten compounds as sole terminal electron acceptor." Microbiological Research **155**(2): 87-94.

Bond, A. M. (1994). "Past, Present and Future Contributions of Microelectrodes to Analytical Studies Employing Voltammetric Detection - a Review." Analyst **119**(11): R1-R21.

Bond, A. M., K. Z. Brainina, et al. (1994). "Voltammetric Studies with Copper Microelectrodes Fabricated from Borosilicate-Coated Copper Microwire." Electroanalysis **6**(4): 275-284.

Bond, A. M., M. Fleischmann, et al. (1984). "Electrochemistry in Organic-Solvents without Supporting Electrolyte Using Platinum Microelectrodes." Journal of Electroanalytical Chemistry **168**(1-2): 299-312.

Bond, A. M., M. Fleischmann, et al. (1984). "The Use of Platinum Microelectrodes for Electrochemical Investigations in Low-Temperature Glasses of Non-Aqueous Solvents." Journal of Electroanalytical Chemistry **180**(1-2): 257-263.

Bond, A. M., M. Fleischmann, et al. (1984). "Voltammetric Measurements Using Microelectrodes in Highly Dilute-Solutions - Theoretical Considerations." Journal of Electroanalytical Chemistry **172**(1-2): 11-25.

Bond, A. M., T. L. E. Henderson, et al. (1986). "Theory and Experimental Characterization of Linear Gold Microelectrodes with Submicrometer Thickness." Journal of Physical Chemistry **90**(13): 2911-2917.

Bonneville, S., P. Van Cappellen, et al. (2004). "Microbial reduction of iron(III) oxyhydroxides: effects of mineral solubility and availability." Chemical Geology **212**(3-4): 255-268.

Boudreau, B. P. and B. R. Ruddick (1991). "On a reactive continuum representation of organic matter diagenesis." American Journal of Science **291**: 507-538.

Boussemart, M., C. M. G. Vandenberg, et al. (1992). "The Determination of the Chromium Speciation in Sea-Water Using Catalytic Cathodic Stripping Voltammetry." Analytica Chimica Acta **262**(1): 103-115.

Brand, L. E., W. G. Sunda, et al. (1986). "Reduction of Marine-Phytoplankton Reproduction Rates by Copper and Cadmium." Journal of Experimental Marine Biology and Ecology **96**(3): 225-250.

Brendel, P. and G. W. Luther III (1995). "Develpment of a Gold Amalgam Voltammetric Microelectrode for the Determination of Dissolved

Fe, Mn, O2, and S(-II) in Porewater of Marine and Freshwater Sediments." Environmental Sciences & Technology **29**: 751-761.

Brendel, P. J. and G. W. Luther (1995). "Development of a Gold Amalgam Voltammetric Microelectrode for the Determination of Dissolved Fe, Mn, O-2, and S(-Ii) in Porewaters of Marine and Fresh-Water Sediments." Environmental Science & Technology **29**(3): 751-761.

Brown, G. E., V. E. Henrich, et al. (1999). "Metal oxide surfaces and their interactions with aqueous solutions and microbial organisms." Chemical Reviews **99**(1): 77-174.

Bruland, K. W., J. R. Donat, et al. (1991). "Interactive Influences of Bioactive Trace-Metals on Biological Production in Oceanic Waters." Limnology and Oceanography **36**(8): 1555-1577.

Buffle, J., R. S. Altmann, et al. (1990). "Complexation by Natural Heterogeneous Compounds - Site Occupation Distribution-Functions, a Normalized Description of Metal Complexation." Geochimica et Cosmochmica Acta **54**(6): 1535-1553.

Buffle, J. and G. Horvai (2000). In Situ Monitoring of Aquatic Systems - Chemical Analysis and Speciation. New York, Wiley.

Buffle, J., M. L. Tercier, et al. (1997). "Analytical techniques for the in situ measurement and speciation of trace compounds in natural waters." Chimia **51**(10): 690-693.

Buffle, J. and M.-L. Tercier-Waeber (2000). *In Situ* Voltammetry: Concepts and Practise for Trace Analysis and Speciation. In Situ Monitoring of Aquatic Systems - Chemical Analysis and Speciation. G. Horvai. New York, Wiley. **6:** 279-408.

Buffle, J., K. J. Wilkinson, et al. (1997). "In situ monitoring and speciation of trace metals in natural waters." Annali Di Chimica **87**(1-2): 67-82.

Buswell, A. M. and M. J. Nicol (2002). "Some aspects of the electrochemistry of the flotation of pyrrhotite." Journal of Applied Electrochemistry **32**: 1321-1329.

Caccavo, F. (1999). "Protein-mediated adhesion of the dissimilatory Fe(III)-reducing bacterium Shewanella alga BrY to hydrous ferric oxide." Applied and Environmental Microbiology **65**(11): 5017-5022.

Caccavo, F., D. J. Lonergan, et al. (1994). "Geobacter Sulfurreducens Sp-Nov, a Hydrogen-Oxidizing and Acetate-Oxidizing Dissimilatory Metal-Reducing Microorganism." Applied and Environmental Microbiology **60**(10): 3752-3759.

Campos, M. and C. M. G. Van den Berg (1994). "Determination of Copper Complexation in Sea-Water by Cathodic Stripping Voltammetry and Ligand Competition with Salicylaldoxime." Analytica Chimica Acta **284**(3): 481-496.

Campos, M. and C. M. G. Vandenberg (1994). "Determination of Copper Complexation in Sea-Water by Cathodic Stripping Voltammetry and Ligand Competition with Salicylaldoxime." Analytica Chimica Acta **284**(3): 481-496.

Canfield, D. E. (1989). "Reactive iron in marine sediments." Geochimica et Cosmochmica Acta **53**: 619-632.

Canfield, D. E. (1993). Organic matter degradation in marine sediments. Interactions of C, N, P, and S biogeochemical cycles. F. Mackenzie. Berlin, Heidelberg, Springer.

Canfield, D. E. (1993). "Organic matter oxidation in marine sediments." NATO ASI Series **14**: 333-363.

Canfield, D. E. (1998). "A new model for Proterozoic ocean chemistry." Nature **396**(6710): 450-453.

Canfield, D. E. (2001). Biogeochemistry of sulfur isotopes. Stable Isotope Geochemistry. **43:** 607-636.

Canfield, D. E., B. P. Boudreau, et al. (1998). "The early diagenetic formation of organic sulfur in the sediments of Mangrove Lake, Bermuda." Geochimica et Cosmochmica Acta **62**(5): 767-781.

Canfield, D. E., B. B. Jørgensen, et al. (1993). "Pathways of organic carbon oxidation in three continental margin sediments." Marine Geology **113**: 27-40.

Canfield, D. E. and R. Raiswell (1999). "The evolution of the sulfur cycle." American Journal of Science **299**(7-9): 697-723.

Canfield, D. E., R. Raiswell, et al. (1992). "The Reactivity of Sedimentary Iron Minerals toward Sulfide." American Journal of Science **292**(9): 659-683.

Canfield, D. E., B. Thamdrup, et al. (1993). "The anaerobic degradation of organic matter in Danish coastal sediments: Iron reduction, manganese reduction, and sulfate reduction." Geochimica et Cosmochmica Acta **57**: 3867-3883.

Canfield, D. E., B. Thamdrup, et al. (1993). "The Anaerobic Degradation of Organic-Matter in Danish Coastal Sediments - Iron Reduction, Manganese Reduction, and Sulfate Reduction." Geochimica et Cosmochmica Acta **57**(16): 3867-3883.

Cappenberg, T. E. and R. A. Prins (1974). "Interrelations between sulfate-reducing and methane-producing bacteria in bottom deposits of a fresh-water lake. III. Experiments with 14C-labelled substrates." Journal of Microbiology and Serology **40**: 457-469.

Chau, Y. K., R. Gachter, et al. (1974). Determination of Apparent Complexing Capacity of Lake Waters. Journal of the Fisheries Research Board of Canada. **31:** 1515.

Christoffersen, J. and M. R. Christoffersen (1976). "The kinetics of dissolution of calcium sulphate dihydrate in water." Journal of Crystal Growth **35**: 79-88.

Church, T. M., M. M. Sarin, et al. (1996). "Salt marshes: An important coastal sink for dissolved uranium." Geochimica et Cosmochmica Acta **60**(20): 3879-3887.

Ciszkowska, M., M. Donten, et al. (1994). "Preparation of a Mercury Disk Microelectrode Based on Solid Silver Amalgam." Analytical Chemistry **66**(22): 4112-4115.

Coale, K. H. and K. W. Bruland (1988). "Copper Complexation in the Northeast Pacific." Limnology and Oceanography **33**(5): 1084-1101.

Coale, K. H. and K. W. Bruland (1990). "Spatial and Temporal Variability in Copper Complexation in the North Pacific." Deep-Sea Research Part A-Oceanographic Research Papers **37**(2): 317-336.

Coates, J. D., E. J. P. Phillips, et al. (1996). "Isolation of Geobacter species from diverse sedimentary environments." Applied and Environmental Microbiology **62**(5): 1531-1536.

Colombo, C. and C. M. G. Van den Berg (1998). "Determination of trace metals (Cu, Pb, Zn and Ni) in soil extracts by flow analysis with voltametric detection." International Journal of Environmental Analytical Chemistry **71**(1): 1-17.

Cooper, D. C., F. Picardal, et al. (2000). "Zinc immobilization and magnetite formation via ferric oxide reduction by Shewanella putrefaciens 200." Environmental Science & Technology **34**(1): 100-106.

Cornell, R. M., A. M. Posner, et al. (1974). "Dissolution of Synthetic Goethites - Early Stage." Soil Science Society of America Journal **38**(2): 377-378.

Cornell, R. M., A. M. Posner, et al. (1976). "Kinetics and Mechanisms of Acid Dissolution of Goethite Alpha-Feooh)." Journal of Inorganic & Nuclear Chemistry **38**(3): 563-567.

Cornell, R. M. and U. Schwertmann (1996). The Iron Oxides: Structure, Properties, Reactions, Occurences, and Uses. New York, VCH.

Cornell, R. M. and U. Schwertmann (2003). The Iron Oxides. Weinheim, Wiley-VCH.

Croot, P. L. and K. A. Hunter (2000). "Labile forms of iron in coastal seawater: Otago Harbour, New Zealand." Marine and Freshwater Research **51**(3): 193-203.

Daniele, S., M. A. Baldo, et al. (2002). "In situ monitoring of electroactive species by using voltammetry at microelectrodes." Journal of the Brazilian Chemical Society **13**(4): 425-432.

Daniele, S., C. Bragato, et al. (2002). "Square wave voltammetry of strong acids at platinum microelectrodes." Electrochemistry Communications **4**(5): 374-378.

Das, A. and F. Caccavo (2000). "Dissimilatory Fe(III) oxide reduction by Shewnnella alga BrY requires adhesion." Current Microbiology **40**(5): 344-347.

Davis, A. R. and R. M. Chatterjee (1975). Journal of Solution Chemistry **4**: 399-405.

Davison, W., G. R. Fones, et al. (1997). "Dissolved metals in surface sediment and a microbial mat at 100-mu m resolution." Nature **387**(6636): 885-888.

Davison, W., G. R. Fones, et al. (2000). Dialysis, DET, DGT: *In Situ* Diffusional Techniques for Studying Water, Sediments, and Soils. In Situ Monitoring of Aquatic Systems. G. Horvai. New York, Wiley. **6:** 495-570.

Davison, W., G. W. Grime, et al. (1991). "Distribution of Dissolved Iron in Sediment Pore Waters at Submillimeter Resolution." Nature **352**(6333): 323-325.

Davison, W., G. W. Grime, et al. (1991). "Distribution of dissolved iron in sediment pore waters at submillimetre resolution." Nature **352**: 323-324.

Davison, W. and H. Zhang (1994). "In-Situ Speciation Measurements of Trace Components in Natural-Waters Using Thin-Film Gels." Nature **367**(6463): 546-548.

Davison, W., H. Zhang, et al. (1994). "Performance-Characteristics of Gel Probes Used for Measuring the Chemistry of Pore Waters." Environmental Science & Technology **28**(9): 1623-1632.

Deakin, M. R., D. Wipf, et al. (1986). "Ultramicroelectrodes." Journal of the Electrochemical Society **133**(3): C135-C135.

Debeer, D., J. Sweerts, et al. (1991). "Microelectrode Measurement of Ammonium Profiles in Fresh-Water Sediments." FEMS Microbiology Ecology **86**(1): 1-6.

Dekkers, M. J., H. F. Passier, et al. (2000). "Magnetic properties of hydrothermally synthesized greigite (F3S4) - II. High- and low-temperature characteristics." Geophysical Journal International **141**(3): 809-819.

Deng, Y. W. and W. Stumm (1994). "Reactivity of Aquatic Iron(III) Oxyhydroxides Implications for Redox Cycling of Iron in Natural-Waters." Applied Geochemistry **9**(1): 23-36.

Devries, W. T. and E. Vandalen (1964). "Theory of Anodic Stripping Voltammetry with a Plane Thin Mercury-Film Electrode." Journal of Electroanalytical Chemistry **8**(5): 366-&.

Dichristina, T. J. (1992). "Effects of Nitrate and Nitrite on Dissimilatory Iron Reduction by Shewanella-Putrefaciens Strain-200." Abstracts of Papers of the American Chemical Society **203**: 127-GEOC.

Diem, D. and W. Stumm (1984). "Is Dissolved Mn-2+ Being Oxidized by O-2 in Absence of Mn-Bacteria or Surface Catalysts." Geochimica et Cosmochmica Acta **48**(7): 1571-1573.

Dixon, D. G. and J. L. Hendrix (1993). "Theoretical Basis for Variable Order Assumption in the Kinetics of Leaching of Discrete Grains." Aiche Journal **39**(5): 904-907.

Dixon, J. B. and H. C. W. Skinner (1992). Manganese Minerals in Surface Environments. Biomineralziation of Iron and Mnaganese. R. W. Fitzpatrick. Cremlingen-Destedt, Catena-Verlag**:** 7-30.

Dollhopf, M. E., K. H. Nealson, et al. (1999). "In situ solid state Au/Hg voltammetric microelectrodes to analyze microbial metal reduction." Abstracts of Papers of the American Chemical Society **217**: U853-U853.

Dollhopf, M. E., K. H. Nealson, et al. (2000). "Kinetics of Fe(III) and Mn(IV) reduction by the Black Sea strain of Shewanella putrefaciens using in situ solid state voltammetric Au/Hg electrodes." Marine Chemistry **70**(1-3): 171-180.

Donat, J. R., K. A. Lao, et al. (1994). "Speciation of Dissolved Copper and Nickel in South San-Francisco Bay - a Multimethod Approach." Analytica Chimica Acta **284**(3): 547-571.

Donat, J. R. and C. M. G. Van den Berg (1992). "A New Cathodic Stripping Voltammetric Method for Determining Organic Copper Complexation in Seawater." Marine Chemistry **38**(1-2): 69-90.

Doyle, F. M. and A. H. Mirza (1886). Electrochemical oxidation of pyrite samples with known composition and electrical properties. Electrochemistry in Mineral and Metal Processing.

Drever, J. I. (1997). The Geochemistry of Natrual Waters. NJ, Prenctice.

Dzombak, D. A. and F. M. M. Morel (1986). "Sorption of Cadmium on Hydrous Ferric-Oxide at High Sorbate/Sorbent Ratios - Equilibrium, Kinetics, and Modeling." Journal of Colloid and Interface Science **112**(2): 588-598.

Ehrlich, H. L. (1998). "Geomicrobiology: its significance for geology." Earth-Science Reviews **45**: 45-60.

Elbaz-Poulichet, F., C. Dupuy, et al. (2000). "Influence of sorption processes by iron oxides and algae fixation on arsenic and phosphate cycle in an acidic estuary (Tinto river, Spain)." Water Research **34**(12): 3222-3230.

Ellwood, M. J. and C. M. G. van den Berg (2001). "Determination of organic complexation of cobalt in seawater by cathodic stripping voltammetry." Marine Chemistry **75**(1-2): 33-47.

Erel, Y., J. J. Morgan, et al. (1991). "Natural Levels of Lead and Cadmium in a Remote Mountain Stream." Geochimica et Cosmochmica Acta **55**(3): 707-719.

Ewing, A. G., R. Withnell, et al. (1981). "Instrument Design for Pulse Voltammetry with Microvoltammetric Electrodes." Review of Scientific Instruments **52**(3): 454-458.

Farrell, R. E., P. M. Huang, et al. (1998). "Biomethylation of mercury(II) adsorbed on mineral colloids common in freshwater sediments." Applied Organometallic Chemistry **12**(8-9): 613-620.

Fenchel, T. (1996). "Worm burrows and oxic microniches in marine sediments. 1. Spatial and temporal scales." Marine Biology **127**: 289-295.

Fenchel, T. (1996). "Worm burrows and oxic microniches in marine sediments. 2. Distribution patterns of ciliated protozoa." Marine Biology **127**: 297-301.

Ferdelman, T. G., T. M. Church, et al. (1991). "Sulfur enrichment of humic substances in a Delaware salt marsh sediment core." Geochimica et Cosmochmica Acta **55**: 979-988.

Ferris, F. G., R. O. Hallberg, et al. (2000). "Retention of strontium, cesium, lead and uranium by bacterial iron oxides from a subterranean environment." Applied Geochemistry **15**(7): 1035-1042.

Ferris, F. G., K. O. Konhauser, et al. (1999). "Accumulation of metals by bacteriogenic iron oxides in a subterranean environment." Geomicrobiology Journal **16**(2): 181-192.

Ferro, I. (2003). Cycling of iron and manganese in freshwater, estuarine, and deep sediments, Groningen University.

Fiedler, D. A. and F. Scholz (2002). Electrochemical Studies of Solid Compounds and Materials. Electroanalytical Methods - Guide to Experiments and Applications. F. Scholz. Berlin, Springer**:** 211-222.

Filella, M., J. Buffle, et al. (1990). "Effect of Physicochemical Heterogeneity of Natural Complexants .1. Voltammetry of Labile Metal Fulvic Complexes." Analytica Chimica Acta **232**(1): 209-223.

Fleischmann, M., F. Lasserre, et al. (1984). "The Application of Microelectrodes to the Study of Homogeneous Processes Coupled to Electrode-Reactions .1. Ec' and Ce Reactions." Journal of Electroanalytical Chemistry **177**(1-2): 97-114.

Fones, G. R., W. Davison, et al. (1998). "Development of constrained DET for measurements of dissolved iron in surface sediments at sub-mm resolution." Science of the Total Environment **221**(2-3): 127-137.

Fones, G. R., W. Davison, et al. (2001). "High-resolution metal gradients measured by in situ DGT/DET deployment in Black Sea sediments using an autonomous benthic lander." Limnology and Oceanography **46**(4): 982-988.

Fossing, H. and B. B. Jørgensen (1989). "Measurement of Bacterial Sulfate Reduction in Sediments - Evaluation of a Single-Step Chromium Reduction Method." Biogeochemistry **8**(3): 205-222.

Foster, A. L., G. E. Brown, et al. (1997). "XAFS determination of As(V) associated with Fe(III) oxyhydroxides in weathered mine tailings and contaminated soil from California, USA." Journal De Physique IV **7**(C2): 815-816.

Fredrickson, J. K., J. M. Zachara, et al. (1998). "Biogenic iron mineralization accompanying the dissimilatory reduction of hydrous ferric oxide by a groundwater bacterium." Geochimica et Cosmochmica Acta **62**(19-20): 3239-3257.

Froelich, P. N., G. P. Klinkhammer, et al. (1979). "Early Oxidation of Organic-Matter in Pelagic Sediments of the Eastern Equatorial Atlantic - Suboxic Diagenesis." Geochimica et Cosmochmica Acta **43**(7): 1075-1090.

Galus, Z. (1975). "Electrochemical Behaviors of Metal Amalgams." CRC Critical Reviews in Analytical Chemistry **4**: 359-422.

Galus, Z. (1984). "Diffusion-Coefficients of Metals in Mercury." Pure and Applied Chemistry **56**(5): 635-644.

Gerringa, L. J. A., P. M. J. Herman, et al. (1995). "Comparison of the Linear Van den Berg Ruzic Transformation and a Nonlinear Fit of the Langmuir Isotherm Applied to Cu Speciation Data in the Estuarine Environment." Marine Chemistry **48**(2): 131-142.

Gledhill, M. and C. M. G. Van den Berg (1994). "Determination of Complexation of Iron(III) with Natural Organic Complexing Ligands in Seawater Using Cathodic Stripping Voltammetry." Marine Chemistry **47**(1): 41-54.

Gledhill, M. and C. M. G. Vandenberg (1994). "Determination of Complexation of Iron(III) with Natural Organic Complexing Ligands in Seawater Using Cathodic Stripping Voltammetry." Marine Chemistry **47**(1): 41-54.

Glud, R. N., N. B. Ramsing, et al. (1996). "Planar optrodes: a new tool for fine scale measruements of two-dimensional O2 distribution in benthic communities." Marine Ecology Progress Series **140**: 217-226.

Gordon, L. I., L. A. Codispoti, et al. (2000). "Seasonal evolution of hydrographic properties in the Ross Sea, Antarctica, 1996-1997." Deep-Sea Research Part II-Topical Studies in Oceanography **47**(15-16): 3095-3117.

Grygar, T. (1995). "Kinetics of Electrochemical Reductive Dissolution of Iron(III) Hydroxy-Oxides." Collection of Czechoslovak Chemical Communications **60**(8): 1261-1273.

Grygar, T. (1996). "The electrochemical dissolution of iron(III) and chromium(III) oxides and ferrites under conditions of abrasive stripping voltammetry." Journal of Electroanalytical Chemistry **405**(1-2): 117-125.

Grygar, T. (1997). "Dissolution of pure and substituted goethites controlled by the surface reaction under conditions of abrasive stripping voltammetry." Journal of Solid State Electrochemistry **1**(1): 77-82.

Grygar, T. (1998). "Phenomenological kinetics of irreversible electrochemical dissolution of metal-oxide microparticles." Journal of Solid State Electrochemistry **2**(3): 127-136.

Grygar, T., P. Bezdicka, et al. (1999). "Electrochemical dissolution of immobilized alpha-(FexCr1-x)(2)O-3 microparticles." Journal of the Electrochemical Society **146**(9): 3234-3237.

Grygar, T., J. Dedecek, et al. (2003). "Iron oxide mineralogy in late Miocene red beds from La Gloria, Spain: rock-magnetic, voltammetric and Vis spectroscopy analyses." Catena **53**(2): 115-132.

Grygar, T., J. Subrt, et al. (1995). "Electrochemical Dissolution of Goethite by Abrasive Stripping Voltammetry." Collection of Czechoslovak Chemical Communications **60**(6): 950-959.

Grygar, T. and I. H. M. van Oorschot (2002). "Voltammetric identification of pedogenic iron oxides in paleosol and loess." Electroanalysis **14**(5): 339-344.

Gundersen, J. K. and B. B. Jørgensen (1990). "Microstructure of diffusive boundary layers and the oxygen uptake of the sea floor." Nature **345**: 604-607.

Gundersen, J. K., B. B. Jørgensen, et al. (1992). "Mats of Giant Sulfur Bacteria on Deep-Sea Sediments Due to Fluctuating Hydrothermal Flow." Nature **360**(6403): 454-456.

Habicht, K. S., D. E. Canfield, et al. (1998). "Sulfur isotope fractionation during bacterial reduction and disproportionation of thiosulfate and sulfite." Geochimica et Cosmochmica Acta **62**(15): 2585-2595.

Haese, R. R. (2000). The Reactivity of Iron. Marine Geochemistry. M. Zabel. Heidelberg, Springer**:** 233-261.

HamiltonTaylor, J., W. Davison, et al. (1996). "The biogeochemical cycling of Zn, Cu, Fe, Mn, and dissolved organic C in a seasonally anoxic lake." Limnology and Oceanography **41**(3): 408-418.

Harper, M. P., W. Davison, et al. (1997). "Temporal, spatial, and resolution constraints for in situ sampling devices using diffusional equilibration: Dialysis and DET." Environmental Science & Technology **31**(11): 3110-3119.

Heinze, J. (1993). "Ultramicroelectrodes in Electrochemistry." Angewandte Chemie-International Edition in English **32**(9): 1268-1288.

Hering, J. G., W. G. Sunda, et al. (1987). "A Field Comparison of 2 Methods for the Determination of Copper Complexation - Bacterial Bioassay and Fixed-Potential Amperometry." Marine Chemistry **20**(4): 299-312.

Holman, D. A., A. W. Thompson, et al. (1994). Analytical Chemistry **66**: 1378.

Howell, J. O. and R. M. Wightman (1984). "Ultrafast voltammetry and voltammetry in highly resistive solutions with microvoltammetric electrodes." Analytical Chemistry **56**: 524-529.

Hoyer, B. and T. M. Florence (1987). "Application of Polymer-Coated Glassy-Carbon Electrodes to the Direct Determination of Trace-Metals in Body-Fluids by Anodic-Stripping Voltammetry." Analytical Chemistry **59**(24): 2839-2842.

Huang, P. (1991). Kinetics of Redox reactions on manganese oxides and its impact on environmental quality. Rates of Soil Chemical Processes. D. Suarez. Madison, Soil Science of Amerika**:** 191-230.

Hudson, R. J. M. and F. M. M. Morel (1989). "Chemical-Kinetics of Biological Iron Uptake." Abstracts of Papers of the American Chemical Society **198**: 99-GEOC.

Hunter, K. A. (1983). "The Adsorptive Properties of Sinking Particles in the Deep Ocean." Deep-Sea Research Part A-Oceanographic Research Papers **30**(6): 669-675.

Hunter, K. A. (1983). "On the Estuarine Mixing of Dissolved Substances in Relation to Colloid Stability and Surface-Properties." Geochimica et Cosmochmica Acta **47**(3): 467-473.

Hyacinthe, C., P. Anschutz, et al. (2001). "Early diagenetic processes in the muddy sediments of the Bay of Biscay." Marine Geology **177**(1-2): 111-128.

Jensen, H. S. and B. Thamdrup (1993). "Iron-Bound Phosphorus in Marine-Sediments as Measured by Bicarbonate-Dithionite Extraction." Hydrobiologia **253**(1-3): 47-59.

Jørgensen, B. B. (1977). "Bacterial sulfate reduction within reduced microniches of oxidized marine sediments." Marine Biology **41**: 7-17.

Jørgensen, B. B. and T. Fenchel (1974). "The sulfur cycle of a marine sediment model system." Marine Biology **24**: 189-201.

Jørgensen, B. B. (1977). "Sulfur Cycle of a Coastal Marine Sediment (Limfjorden, Denmark)." Limnology and Oceanography **22**(5): 814-832.

Jørgensen, B. B. (1978). "Comparison of Methods for the Quantification of Bacterial Sulfate Reduction in Coastal Marine-Sediments .1. Measurement with Radiotracer Techniques." Geomicrobiology Journal **1**(1): 11-27.

Jørgensen, B. B. (1978). "Comparison of Methods for the Quantification of Bacterial Sulfate Reduction in Coastal Marine-Sediments .2. Calculation from Mathematical-Models." Geomicrobiology Journal **1**(1): 29-47.

Jørgensen, B. B. (1978). "Comparison of Methods for the Quantification of Bacterial Sulfate Reduction in Coastal Marine-Sediments .3. Estimation from Chemical and Bacteriological Field Data." Geomicrobiology Journal **1**(1): 49-64.

Jørgensen, B. B. (1982). "Mineralization of Organic-Matter in the Sea Bed - the Role of Sulfate Reduction." Nature **296**(5858): 643-645.

Jørgensen, B. B. (1990). "The Sulfur Cycle of Fresh-Water Sediments - Role of Thiosulfate." Limnology and Oceanography **35**(6): 1329-1342.

Jørgensen, B. B. (1990). "A Thiosulfate Shunt in the Sulfur Cycle of Marine-Sediments." Science **249**(4965): 152-154.

Jørgensen, B. B., N. P. Revsbech, et al. (1983). "Photosynthesis and Structure of Benthic Microbial Mats - Microelectrode and Sem Studies of 4 Cyanobacterial Communities." Limnology and Oceanography **28**(6): 1075-1093.

Junta, J. and M. F. Hochella (1994). "Manganese(II) Oxidation at Mineral Surfaces - a Microscopic and Spectroscopic Study." Geochimica et Cosmochmica Acta **58**(22): 4985-4999.

Kappler, A., R. Ji, et al. (2001). "Dynamics in composition and size-class distribution of humic substances in profundal sediments of Lake Constance." Organic Geochemistry **32**(1): 3-10.

Kelsall, G. H., Q. Yin, et al. (1999). "Electrochemical oxidation of pyrite (FeS_2) in aqueous electrolytes." Journal of Electroanalytical Chemistry **471**: 116-125.

Kogut, M. B. and B. M. Voelker (2001). "Strong copper-binding behavior of terrestrial humic substances in seawater." Environmental Science & Technology **35**(6): 1149-1156.

Komorsky-Lovric, S., V. Mirceski, et al. (1999). "Voltammetry of organic microparticles." Mikrochimica Acta **132**(1): 67-77.

Komorsky-Lovric, S. and F. Scholz (1998). "Stripping chronopotentiometry of immobilized microparticles." Journal of Electroanalytical Chemistry **445**(1-2): 81-87.

Kostka, J., G. W. Luther, et al. (1992). "Coupling the Growth and Carbon Conversion of Shewanella-Putrefaciens to the Reduction Solubilization of Fe." Abstracts of Papers of the American Chemical Society **203**: 126-GEOC.

Kostka, J. E. and G. W. Luther (1994). "Partitioning and Speciation of Solid-Phase Iron in Salt-Marsh Sediments." Geochimica et Cosmochmica Acta **58**(7): 1701-1710.

Kostka, J. E., J. W. Stucki, et al. (1996). "Reduction of structural Fe(III) in smectite by a pure culture of Shewanella putrefaciens strain MR-1." Clays and Clay Minerals **44**(4): 522-529.

Kounaves, S. P. and W. Deng (1991). "An Iridium Based Mercury Ultramicroelectrode - Fabrication and Characterization." Journal of Electroanalytical Chemistry **301**(1-2): 77-85.

Kounaves, S. P. and W. Deng (1993). "Analytical Utility of the Iridium-Based Mercury Ultramicroelectrode with Square-Wave Anodic-Stripping Voltammetry." Analytical Chemistry **65**(4): 375-379.

Kozelka, P. B. and K. W. Bruland (1998). "Chemical speciation of dissolved Cu, Zn, Cd, Pb in Narragansett Bay, Rhode Island." Marine Chemistry **60**(3-4): 267-282.

Krom, M. D., R. J. G. Mortimer, et al. (2002). "In-situ determination of dissolved iron production in recent marine sediments." Aquatic Sciences **64**(3): 282-291.

Kusel, K., T. Dorsch, et al. (1999). "Microbial reduction of Fe(III) in acidic sediments: Isolation of Acidiphilium cryptum JF-5 capable of coupling the reduction of Fe(III) to

the oxidation of glucose." Applied and Environmental Microbiology **65**(8): 3633-3640.

Laglera, L. M. and C. M. G. van den Berg (2003). "Copper complexation by thiol compounds in estuarine waters." Marine Chemistry **82**(1-2): 71-89.

Laglera, L. M. and C. M. G. van den Berg (2003). Copper complexation by thiol compounds in estuarine waters. Marine Chemistry. **82:** 71-89.

Lakind, J. S. and A. T. Stone (1989). "Reductive Dissolution of Goethite by Phenolic Reductants." Geochimica et Cosmochmica Acta **53**(5): 961-971.

Lam, M. T., J. Murimboh, et al. (1999). "Competitive ligand exchange/adsorptive cathodic stripping voltammetry (CLE/AdCSV) for kinetic studies of nickel speciation in aqueous environmental samples containing heterogeneous, macromolecular, organic complexants." Analytica Chimica Acta **402**(1-2): 195-209.

Larsen, O. and D. Postma (2001). "Kinetics of reductive bulk dissolution of lepidocrocite, ferrihydrite, and goethite." Geochimica et Cosmochmica Acta **65**(9): 1367-1379.

Lasalle, A. L., B. Limoges, et al. (1994). "Determination of Alkaline-Phosphatase Using a Nafion(R)-Modified Electrode." Journal of Electroanalytical Chemistry **379**(1-2): 281-291.

Le Gall, A. C. A. and C. M. G. Van Den Berg (1998). "Folic acid and glutathione in the water column of the north east Atlantic." Deep-Sea Research Part I-Oceanographic Research Papers **45**(11): 1903-1918.

Lennie, A. R., S. A. T. Redfern, et al. (1997). "Transformation of mackinawite to greigite: An in situ X-ray powder diffraction and transmission electron microscope study." American Mineralogist **82**(3-4): 302-309.

Lennie, A. R. and D. H. Vaughan (1996). Spectroscopic studies of iron sulfide formation and phase relation at low temperatures. Mineral Spectroscopy: A tribute to Roger G. Burns. M. W. Schaefer**:** 117-156.

Liang, L. Y., A. Hofmann, et al. (2000). "Ligand-induced dissolution and release of ferrihydrite colloids." Geochimica et Cosmochmica Acta **64**(12): 2027-2037.

Liu, C. X., S. Kota, et al. (2001). "Kinetic analysis of the bacterial reduction of goethite." Environmental Science & Technology **35**(12): 2482-2490.

Loveland, J. W. and P. J. Elving (1952). "Cathode-Ray Oscilloscopic Investigation of Phenomena at Polarizable Mercury Electrodes." Chemical Reviews **51**(1): 67-117.

Lovley, D. R. (1987). "Organic matter mineralization with the reduction of ferric iron: a review." Geomicrobiology Journal **5**: 375-399.

Lovley, D. R. (1991). "Dissimilatory Fe(III) and Mn(IV) Reduction." Microbiological Reviews **55**(2): 259-287.

Lovley, D. R., M. J. Baedecker, et al. (1989). "Oxidation of Aromatic Contaminants Coupled to Microbial Iron Reduction." Nature **339**(6222): 297-300.

Lovley, D. R., J. D. Coates, et al. (1996). "Humic substances as electron acceptors for microbial respiration." Nature **382**(6590): 445-448.

Lovley, D. R., D. E. Holmes, et al. (2004). "Dissimilatory Fe(III) and Mn(IV) Reduction." Advances in Microbial Physiology(49): 219-286.

Lovley, D. R. and E. J. P. Phillips (1986). "Availability of ferric iron for microbial reduction in bottom sediments of the freshwater tidal Potomac River." Applied and Environmental Microbiology **52**(4): 751-757.

Lovley, D. R. and E. J. P. Phillips (1986). "Organic matter mineralization with reduction of ferric iron in anaerobic sediments." Applied and Environmental Microbiology **51**: 683-689.

Lovley, D. R. and E. J. P. Phillips (1987). "Rapid Assay for Microbially Reducible Ferric Iron in Aquatic Sediments." Applied and Environmental Microbiology **53**(7): 1536-1540.

Lovley, D. R. and E. J. P. Phillips (1988). "Novel Mode of Microbial Energy-Metabolism - Organic-Carbon Oxidation Coupled to Dissimilatory Reduction of Iron or Manganese." Applied and Environmental Microbiology **54**(6): 1472-1480.

Lower, B. H., M. F. Hochella, et al. (in review). "Putative mineral-specific proteins synthesized by a metal reducing bacteria." submitted to Geochimica et Cosmochmica Acta.

Lower, S. K., M. F. Hochella, et al. (2001). "Bacterial recognition of mineral surfaces: Nanoscale interactions between Shewanella and alpha-FeOOH." Science **292**(5520): 1360-1363.

Lower, S. K., C. J. Tadanier, et al. (2000). "Measuring interfacial and adhesion forces between bacteria and mineral surfaces with biological force microscopy." Geochimica et Cosmochmica Acta **64**(18): 3133-3139.

Luther, G. W. (1989). "Frontier Molecular-Orbital Theory Analysis of Fe(II) and Mn(II) Oxidation by O-2 and Mno2 and Fe(III) Mineral Reduction by Sh." Abstracts of Papers of the American Chemical Society **198**: 55-GEOC.

Luther, G. W., P. J. Brendel, et al. (1998). "Simultaneous measurement of O-2, Mn, Fe, I-, and S(-II) in marine pore waters with a solid-state voltammetric microelectrode." Limnology and Oceanography **43**(2): 325-333.

Luther, G. W., B. Glazer, et al. (2003). "Iron and sulfur chemistry in a stratified lake: Evidence for iron-rich sulfide complexes." Aquatic Geochemistry **9**(2): 87-110.

Luther, G. W., B. T. Glazer, et al. (2001). "Sulfur speciation monitored in situ with solid state gold amalgam voltammetric microelectrodes: polysulfides as a special case in sediments, microbial mats and hydrothermal vent waters." Journal of Environmental Monitoring **3**(1): 61-66.

Luther, G. W. and E. Tsamakis (1989). "Concentration and Form of Dissolved Sulfide in the Oxic Water Column of the Ocean." Marine Chemistry **27**(3-4): 165-177.

Macrellis, H. M., C. G. Trick, et al. (2001). "Collection and detection of natural iron-binding ligands from seawater." Marine Chemistry **76**(3): 175-187.

Madden, A. S. and M. F. Hochella (2005). "A test of geochemical reactivity as a function of mineral size: Manganese oxidation promoted by hematite nanoparticles." Geochimica et Cosmochmica Acta **69**(2): 389-398.

Mandernack, K. W., J. Post, et al. (1995). "Manganese Mineral Formation by Bacterial-Spores of the Marine Bacillus, Strain Sg-1 - Evidence for the Direct Oxidation of Mn(II) to Mn(IV)." Geochimica et Cosmochmica Acta **59**(21): 4393-4408.

Mandernack, K. W. and B. M. Tebo (1993). "Manganese Scavenging and Oxidation at Hydrothermal Vents and in Vent Plumes." Geochimica et Cosmochmica Acta **57**(16): 3907-3923.

Martens, C. S. and R. A. Berner (1974). "Methane Production in Interstitial Waters of Sulfate-Depleted Marine Sediments." Science **185**(4157): 1167-1169.

Martin, S. T. (in press). Precipitation and dissolution of Iron and Manganese Oxides. Environmental Catalysis. V. H. Grassian. New York, Marcel Dekker.

Mehra, O. P. and M. L. Jackson (1960). "Iron oxide removal from soils and clays by a dithionite-citrate system buffered with sodium carbonate." Proceedings of the national conference on clays and clay mineralogy **7**: 317-327.

Meyer, B., M. Ospina, et al. (1980). Analytica Chimica Acta **117**: 301-309.

Middelburg, J. J. (1989). "A simple rate model for organic matter decomposition in marine sediments." Geochimica et Cosmochmica Acta **53**: 1577-1581.

Mikhlin, Y. (2000). "Reactivity of pyrrhotite surfaces: an electrochemical study." Physical Chemistry Chemical Physics **2**: 5672-5677.

Millero, F. J., S. Sotolongo, et al. (1987). "The oxidation kinetics of Fe(II) in seawater." Geochimica et Cosmochmica Acta **51**: 793-801.

Moffett, J. W. (1995). Temporal and spatial variability of copper complexation by strong chelators in the Sargasso Sea. Deep-Sea Research Part I-Oceanographic Research Papers. **42:** 1273-1295.

Moffett, J. W. (1995). "Temporal and Spatial Variability of Copper Complexation by Strong Chelators in the Sargasso-Sea." Deep-Sea Research Part I-Oceanographic Research Papers **42**(8): 1273-1295.

Moffett, J. W. and R. G. Zika (1987a). Solvent-Extraction of Copper Acetylacetonate in Studies of Copper(II) Speciation in Seawater. Marine Chemistry. **21:** 301-313.

Moffett, J. W. and R. G. Zika (1987b). Reaction-Kinetics of Hydrogen-Peroxide with Copper and Iron in Seawater. Environmental Science & Technology. **21:** 804-810.

Moffett, J. W., R. G. Zika, et al. (1990). "Distribution and Potential Sources and Sinks of Copper Chelators in the Sargasso Sea." Deep-Sea Research Part a-Oceanographic Research Papers **37**(1): 27-36.

Morgan, J. J. (2000). Manganese in natural waters and Earth´s Crust: Its availability to organisms. Metal ions in biological systems. H. Sigel. New York, Dekker**:** 1-34.

Morse, J. W. (1994). "Interactions of Trace-Metals with Authigenic Sulfide Minerals - Implications for Their Bioavailability." Marine Chemistry **46**(1-2): 1-6.

Morse, J. W. (1994). Release of Toxic Metals Via Oxidation of Authigenic Pyrite in Resuspended Sediments. Environmental Geochemistry of Sulfide Oxidation. **550:** 289-297.

Myers, C. R. and J. M. Myers (1994). "Ferric Iron Reduction-Linked Growth Yields of Shewanella-Putrefaciens Mr-1." Journal of Applied Bacteriology **76**(3): 253-258.

Myers, C. R. and J. M. Myers (1997). "Outer membrane cytochromes of Shewanella putrefaciens MR-1: Spectral analysis, and purification of the 83-kDa c-type cytochrome." Biochimica Et Biophysica Acta-Biomembranes **1326**(2): 307-318.

Myers, C. R. and J. M. Myers (1998). "Iron stimulates the rate of reduction of hexavalent chromium by human microsomes." Carcinogenesis **19**(6): 1029-1038.

Myers, J. M. and C. R. Myers (1998). "Isolation and sequence of omcA, a gene encoding a decaheme outer membrane cytochrome c of Shewanella putrefaciens MR-1, and detection of omcA homologs in other strains of S-putrefaciens." Biochimica Et Biophysica Acta-Biomembranes **1373**(1): 237-251.

Nealson, K. H. (1983). Microbial oxidation and reduction of manganese and iron. Biomineralization and Biological Metal Accumulation**:** 459-479.

Nealson, K. H., D. P. Moser, et al. (1995). "Anaerobic Electron-Acceptor Chemotaxis in Shewanella-Putrefaciens." Applied and Environmental Microbiology **61**(4): 1551-1554.

Nealson, K. H. and C. R. Myers (1992). "Microbial Reduction of Manganese and Iron - New Approaches to Carbon Cycling." Applied and Environmental Microbiology **58**(2): 439-443.

Neubauer, U., G. Furrer, et al. (2002). "Heavy metal sorption on soil minerals affected by the siderophore desferrioxamine B: the role of Fe(III) (hydr)oxides and dissolved Fe(III)." European Journal of Soil Science **53**(1): 45-55.

Nevin, K. P. and D. R. Lovley (2000). "Lack of production of electron-shuttling compounds or solubilization of Fe(III) during reduction of insoluble Fe(III) oxide by Geobacter metallireducens." Applied and Environmental Microbiology **66**(5): 2248-2251.

Newman, D. K. and R. Kolter (2000). "A role for excreted quinones in extracellular electron transfer." Nature **405**(6782): 94-97.

Nielsen, O. I., B. Gribsholt, et al. (2004). "Microscale distribution of oxygen and nitrate in sediment inhabited by Nereis diversicolor: spatial patterns and estimated reaction rates." Aquatic Microbial Ecology **34**(1): 23-32.

Ostapczuk, P. and Z. Kublik (1978). "Silver Based Mercury Film Electrode .4. Comparison of Theoretical and Experimental Voltammetric Results Obtained for Cadmium." Journal of Electroanalytical Chemistry **93**(3): 195-212.

Osteryoung, J. and J. J. Odea (1986). "Square-Wave Voltammetry." Electroanalytical Chemistry **14**: 209-308.

Osteryoung, J. G. and R. A. Osteryoung (1985). "Square-Wave Voltammetry." Analytical Chemistry **57**(1): A101-&.

Osteryoung, R. A., J. H. Christie, et al. (1975). "Innovations in Pulse Polarography." Abstracts of Papers of the American Chemical Society(169): 27-27.

Osteryoung, R. A., J. H. Christie, et al. (1979). "Advances in Pulsed Voltammetric Methodology." Abstracts of Papers of the American Chemical Society(APR): 78-78.

Ottley, C. J., W. Davison, et al. (1997). "Chemical catalysis of nitrate reduction by iron(II)." Geochimica et Cosmochmica Acta **61**(9): 1819-1828.

Phillips, E. J. P. and D. R. Lovley (1987). "Determination of Fe(III) and Fe(II) in Oxalate Extracts of Sediment." Soil Science Society of America Journal **51**(4): 938-941.

Phillips, E. J. P., D. R. Lovley, et al. (1993). "Composition of Non-Microbially Reducible Fe(III) in Aquatic Sediments." Applied and Environmental Microbiology **59**(8): 2727-2729.

Pizeta, I., G. Billon, et al. (2003). "Solid microelectrodes for in situ voltammetric measurements." Electroanalysis **15**(17): 1389-1396.

Polerecky, L., U. Franke, et al. (2005). "High spatial resolution measurement of oxygen consumption rates in permeable sediments." Limnology and Oceanography-Methods **3**: 75-85.

Postma, D. (1985). "Concentration of Mn and separation from Fe in sediments - I. Kinetics and stoichiometry of the reaction between birnessite and dissolved Fe(II) at 10oC." Geochimica et Cosmochmica Acta **49**: 1023-1033.

Postma, D. (1993). "The Reactivity of Iron-Oxides in Sediments - a Kinetic Approach." Geochimica et Cosmochmica Acta **57**(21-22): 5027-5034.

Postma, D. and R. Jakobsen (1996). "Redox zonation: Equilibrium constraints on the Fe(III)/SO4-reduction interface." Geochimica et Cosmochmica Acta **60**(17): 3169-3175.

Poulton, S. W., M. D. Krom, et al. (2004). "A revised scheme for the reactivity of iron (oxyhydr)oxide minerals towards dissolved sulfide." Geochimica et Cosmochmica Acta **68**(18): 3703-3715.

Poulton, S. W., M. D. Krom, et al. (2002). "The use of hydrous iron (III) oxides for the removal of hydrogen sulphide in aqueous systems." Water Research **36**(4): 825-834.

Pyzik, A. J. and S. E. Sommer (1981). "Sedimentary iron monosulfides: kinetics and mechanism of formation." Geochimica et Cosmochmica Acta **45**: 687-698.

Raiswell, R. and D. E. Canfield (1996). "Rates of reaction between silicate iron and dissolved sulfide in Peru Margin sediments." Geochimica et Cosmochmica Acta **60**(15): 2777-2787.

Raiswell, R., D. E. Canfield, et al. (1994). "A Comparison of Iron Extraction Methods for the Determination of Degree of Pyritisation and the Recognition of Iron-Limited Pyrite Formation." Chemical Geology **111**(1-4): 101-110.

Randles, J. E. B. (1948). Trans. Faraday Soc. **44**: 327.

Reimers, C. E., K. M. Fischer, et al. (1986). "Oxygen Microprofiles Measured Insitu in Deep Ocean Sediments." Nature **320**(6064): 741-744.

Revsbech, N. P., B. B. Jørgensen, et al. (1980). "Oxygen in the sea bottom measured with a microelectrode." Science **207**: 1355-1356.

Revsbech, N. P., B. B. Jørgensen, et al. (1983). "Microelectrode studies of the photosynthesis and O2, H2S, and pH profiles of a microbial mat." Limnology and Oceanography **28**: 1062-1074.

Revsbech, N. P. and B. B. Jørgensen (1986). "Microelectrodes - Their Use in Microbial Ecology." Advances in Microbial Ecology **9**: 293-352.

Revsbech, N. P., B. B. Jørgensen, et al. (1980). "Oxygen in the Sea Bottom Measured with a Microelectrode." Science **207**(4437): 1355-1356.

Reynolds, R. L., M. L. Tuttle, et al. (1994). "Magnetization and Geochemistry of Greigite-Bearing Cretaceous Strata, North-Slope Basin, Alaska." American Journal of Science **294**(4): 485-528.

Rickard, D. (1997). "Kinetics of pyrite formation by the H2S oxidation of iron (II) monosulfide in aqueous solutions between 25 and 125 degrees Celsius: The rate equation." Geochimica et Cosmochmica Acta **61**(1): 115-134.

Rickard, D. and G. W. I. Luther (1997). "Kinetics of pyrite formation by the H2S oxidation of iron (II) monosulfide in aqueous solutions between 25 and 125 degrees Celsius: The mechanism." Geochimica et Cosmochmica Acta **61**(1): 135-147.

Rifkin, S. C. and D. H. Evans (1976). "General Equation for Voltammetry with Step-Functional Potential Changes Applied to Differential Pulse Voltammetry." Analytical Chemistry **48**(11): 1616-1618.

Roberts, A. P. (1995). "Magnetic-Properties of Sedimentary Greigite (Fe3s4)." Earth and Planetary Science Letters **134**(3-4): 227-236.

Roberts, A. P. and G. M. Turner (1993). "Diagenetic Formation of Ferrimagnetic Iron Sulfide Minerals in Rapidly Deposited Marine-Sediments, South-Island, New-Zealand." Earth and Planetary Science Letters **115**(1-4): 257-273.

Roden, E. E. (2003). "Fe(III) oxide reactivity toward biological versus chemical reduction." Environmental Science & Technology **37**(7): 1319-1324.

Roden, E. E., M. R. Leonardo, et al. (2002). "Immobilization of strontium during iron biomineralization coupled to dissimilatory hydrous ferric oxide reduction." Geochimica et Cosmochmica Acta **66**(16): 2823-2839.

Roden, E. E. and M. M. Urrutia (1999). "Ferrous iron removal promotes microbial reduction of crystalline iron(III) oxides." Environmental Science & Technology **33**(11): 1847-1853.

Roden, E. E. and R. G. Wetzel (1996). "Organic carbon oxidation and suppression of methane production by microbial Fe(III) oxide reduction in vegetated and unvegetated freshwater wetland sediments." Limnology and Oceanography **41**(8): 1733-1748.

Roden, E. E. and R. G. Wetzel (2002). "Kinetics of microbial Fe(III) oxide reduction in freshwater wetland sediments." Limnology and Oceanography **47**(1): 198-211.

Roden, E. E. and J. M. Zachara (1996). "Microbial reduction of crystalline iron(III) oxides: Influence of oxide surface area and potential for cell growth." Environmental Science & Technology **30**(5): 1618-1628.

Rozan, T. F., M. E. Lassman, et al. (2000). "Evidence for iron, copper and zinc complexation as multinuclear sulphide clusters in oxic rivers." Nature **406**(6798): 879-882.

Rue, E. L. and K. W. Bruland (1995). "Complexation of Iron(III) by Natural Organic-Ligands in the Central North Pacific as Determined by a New Competitive Ligand Equilibration Adsorptive Cathodic Stripping Voltammetric Method." Marine Chemistry **50**(1-4): 117-138.

Ruzic, I. (1982). "Theoretical Aspects of the Direct Titration of Natural-Waters and Its Information Yield for Trace-Metal Speciation." Analytica Chimica Acta **140**(1): 99-113.

Ruzic, I. and S. Nikolic (1982). "The Influence of Kinetics on the Direct Titration Curves of Natural-Water Systems - Theoretical Considerations." Analytica Chimica Acta **140**(1): 331-334.

Saito, M. A. and J. W. Moffett (2001). "Complexation of cobalt by natural organic ligands in the Sargasso Sea as determined by a new high-sensitivity electrochemical cobalt speciation method suitable for open ocean work." Marine Chemistry **75**(1-2): 49-68.

Samson, S. D. and C. M. Eggleston (2000). "The depletion and regeneration of dissolution-active sites at the mineral-water interface: II. Regeneration of active sites on alpha-Fe2O3 at pH 3 and pH 6." Geochimica et Cosmochmica Acta **64**(21): 3675-3683.

Samson, S. D., L. L. Stillings, et al. (2000). "The depletion and regeneration of dissolution-active sites at the mineral-water interface: I. Fe, Al, and In sesquioxides." Geochimica et Cosmochmica Acta **64**(20): 3471-3484.

Sanders, B. M., K. D. Jenkins, et al. (1983). "Free Cupric Ion Activity in Seawater - Effects on Metallothionein and Growth in Crab Larvae." Science **222**(4619): 53-55.

Santschi, P., P. Hohener, et al. (1990). "Chemical Processes at the Sediment Water Interface." Marine Chemistry **30**(1-3): 269-315.

Schippers, A. and B. B. Jørgensen (2001). "Oxidation of pyrite and iron sulfide by manganese dioxide in marine sediments." Geochimica et Cosmochmica Acta **65**(6): 915-922.

Schippers, A. and B. B. Jørgensen (2001). "Oxidation of pyrite and iron sulfide by manganese dioxide in marine sediments." Geochimica et Cosmochmica Acta **65**(6): 915-922.

Schippers, A. and B. B. Jørgensen (2002). "Biogeochemistry of pyrite and iron sulfide oxidation in marine sediments." Geochimica et Cosmochmica Acta **66**(1): 85-92.

Schippers, A., P. G. Jozsa, et al. (1996). "Sulfur chemistry in bacterial leaching of pyrite." Applied and Environmental Microbiology **62**(9): 3424-3431.

Scholz, F. and B. Lange (1990). "High-Performance Abrasive Stripping Voltammetry." Fresenius Journal of Analytical Chemistry **338**(3): 293-294.

Scholz, F. and B. Lange (1992). "Abrasive Stripping Voltammetry - an Electrochemical Solid-State Spectroscopy of Wide Applicability." TRAC-Trends in Analytical Chemistry **11**(10): 359-367.

Scholz, F. and B. Meyer (1998). Voltammetry of solid microparticles immobilized on electrode surfaces. Electroanalytical Chemistry **20:** 1-86.

Scholz, F., L. Nitschke, et al. (1989). "Identification of Solid Materials with a New Electrochemical Technique - the Abrasive Stripping Analysis." Fresenius Zeitschrift Fur Analytische Chemie **334**(1): 56-58.

Scholz, F., L. Nitschke, et al. (1989). "A New Procedure for Fast Electrochemical Analysis of Solid Materials." Naturwissenschaften **76**(2): 71-72.

Scholz, F., L. Nitschke, et al. (1989). "Abrasive Stripping Voltammetry - the Electrochemical Spectroscopy for Solid-State - Application for Mineral Analysis." Fresenius Zeitschrift Fur Analytische Chemie **335**(2): 189-194.

Scholz, F., L. Nitschke, et al. (1989). "A Technique to Study the Electrochemistry of Minerals." Naturwissenschaften **76**(4): 167-168.

Scholz, F., L. Nitschke, et al. (1989). "A Simple and Convenient Solid-State Microanalytical Technique for Identification and Characterization of the High-Temperature Superconductor Yba2cu3o7-X." Fresenius Zeitschrift Fur Analytische Chemie **335**(6): 571-572.

Schramm, A., C. M. Stantegoeds, et al. (1999). "On the occurrence of anoxic microniches, denitrification, and sulfate reduction in aerated activated sludge." Applied and Environmental Microbiology **65**(9): 4189-4196.

Schroder, U., K. B. Oldham, et al. (2000). "Modelling of solid state voltammetry of immobilized microcrystals assuming an initiation of the electrochemical reaction at a three-phase junction." Journal of Solid State Electrochemistry **4**(6): 314-324.

Schwertmann, U. (1964). "Differenzierung der Eisenoxide des Bodens durch photochemische Extraktion mit saurer Ammoniumoxalat-Lösung (in German)." Zeitschrift zur Pflanzenernährung und Bodenkunde **195**: 194-202.

Schwertmann, U. (1984). "Citation Classic - the Differentiation of Iron-Oxides in Soils by Extraction with Ammonium Oxalate Solution." Current Contents/Agriculture Biology & Environmental Sciences(22): 20-20.

Schwertmann, U. (1991). "Solubility and Dissolution of Iron-Oxides." Plant and Soil **130**(1-2): 1-25.

Schwertmann, U. and R. M. Cornell (1991). Iron oxides in the laboratory. Weinheim, VCH Verlagsgesellschaft.

Schwertmann, U. and R. W. Fitzpatrick (1992). Iron Minerals in Surface Environments. Biomineralization Processes of Iron and Manganese. R. W. Fitzpatrick. Cremlingen-Destedt, Catena Verlag**:** 7-30.

Schwertmann, U. and E. Murad (1983). "Effect of Ph on the Formation of Goethite and Hematite from Ferrihydrite." Clays and Clay Minerals **31**(4): 277-284.

Seeliger, S., R. Cord-Ruwisch, et al. (1998). "A periplasmic and extracellular c-type cytochrome of Geobacter sulfurreducens acts as a ferric iron reductase and as an electron carrier to other acceptors or to partner bacteria." Journal of Bacteriology **180**(14): 3686-3691.

Shain, I. and J. Lewinson (1961). "Stripping Analysis with Spherical Mercury Electrodes." Analytical Chemistry **33**(2): 187-&.

Shuttleworth, S. M., W. Davison, et al. (1999). "Two-dimensional and fine structure in the concentrations of iron and manganese in sediment pore-waters." Environmental Science & Technology **33**(23): 4169-4175.

Sidhu, P. S., R. J. Gilkes, et al. (1981). "Dissolution of Iron-Oxides and Oxyhydroxides in Hydrochloric and Perchloric Acids." Clays and Clay Minerals **29**(4): 269-276.

Skei, J. M., D. H. Loring, et al. (1988). "Partitioning and enrichment of trace metals in a sediment core from Framvaren, South Norway." Marine Chemistry **23**: 269-281.

Sorensen, J. and B. B. Jørgensen (1987). "Early Diagenesis in Sediments from Danish Coastal Waters - Microbial Activity and Mn-Fe-S Geochemistry." Geochimica et Cosmochmica Acta **51**(6): 1583-1590.

Stojek, Z. (2002). The Electrical Double Layer and Its Structure. Electroanalytical Methods - Guide to Experiments and Applications. F. Scholz. Berlin, Springer**:** 3-8.

Stone, A. T. and J. J. Morgan (1987). Reductive dissolution of metal oxides. Aquatic Surface Chemistry. W. Stumm. New York, Wiley**:** 221-254.

Stookey, L. L. (1970). "Ferrozine - a New Spectrophotometric Reagent for Iron." Analytical Chemistry **42**(7): 779-&.

Straub, K. L., M. Benz, et al. (2001). "Iron metabolism in anoxic environments at near neutral pH." Fems Microbiology Ecology **34**(3): 181-186.

Straub, K. L., M. Benz, et al. (1996). "Anaerobic, nitrate-dependent microbial oxidation of ferrous iron." Applied and Environmental Microbiology **62**(4): 1458-1460.

Stumm, W. and J. J. Morgan (1996). Aquatic chemistry. New York, Wiley.

Stumm, W. and B. Sulzberger (1992). "The Cycling of Iron in Natural Environments - Considerations Based on Laboratory Studies of Heterogeneous Redox Processes." Geochimica et Cosmochmica Acta **56**(8): 3233-3257.

Sulzberger, B. and H. Laubscher (1995). "Reactivity of Various Types of Iron(III) (Hydr)Oxides Towards Light-Induced Dissolution." Marine Chemistry **50**(1-4): 103-115.

Sulzberger, B., D. Suter, et al. (1989). "Dissolution of Fe(III)(Hydr)Oxides in Natural-Waters - Laboratory Assessment on the Kinetics Controlled by Surface Coordination." Marine Chemistry **28**(1-3): 127-144.

Suter, D., S. Banwart, et al. (1991). "Dissolution of Hydrous Iron(III) Oxides by Reductive Mechanisms." Langmuir **7**(4): 809-813.

Sweeney, R. E. and I. R. Kaplan (1973). "Pyrite framboid formation: Laboratory synthesis and marine sediments." Economic Geology **68**: 618-634.

Taillefert, M., A. B. Bono, et al. (2000). "Reactivity of freshly formed Fe(III) in synthetic solutions and (pore)waters: Voltammetric evidence of an aging process." Environmental Science & Technology **34**(11): 2169-2177.

Tallman, D. E. (1994). "Square-Wave Voltammetry of Reversible-Systems at Ring Microelectrodes .1. Theoretical-Study." Analytical Chemistry **66**(4): 557-565.

Tang, D. G., K. W. Warnken, et al. (2001). "Organic complexation of copper in surface waters of Galveston Bay." Limnology and Oceanography **46**(2): 321-330.

Taplin, J. H. (1974). "Index of Reaction - Unifying Concept for Reaction-Kinetics of Powders." Journal of the American Ceramic Society **57**(3): 140-143.

Tercier, M. L. and J. Buffle (1996). "Antifouling membrane-covered voltammetric microsensor for in situ measurements in natural waters." Analytical Chemistry **68**(20): 3670-3678.

Tercier, M. L., N. Parthasarathy, et al. (1995). "Reproducible, Reliable and Rugged Hg-Plated Ir-Based Microelectrode for in-Situ Measurements in Natural-Waters." Electroanalysis **7**(1): 55-63.

Tercier-Waeber, M. L., C. Belmont-Hebert, et al. (1998). "Real-time continuous Mn(II) monitoring in lakes using a novel voltammetric in situ profiling system." Environmental Science & Technology **32**(10): 1515-1521.

Tercier-Waeber, M. L., J. Pei, et al. (2000). "A novel voltammetric probe with individually addressable gel-integrated microsensor arrays for real-time high spatial resolution concentration profile measurements." Electroanalysis **12**(1): 27-34.

Tessier, A., D. Fortin, et al. (1996). "Metal sorption to diagenetic iron and manganese oxyhydroxides and associated organic matter: Narrowing the gap between field and laboratory measurements." Geochimica et Cosmochmica Acta **60**(3): 387-404.

Thamdrup, B. (2000). Bacterial manganese and iron reduction in aquatic sediments. Advances in Microbial Ecology **16:** 41-84.

Thamdrup, B. and D. E. Canfield (1996). "Pathways of carbon oxidation in continental margin sediments off central Chile." Limnology and Oceanography **41**(8): 1629-1650.

Thamdrup, B., K. Finster, et al. (1994). "Thiosulfate and Sulfite Distributions in Porewater of Marine-Sediments Related to Manganese, Iron, and Sulfur Geochemistry." Geochimica et Cosmochmica Acta **58**(1): 67-73.

Thamdrup, B., H. Fossing, et al. (1994). "Manganese, iron, and sulfur cycling in a coastal marine sediment, Aarhus Bay, Denmark." Geochimica et Cosmochmica Acta **58**(23): 5115-5129.

Thamdrup, B., H. Fossing, et al. (1994). "Manganese, Iron, and Sulfur Cycling in a Coastal Marine Sediment, Aarhus Bay, Denmark." Geochimica et Cosmochmica Acta **58**(23): 5115-5129.

Thamdrup, B., R. Rossello-Mora, et al. (2000). "Microbial manganese and sulfate reduction in Black Sea shelf sediments." Applied and Environmental Microbiology **66**(7): 2888-2897.

Turick, C. E., F. Caccavo, et al. (2003). "Electron transfer from Shewanella algae BrY to hydrous ferric oxide is mediated by cell-associated melanin." FEMS Microbiology Letters **220**(1): 99-104.

Turick, C. E., L. S. Tisa, et al. (2002). "Melanin production and use as a soluble electron shuttle for Fe(III) oxide reduction and as a terminal electron acceptor by Shewanella algae BrY." Applied and Environmental Microbiology **68**(5): 2436-2444.

Van den Berg, C. M. G. (1984). "Organic and Inorganic Speciation of Copper in the Irish Sea." Marine Chemistry **14**(3): 201-212.

van den Berg, C. M. G. (1984). Organic and inorganic speciation of copper in the Irish Sea. Marine Chemistry. **14:** 201-212.

Van den Berg, C. M. G. (1988). "Cathodic Stripping Voltammetry and Chronopotentiometry of Trace-Metals in Seawater." Abstracts of Papers of the American Chemical Society **195**: 10-17.

Van den Berg, C. M. G. (1991). "Potentials and Potentialities of Cathodic Stripping Voltammetry of Trace-Elements in Natural-Waters." Analytica Chimica Acta **250**(1): 265-276.

Van den Berg, C. M. G. (1995). "Evidence for Organic Complexation of Iron in Seawater." Marine Chemistry **50**(1-4): 139-157.

van Oorschot, I. H. M., T. Grygar, et al. (2001). "Detection of low concentrations of fine-grained iron oxides by voltammetry of microparticles." Earth and Planetary Science Letters **193**(3-4): 631-642.

Vandenberg, C. M. G. (1982). "Determination of Copper Complexation with Natural Organic-Ligands in Sea-Water by Equilibration with Mno2 .1. Theory." Marine Chemistry **11**(4): 307-322.

Vandenberg, C. M. G. (1982). "Determination of Copper Complexation with Natural Organic-Ligands in Sea-Water by Equilibration with Mno2 .2. Experimental Procedures and Application to Surface Sea-Water." Marine Chemistry **11**(4): 323-342.

Vandenberg, C. M. G. (1984). "Determination of Copper in Sea-Water by Cathodic Stripping Voltammetry of Complexes with Catechol." Analytica Chimica Acta **164**(OCT): 195-207.

Vandenberg, C. M. G. (1984). "Determination of the Complexing Capacity and Conditional Stability-Constants of Complexes of Copper(II) with Natural Organic-Ligands in Seawater by Cathodic Stripping Voltammetry of Copper Catechol Complex-Ions." Marine Chemistry **15**(1): 1-18.

Vandenberg, C. M. G. and J. R. Donat (1992). "Determination and Data Evaluation of Copper Complexation by Organic-Ligands in Sea-Water Using Cathodic Stripping Voltammetry at Varying Detection Windows." Analytica Chimica Acta **257**(2): 281-291.

Vandenberg, C. M. G. and J. R. Kramer (1979). "Determination of Complexing Capacities of Ligands in Natural-Waters and Conditional Stability-Constants of the Copper-Complexes by Means of Manganese-Dioxide." Analytica Chimica Acta **106**(1): 113-120.

Visscher, P. T., J. Beukema, et al. (1991). "In situ characterization of sediments: Measurements of oxygen and sulfide profiles with a novel combined needle electrode." Limnology and Oceanography **36**: 1476-1480.

Voigt, D. E., S. L. Brantley, et al. (1996). "Chemical fixation of arsenic in contaminated soils." Applied Geochemistry **11**(5): 633-&.

von Gunten, U. and G. Furrer (2000). "Steady-state modelling of biogeochemical processes in columns with aquifer material: 2. Dynamics of iron-sulfur interactions." Chemical Geology **167**(3-4): 271-284.

Waite, T. D., J. A. Davis, et al. (1994). "Uranium(Vi) Adsorption to Ferrihydrite - Application of a Surface Complexation Model." Geochimica et Cosmochmica Acta **58**(24): 5465-5478.

Wang, F. Y. and A. Tessier (1999). "Cadmium complexation with bisulfide." Environmental Science & Technology **33**(23): 4270-4277.

Wang, Q. W. and J. W. Morse (1996). "Pyrite formation under conditions approximating those in anoxic sediments .1. Pathway and morphology." Marine Chemistry **52**(2): 99-121.

Wang, X. H. and K. S. E. Forssberg (1996). "Solution electrochemistry of sulfide-xanthate-cyanide systems in sulfide mineral flotation." Minerals Engineering **9**(5): 527-546.

Waychunas, G. A., B. A. Rea, et al. (1993). "Surface-Chemistry of Ferrihydrite .1. Exafs Studies of the Geometry of Coprecipitated and Adsorbed Arsenate." Geochimica et Cosmochmica Acta **57**(10): 2251-2269.

Wedepohl, K. H. (1995). "The composition of the continental crust." Geochimica et Cosmochmica Acta **59**(7): 1217-1232.

Wightman, R. M. and (1981). "Microvoltammetric electrodes." Analytical Chemistry **53**: 1125A-1130A.

Wightman, R. M. and D. O. Wipf (1989). "Voltammetry at Ultramicroelectrodes." Electroanalytical Chemistry **15**: 267-353.

Wilkin, R. T. and H. L. Barnes (1996). "Pyrite formation by reactions of iron monosulfides with dissolved inorganic and organic sulfur species." Geochimica et Cosmochmica Acta **60**(21): 4167-4179.

Witter, A. E., B. L. Lewis, et al. (2000). "Iron speciation in the Arabian Sea." Deep-Sea Research Part II-Topical Studies in Oceanography **47**(7-8): 1517-1539.

Wolthers, M., C. H. van der Weijden, et al. (2002). "Arsenic association with iron sulphides, adsorption and incorporation." Geochimica et Cosmochmica Acta **66**(15A): A843-A843.

Xue, H. and L. Sigg (1993). Free cupric ion concentration and Cu(II) speciation in a eutrophic lake. Limnology and Oceanography. **38:** 1200-1213.

Yao, W. S. and F. J. Millero (1996). "Oxidation of hydrogen sulfide by hydrous Fe(III) oxides in seawater." Marine Chemistry **52**(1): 1-16.

Zachara, J. M., R. K. Kukkadapu, et al. (2004). "Biogeochemical transformation of Fe minerals in a petroleum-contaminated aquifer." Geochimica et Cosmochmica Acta **68**(8): 1791-1805.

Zachara, J. M., S. C. Smith, et al. (1992). "Cadmium Sorption to Soil Separates Containing Layer Silicates and Iron and Aluminum-Oxides." Soil Science Society of America Journal **56**(4): 1074-1084.

Zhang, X. J. and B. Ogorevc (1998). "Poly(tetrafluoroethylene) film housing of carbon fibers using capillary-pull technology for one-stage fabrication of carbon disk ultramicroelectrodes and their characterization." Analytical Chemistry **70**(8): 1646-1651.

Ziebis, W., S. Forster, et al. (1996). "Complex burrows of the mud shrimp Callianassa truncata and their geochemical impact in the sea bed." Nature **382**(6592): 619-622.

Zinder, B., G. Furrer, et al. (1986). "The Coordination Chemistry of Weathering .2. Dissolution of Fe(III) Oxides." Geochimica et Cosmochmica Acta **50**(9): 1861-1869.

Zopfi, J., T. G. Ferdelman, et al. (2001). "Influence of water column dynamics on sulfide oxidation and other major biogeochemical processes in the chemocline of Mariager Fjord (Denmark)." Marine Chemistry **74**(1): 29-51.